SERI/TP-49-185

Photovoltaic Material & Device Measurements Workshop

Focus on Polycrystalline Thin Film Cells

June 11-13, 1979

Stouffer's
National Center Hotel
Arlington, Virginia

Sponsored by
Solar Energy Research Institute
under contract to the U.S. Department of Energy

DISCLAIMER

NOTICE

This report was prepared as an account of the meeting sponsored by the United States Government. Neither the United States nor the United States Department of Energy, nor any of their employees, nor any of their contractors, subcontractors, or their employees, makes any warranty, express or implied, or assumes any legal liability or responsibility for the accuracy, completeness or usefulness of any information, apparatus, product or process disclosed, or represents that its use would not infringe privately owned rights.

This report has been reproduced directly from the best available copy.

SERI/TP-49-185

Distribution Category: UC-63e

Photovoltaic Material & Device Measurements Workshop

Focus on Polycrystalline Thin Film Cells

June 11-13, 1979

Stouffer's
National Center Hotel
Arlington, Virginia

Co-Chairmen

David Sawyer
National Bureau of Standards

Joseph Morabito
Bell Laboratories

Sponsored by
Solar Energy Research Institute
under contract to the U.S. Department of Energy

Report Number:
Conf. 790601

THIS PAGE

WAS INTENTIONALLY

LEFT BLANK

TABLE OF CONTENTS

OPTICAL/ECTRO-OPTICAL SESSION

CHARGE TRANSPORT SESSION

POSTER SESSION

TABLE OF CONTENTS (con't.) Page No.

PHOTOVOLTAICS MATERIAL AND DEVICE MEASUREMENTS WORKSHOP

INTRODUCTION

This is the first meeting of the Photovoltaics Material and Device Measurements Workshop. It is being conducted for the Department of Energy by the Photovoltaics Program Office of the Solar Energy Research Institute in association with the National Bureau of Standards. The general purpose of the workshop is to accelerate the development of thin film solar cells by improving the versatility and reliability of material and device measurement techniques.

This meeting focuses on polycrystalline materials and the associated thin film devices. Another meeting, being planned for early 1980, will emphasize amorphous materials and device measurements. Findings and conclusions will be the basis for future meetings to examine other photovoltaic materials and/or technologies.

The objectives of this meeting of the workshop are:

1. Identify and discuss the techniques which have been used to measure selected key characteristics of thin film polycrystalline materials and devices.

2. Discuss the applicability of these techniques to the understanding of thin film polycrystalline materials and devices.

3. Identify measurement techniques which require improvements.

4. Identify new measurement techniques.

5. Suggest methods for achieving:

   - more meaningful material and device measurements
   - greater measurement reproducibility
   - greater efficiency in the development and fabrication of thin film devices
   - greater confidence in comparing and evaluating thin film device measurements.

6. Foster greater communication between device researchers and experts in measurement techniques.

Presentations and discussion are divided into five sessions. Three are devoted to formal presentations, a fourth to poster papers, and a fifth to discussion of key issues and recommendations for future work. The papers for presentation were selected on the basis of addressing the following selected key topics:

Structural/Chemical Session

- o Grain structure: size, texture, morphology, boundaries;
- o Defects: planar, line, point;
- o Interfaces: surface, grain, junction;
- o Impurities: dopants, stoichiometry; and
- o Macroscopic features: cracks, pinholes, evidence of stress.

Optical/Electro-optical Session

- o Electronic structure of dislocations and grain boundaries;
- o Interface and grain boundary barrier heights;
- o Surface and grain boundary recombination velocities;
- o Diffusion lengths for photo-generated minority carriers; and
- o Aspects of optical absorption unique to polycrystalline films.

Charge Transport Session

- o Majority carrier transport properties in polycrystalline materials: resistivity carrier concentration, mobility;
- o Minority carrier transport properties in polycrystalline materials: bulk, defect and grain boundary recombination;
- o Current transport mechanisms in polycrystalline junctions: Schottky barrier, MIS, p-n junction, heterojunction;
- o Electronic structure of grain boundaries (electrical measurements): barrier height, interface states, recombination velocity; and
- o Effects of surface on transport properties in polycrystalline materials.

These topics were selected by the Steering Committee using input obtained from the questionnaire distributed at the Photovoltaics R&D Review Meeting held during October 24-26, 1978, at Vail, Colorado.

Poster papers will also emphasize these topics.

Since there will be no workshop proceedings, the Steering Committee has arranged for a special issue of the Elsevier Sequoia Journal, Solar Cells: Their Science, Technology, Applications and Economics, to be devoted to the workshop. Dr. David Sawyer of the National Bureau of Standards, will be the editor for this special issue that will be published in the fall of 1979. All speakers have been invited to either submit papers or extended summaries of their papers for inclusion in the journal. All papers or summaries submitted will be selected through a peer review process. The journal will not be automatically mailed to workshop attendees and therefore must be obtained individually by those interested.

The workshop Steering Committee wishes to express its thanks to all speakers, persons submitting papers in response to the Call for Papers and those individuals who have helped in the organization. Special thanks to Alan Fahrenbruch, Harry Schafft, Fritz Wald and the very capable staff of the SERI Conferences Group.

Phil Pierce for the Steering Committee:

Richard L. Anderson
University of Vermont

J. Richard Burke
Solar Energy Research Institute

David E. Carlson
RCA Laboratories

Vicky Curry, Workshop Coordinator
Solar Energy Research Institute

P. Daniel Dapkus
Rockwell International

Alfred P. DeFonzo
Naval Research Laboratory

Donald L. Feucht
Solar Energy Research Institute

Lewis M. Fraas
Chevron Research Company

Stephen J. Hogan
Solar Energy Research Institute

Lawrence L. Kazmerski
Solar Energy Research Institute

John D. Meakin
Institute of Energy Conversion

Joseph M. Morabito
Bell Laboratories

Philip R. Pierce, Workshop Coord.
Solar Energy Research Institute

Donald W. Ritchie
Solar Energy Research Institute

David E. Sawyer
National Bureau of Standards

H. Harry Wieder
Naval Ocean Systems Center

THIS PAGE

WAS INTENTIONALLY

LEFT BLANK

Overview Session

PERSPECTIVE ON PHOTOVOLTAIC MATERIAL AND DEVICE MEASUREMENTS

Allen Rothwarf

Institute of Energy Conversion
University of Delaware
Newark, Delaware 19711

INTRODUCTION

The successful development of polycrystalline thin film solar cells can be traced through a number of distinct stages. In each of these stages certain measurement, modeling and testing procedures are essential if systematic progress is to be achieved. It is the purpose of this paper to review these stages and to describe in a general way the type of activities that should be conducted at each stage. Focusing on a solar cell with no prior history the first step would be to identify a possible material for the absorber-generator and establish its vital optical and electronic properties. Following this would be studies of preparation techniques suitable for thin film cells. The next stage is to produce prototype devices which would then form the basis of an optimization effort. As appropriate, durability and failure mode studies would be added leading finally to the development of a large scale production technology.

Figure 1 illustrates the essential interrelationships between the various activities during the research and development effort. A model of cell structure and operation, as detailed and quantitative as possible, forms the basis of a specific cell design. Actual cells, or component parts, are then produced and subjected to such tests as are necessary to show conformation or variance with the cell and material specifications. Production modifications can then be made until the cell design and actual cells essentially match. Cell optimization is then achieved by redesigning the cell until the limits of the component materials is considered to have been reached.

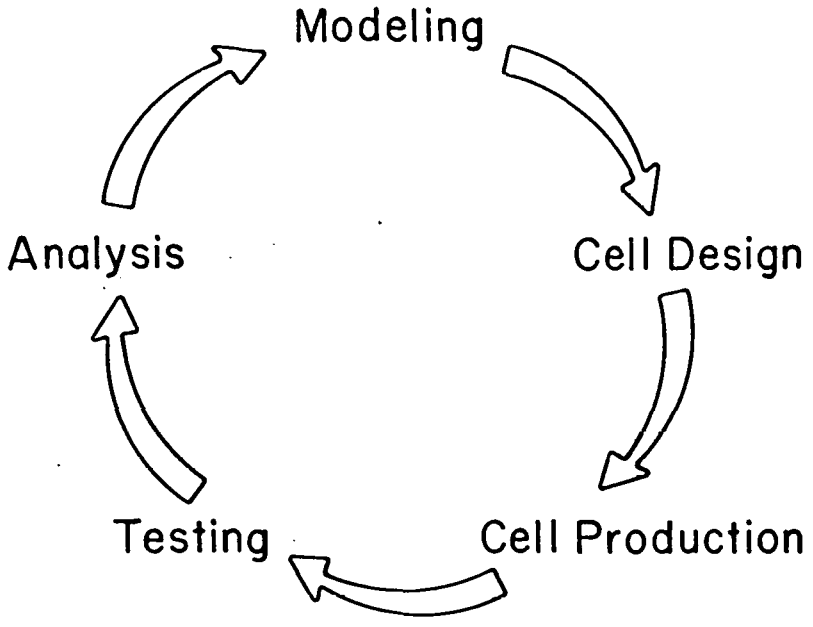

Figure 1. Major information and materials flow. Not shown are the many other linkages between the various activities essential to systematic cell improvement.

CONCEPTUAL STAGE AND MATERIAL STUDIES

In the conceptual stage of the cell the material properties are the key to modeling the eventual device. In Table I we have listed the various material properties which impact solar cell performance classified in one of the numerous possible ways. In this stage a major consideration is the choice of a preparation technique for the component materials. A broad range of techniques include physical or chemical vapor deposition, sputtering, pyrolysis, plating and many others. Whichever technique is used the preparation will determine many of the structural properties of the materials, such as grain size, planar, line and point defect structures and electronic properties which impact the mobility, lifetime, diffusion length and so on. Characterization of the material would initially utilize the traditional techniques such as X-ray diffraction, transmission and scanning electron microscopy, and the now very versatile chemical analysis techniques based on electron and ion spectroscopy. Optical techniques would be used to study absorption behavior and the index of refraction as a function of wavelength and to determine the bandgap. A powerful experimental tool is to construct test devices which are specifically designed to measure key material properties. Schottky diodes or other junctions with well-known materials acting as heterojunctions can be used to study the unknown material being investigated. The techniques applicable to such devices include spectral response as a function of wavelength, photocapacitance measurements, and current-voltage measurements at various wavelengths, intensities and temperatures. Measurements of Hall mobility, resistivity as a function of temperature and thermoelectric power will all have broad applicability in characterizing the properties of the materials under study.

Table 1. Material Properties Impacting Upon Specific Solar Cell Performance

Photon Economy	Carrier Collection
Bandgap	Diffusion Length
Absorption Coefficient	Minority Carrier Mobility
Index of Refraction	Minority Carrier Lifetime
Carrier Concentration	Surface Recombination Velocity
Device Configuration	Resistivity
Doping Type	Interface Recombination Velocity
Lattice Constants	**Structural Stability and Operation**
Electron Affinity	Thermal Expansion Coefficient
Dielectric Constant	Thermal Conductivity

PROTOTYPE DEVICE DESIGN

In this stage the results of stage one are fed into the modeling of a homojunction, heterojunction, heterostructure, or Schottky diode, and the choice of doping levels, partner materials, substrate, ohmic contacts, thickness of layers, gridding and other device characteristics are selected. The modeling is particularly critical at this stage and must take into account to as large an extent as possible the known mechanisms. The expected performance of the device is computed to the degree possible and used as a basis of comparison for measurements on the actual devices. All components selected and their interactions are extremely important, and no component can be ignored. As an example, we can consider the role of the substrate for a thin film polycrystalline cell. There are on the order of ten distinct properties which can affect the final device stability or efficiency. These include lattice match to the material to prevent stress build up and possible fracture, and ohmic contact to the semiconductor. Particularly for thin film cells a high reflectivity of the substrate material is desirable to promote multiple light passes through the absorbing layer. The substrate must also be inert or cause benign or advantageous doping of the adjacent semiconductor. It must be able to sustain temperatures at which growth for optimal properties is to take place, it must be a material rugged enough to serve as one of the outer layers of the cell and it must, of course, be a low cost material. The failure to be acceptable in any one of these properties may at a later stage require the abandonment of the substrate with the possible waste of much of the proceeding cell development efforts. A similar situation applies to the choice of the partner materials for a heterojunction or for a Schottky device.

PROTOTYPE DEVICE DEVELOPMENT

The essential nature of thorough and quantitative modeling during this stage of the solar cell development cannot be over-emphasized. It is against the model that all material and device measurements are compared and steps then taken to remedy any discrepancies. These may prove to be due to a failure to produce the material or structure the cell design calls for, or alternatively measurements may show errors in the modeling which must then be corrected.

The measurements carried out in this stage fall into a number of general categories. The first group provides routine feedback of performance data for many cells to establish a baseline and ensure statistically meaningful data. A second group includes attack on specific problems in which selected devices are subjected to specialized tests. Parameters such as diffusion voltages, carrier mobilities and densities, diffusion lengths, and optical absorption effects may be determined in this group of studies.

A third class are in-depth studies which are designed to extend the basic knowledge of either the materials or the device configuration under study and may involve the development of new or improved techniques to study various phenomena.

OPTIMIZATION

In this stage the goal is to achieve the maximum efficiency which the materials and device design are capable of producing. The loss minimization approach developed at the Institute of Energy Conversion has proved invaluable in this stage. Detailed modeling of all the possible loss mechanisms in the specific cell design are carried out. As necessary, measurements are made to quantify the losses occurring throughout the device. These measurements include detailed optical reflectivity and transmission tests using an integrating sphere. Accurate measurements and analysis of the current-voltage curve determines the series and shunt resistance losses and separates other non-resistive causes of fill factor loss. It is essential to pinpoint whether losses are occurring within the bulk absorbing layers, or at the various surfaces or at interfaces. To do so use is made of techniques such as the spectral response as a function of wavelength and bias voltage, and photocapacitance as a function of wavelength, voltage and intensity of the light. Variations in the current-voltage curve as a function of temperature, intensity and spectral content of the light, and the results of various post-device formation heat treatments have all proved valuable. The results of these measurements are analyzed and fed back into the cell production process until the device design and actual cell performance essentially agree. If necessary appropriate modifications are made to the cell modeling.

In a systematic way the most dominant efficiency loss mechanisms are ameliorated in turn until it is concluded that the inherent material and design limited efficiency has been achieved.

DURABILITY AND FAILURE TESTING

As the initial device efficiency reaches a usable value attention must be given to the potential usable lifetime of the device and its failure modes. In this stage the cell is subjected to a number of stresses which are designed to reveal possible failure modes in the cell and to diagnose the cause of the failure. Again, modeling is important to provide the framework for the experimental studies. Experiments must be designed to identify which mechanisms occur. Many of the measurements which were useful in the optimization phase will again be of value to

determine exactly where the loss in performance is occurring and to identify the structural or electronic mechanism responsible.

LARGE SCALE PRODUCTION TECHNOLOGY

In this final stage a low-cost production technology must be developed to produce large areas of cells without serious loss in efficiency or other essential parameters. A version of loss minimization is invaluable. Each modification to the production entailed by the need for high speed, low-cost processing is subjected to a detailed analysis to determine where losses in performance are taking place and to direct the remedial measures. Some of the test procedures which were useful in the laboratory optimization phase will be modified to serve as the basis of a quality assurance program.

SUMMARY

We have described a methodology for materials and device development for thin film polycrystalline solar cells. The key is the interplay between modeling, device design and production, and materials and device measurement. The parameters of interest have been discussed, the types of measurements needed have been reviewed and the utility of these for polycrystalline thin film cells will be demonstrated by their applicability to the cadmium sulfide/copper sulfide system.

NOTES

Structural/Chemical Session

STRUCTURAL AND CHEMICAL CHARACTERIZATION OF PHOTOVOLTAIC MATERIALS AND DEVICES

John D. Meakin

Institute of Energy Conversion
University of Delaware
Newark, Delaware 19711

INTRODUCTION

In its most general form a solar cell is comprised of five distinct layers. These are the two semiconductors which make up the junction, two ohmic contacts and a transparent encapsulating and anti-reflecting layer. In order to understand the structure and operation of this multi-layer device, generally with a view to improving its performance, it is necessary to build up an extensive data base covering both the individual components and the interfaces and interactions between the discrete layers. A complicating factor is that in many instances the behavior of the component layers cannot be predicted from the known and understood properties of the corresponding bulk material. As a direct consequence of the thickness of the layers, profound effects on phase and chemical stability can frequently be observed. The interface region between contiguous layers may also play a dominant role in the performance of a given cell and regions less than 50 Å thick must often be detected and characterized before a full accounting of cell behavior is possible. Finally we are concerned with a large area device which is inherently susceptible to defects that may be few in number and low in areal density. Unless such flaws can either be eliminated or neutralized many cell measurements will owe more to the defects than to the vast majority of defect free cell area.

To attack the problem of fully characterizing the structural and chemical build up of a thin film solar cell there is now an impressive array of experimental and analytical techniques available. It remains true however that unless the choice of techniques is well planned and the analytical results integrated into a very broad based study, the results of using even the most sophisticated tools will be an accumulation of data and not necessarily an increase in either real knowledge or understanding.

STRUCTURAL CHARACTERIZATION

In this section we are concerned with the morphological, crystallographic and defect structure of the solar cell components. Techniques are available which will provide images with down to virtually atomic resolution. Each increment in detail resolved however is usually only achieved at the cost of a reduction in the total area or volume of material examined. A judicious combination of large area-low resolution and small area-high

resolution studies are generally necessary to provide all the information required.

Optical microscopy still provides the most convenient and accessible techniques for studying the morphology and structure of a photovoltaic device. Simple reflection or transmission imaging can be extended using various interference and phase contrast techniques. A direct way of studying the actual energy conversion operation of the cell is provided by the scanning spot techniques now in use in various laboratories. These techniques in common with all optical based systems are limited in spatial resolution to a few tenths of a micron which is however very adequate for many studies.

In order to extend the fineness of detail that can be resolved we turn to the broad range of electron beam techniques. The surface probing techniques available in a modern scanning electron microscope have,because of their convenience and versatility, become dominant. Most widely used is secondary electron imaging which with virtually no prior sample preparation required, will give images of better than 100 Å resolution, almost unlimited depth of field and good contrast between most cell components. To explore composition variations and enhance the contrast between different phases there are relatively simple modifications to give backscattered electron or cathodeluminescence images. Direct insight into the electronic functioning of a device under study is given by voltage contrast or electron beam induced current imaging.

The convenience of conventional scanning electron microscopy arises in part from the long working distance between the final lens and the sample surface and the ability to directly study almost any free surface. Higher resolution than possible in an SEM is available in the traditional transmission electron microscope (TEM). However to use the TEM necessitates preparing an electron transparent sample of less than about 1 μm thickness. The problems of achieving this in a multi-layer device are not trivial but once achieved it is possible to see detail at virtually atomic resolution and also to obtain direct insight into crystal and defect structures. The latest modification to the TEM is the scanning transmission electron microscope (STEM) which can be used to produce images in the TEM mode or to operate in the scanning mode. The major advantages of the STEM are a better resolution for surface studies than in the SEM and the ability to perform the very small area diffraction and chemical analysis studies described below.

X-ray diffraction maintains its position as the leading system for studying the crystal structure of solids being unrivaled for precision, requiring generally no special sample preparation and being essentially non-destructive. Thin surface films can be characterized by reflection high energy electron diffraction (RHEED) or low energy electron diffraction (LEED). The latter is often combined with Auger electron spectroscopy or other chemical analysis techniques. A relatively recent addition to the arsenal of crystal structure sensitive techniques is the use of electron channeling patterns in the SEM. By rocking the incident beam around a fixed point on the sample surface, a display is generated which reflects the crystal structure and can therefore be used to differentiate between phases or provide the local orientation. The spatial resolution is of the order of 1 μm and will therefore have wide applicability in

polycrystalline solar cells. The STEM is capable of giving diffraction information from regions as small as 50-100 Å.

Imperfections, both planar and line, can be revealed in a number of different ways. In order to render dislocations visible using optical techniques it is usually necessary to etch the sample and produce etch pits at the point of emergence of the defects. Transmission electron microscopy will reveal both dislocations and planar faults more directly as a consequence of the local changes in diffraction conditions. The use of electron channeling has now extended the detection of defects to the conventional SEM allowing multiple mode studies of a given region of a sample surface. If relatively large grain sizes are being used it is also possible to image defects using the various X-ray topography techniques.

CHEMICAL CHARACTERIZATION

There has been a general trend in chemical analysis towards physical rather than chemical techniques. Many of these techniques can be applied to the component materials of a solar cell but of particular interest are those which can be applied to either thin films or to completed devices.

To analyze the bulk composition of a layer requires that an appropriate energy input will cause a detectable and element specific emission. Characteristic X-ray lines form the basis of a number of techniques. The earliest technique was X-ray fluorescence in which the characteristic lines were excited by a suitable short wave X-ray. This system is generally set up in a manner that does not give any laterial resolution. Subsequently, lateral and depth resolution have been added by using either electron or proton excitation. The former is now a standard technique and can be carried out in an electron beam microprobe, an SEM or an STEM. Analysis of the emitted X-ray is generally by means of solid state detectors (EDAX) which have larger acceptance angles and much higher counting efficiencies than crystal monochromators. Dedicated microprocessors and peak de-convolution techniques have largely overcome the reduced resolution of the energy discriminating systems and generally all elements heavier than sodium can be discriminated and detected. The spatial resolution of EDAX with bulk samples is limited to the order of a micron by the range of elastically scattered electrons and by secondary fluorescence effects. A particular advantage of STEM is that when examining a thin sample the spatial resolution for EDAX can be less than 50 Å.

A number of proton microprobes have now been constructed in which either X-ray or γ-ray emission is stimulated by a beam of protons at energies of the order of 2 MeV. The spatial and depth resolution of this system is about 10 μm but a significant advantage over electron beam systems is that the sample need not be in vacuum. Certain elements lighter than sodium can be detected from γ-ray spectroscopy.

Many of the standard analytical techniques can be applied to thin films such as atomic absorption and neutron activation analysis, spark spectrography and so on. In general these are destructive techniques and will give an average analysis of the film.

In order to obtain an analysis of the outer surface of a film the detected

species must be such that it can only derive from the outer layers of interest. Low energy electrons are ideally suited for this purpose and are used in a number of techniques. Auger electron spectroscopy (AES) uses a moderately energetic electron (1-5 KeV) to stimulate the emission of low energy electrons by Auger capture. This technique is now available in a scanning mode (SAM) thus allowing point to point mapping of elemental concentration. A particular advantage of AES is the sensitivity to light elements.

Electron emission can also be stimulated by appropriate X-ray bombardment in a technique generally known as electron spectroscopy for chemical analysis (ESCA). The primary X-ray is usually the characteristic from a light element such as Mg or Al and the detected electrons are produced by ionization from the valence shells. This is generally not a spatially resolving technique but by generating the X-rays from a thin foil by electron bombardment a form of scanning ESCA is now possible. The major advantage of ESCA is that the electron energies give information on the chemical state of the elements detected.

To provide in depth or composition gradient information it is necessary to progressively remove material and then repeat the surface analysis. This is now a well developed procedure using stationary or scanning ion beams. AES and ESCA can thus be extended into a three dimensional analysis. There is however a considerable potential for producing errors and artifacts arising from selective sputtering, channeling effects and so on and as in all analytical studies each result must be subject to test and scrutiny to confirm reliability.

Rather than detecting electrons emitted from the surface it is possible to analyze the ions emitted during the ion bombardment giving so called secondary Ion Mass Spectroscopy or SIMS. This technique can under favorable circumstances be sensitive to parts per million and differentiate between isotopes. SIMS is inherently a depth profiling technique.

Finally a non-destructive technique which given information on the in-depth composition of a film is Rutherford Back Scattering. This must however be viewed as a rather special tool as it requires a particle accelerator to provide the probing beam.

NOTES

THIS PAGE

WAS INTENTIONALLY

LEFT BLANK

MEASURING TRACE ELEMENTS IN SEMICONDUCTORS:
METHODS AND PITFALLS

Richard M. Lindstrom
Center for Analytical Chemistry
National Bureau of Standards
Washington, DC 20234

A full quantitative understanding of the electrical behavior of semiconductors requires, among other parameters, quantitative knowledge of the deliberately and accidently present impurities. The concentrations of interest may be as small as one part per billion, which is the fraction of the volume of a bedroom occupied by a mosquito. Methods available for trace measurements at this level are few in number; for many constituents the number of routine, inexpensive, and reliably accurate methods is zero. If the sample of interest is a thin film on a substrate, the mass of sample available for analysis is small and the difficulties of microanalysis are added to those of trace analysis (1).

Nearly all methods available for approaching this problem rely on physical rather than chemical reactions. The sample (or a separated portion) is probed with an external stimulus, and the response to this stimulus is then detected. The probe and also the response may be photons (from microwaves to gamma rays), electrons, neutrons or other nuclear particles, or ions. A large number of probe-response pairs are available to the analyst, none is as yet universally applicable. Desirable properties of a method are high sensitivity to the signal from the component sought, insensitivity to the presence of uninteresting factors such as the matrix and accidental dirt, and in addition a response related to the stimulus by a known factor of proportionality.

Some analytical methods are direct: the sample is inserted into the instrument for the measurement without pretreatment. Or an indirect procedure may be used, in which the matrix is removed chemically and the residue analyzed. This approach often dramatically improves the detection sensitivity and accuracy, but at the risk of contamination of the sample (positive blank) or of partial loss of the analyte (negative blank) during the preprocessing (2).

Few of the most sensitive methods available are capable of measuring spatial distributions of trace element concentrations. In particular, the problem of separating the analytical signal of a thin film from that of the substrate offers a rich field for fruitful collaboration

between the physicist and the analyst in the design of an experiment.

Although semiquantitative or relative information (e.g., images or ratios) is sufficient to answer many questions, the analyst's goal is to produce measurements of high and known accuracy. The history of blind interlaboratory comparisons of trace element measurements shows that agreement is seldom as good as expected a priori (3). Resolution of discrepancies among analysts is most efficiently done if one or more common lots of material is available for repeated analyses (4). Standard Reference Materials are produced by NBS to assist this process of quality control (5).

References

(1) G. Tölg, Talanta 21 (1974) 327.

(2) T. J. Murphy, in P. D. LaFleur, ed., "Accuracy in Trace Analysis," (NBS Spec. Pub. 422, 1976) p. 509.

(3) R. K. Skogerboe and S. R. Koirtyohann, in NBS Spec. Pub. 422, p. 199.

(4) W. J. Youden, Anal. Chem. 32 (1960) no. 13, p. 23A.

(5) J. P. Cali and W. P. Reed, in "Accuracy in Trace Analysis," NBS Spec. Pub. 422, p. 41.

NOTES

THIS PAGE

WAS INTENTIONALLY

LEFT BLANK

EBIC CHARACTERIZATION OF POLYCRYSTALLINE SILICON SOLAR CELLS

J.I. Hanoka

Mobil Tyco Solar Energy Corporation
16 Hickory Drive
Waltham, Massachusetts 02154

ABSTRACT

INTRODUCTION

The Electron Beam Induced Current (EBIC) mode of the scanning electron microscope is an extremely useful probe for nondestructive, in-situ studies of recombination in polycrystalline solar cells. Within the limits of resolution of the technique, EBIC studies can provide a recombination "map" of a solar cell and thus should be significant in helping to understand in detail recombination processes occurring at defects such as grain boundaries and dislocations. This paper will discuss both the potentialities and the limitations of EBIC for polycrystalline silicon solar cells. Quantitative studies and representative results on EFG ribbon solar cells and refined metallurgical silicon solar cells will be presented and compared.

THE EBIC MODE

Under bombardment from an electron beam, electron-hole pairs are produced in the sample, diffuse toward the space charge region, and are then separated by the built-in field provided by a Schottky barrier or a p-n junction. The amount of current so produced can be considerable by electron microscopy standards and is on the order of micro-amps, a level which facilitates quantitative work. The EBIC at any particular location of the incident scanned electron beam can then be fed into an amplifier whose output is then fed into the CRT video display of the SEM. The latter is scanned synchronously with the incident electron beam and the result is a CRT display of the current collection at every point of the scanned region. Regions which result in recombination will show dark or light contrast on the video display, depending on the amount of current collected in that region. Figure 1 gives examples of such EBIC photographs on both an EFG ribbon solar cell and a highly polycrystalline solar cell sample of refined metallurgical silicon (RMS). The EFG ribbon sample exhibits an EBIC pattern of mostly linear boundaries more or less parallel to the growth direction. The RMS sample, on the other hand, shows an extensive grain boundary and dislocation structure. (Note: dark contrast in these EBIC photos means recombination, light contrast means efficient current collection.)

RESOLUTION

Resolution is principally limited by the electron beam spreading within the silicon. As it reaches the silicon sample, the beam may only be on the order of 100 Å in width, but once inside the silicon, the effective volume of hole-electron pair generation spreads out due to

large-angle elastic collisions and can be roughly approximated by a sphere of diameter, R. R is also called the penetration range and varies with the beam energy, E_B, according to this relationship (1):

$$R_{(\mu)} = 0.0171\ E_B^{1.75}\ (\text{keV}).$$

Thus, a 10 keV beam produces a sphere of ≈1.5 μ diameter and the highest resolution, which would be on the order of ~0.5 μ according to this, is obtained using the lowest possible beam energy.

REPRESENTATIVE RESULTS

Many features commonly found in EBIC images of polycrystalline silicon solar cells can be seen in Fig. 1(a) and Fig. 1(b). Four features in particular are worthy of note:

1. The appearance of the surface of a polycrystalline solar cell and the EBIC image may bear little relation to each other. In Fig. 1 (b) the EBIC image shows much richer detail than the surface micrograph (not shown here) would indicate. The opposite effect is also quite common in ribbon silicon, where twin boundaries visible on the surface show little or no EBIC image (2,3).

2. The degree of recombination along different grain boundaries can vary considerably.

3. Grain boundary recombination can be quite nonuniform along the boundary, and "gaps" of little or no recombination can be seen along a boundary.

4. Recombination exists within grains which shows as areas of varying gray contrast. Some correlation between this sort of recombination and the presence of dislocations does exist (but see below).

QUANTITATIVE STUDIES

Figure 2 shows a quantitative study of some linear boundaries in an EFG ribbon silicon solar cell. The numbers in Fig. 2(a) and Fig. 2(b) show corresponding boundaries, and the numbers in Fig. 2(c) the current collected in the regions intersected by the line scan shown. As has already been noted, a qualitative correlation exists between the recombination contrast and the existence of dislocations. However, on closer quantitative examination it appears that there are interesting exceptions to such a correlation. In particular, the squared region shows no etch pits, but almost identical current collection as the region on the right of Fig. 2(b), which has a significant etch pit density. Many such examples can be cited. Figure 3 shows a region with about 4 etch pits visible, i.e., a very low dislocation density, and a very intense recombination contrast. Figure 4 shows an opposite case. Here, a linear boundary (marked with an arrow) with etch pits shows no recombination contrast in the EBIC photograph.

A full explanation for some of the above observations is not yet available but may well be related to the question of the presence or absence of impurities and to the interactive effects between impurities

on the one hand and dislocations and grain boundaries on the other. Further refinement of EBIC in conjunction with other techniques such as STEM, DLTS, and EPR should help to answer some of these questions and thereby provide a better understanding of recombination in silicon solar cells.

REFERENCES

1. T.E. Everhart and P.H. Hoff, J. Appl. Phys. 42 (1971) 5837.

2. K.V. Ravi et al., 12th IEEE PVSC, Baton Rouge, p. 182 (1976).

3. G.H. Schwuttke et al., J. Crystal Growth 43 (1978) 329-335.

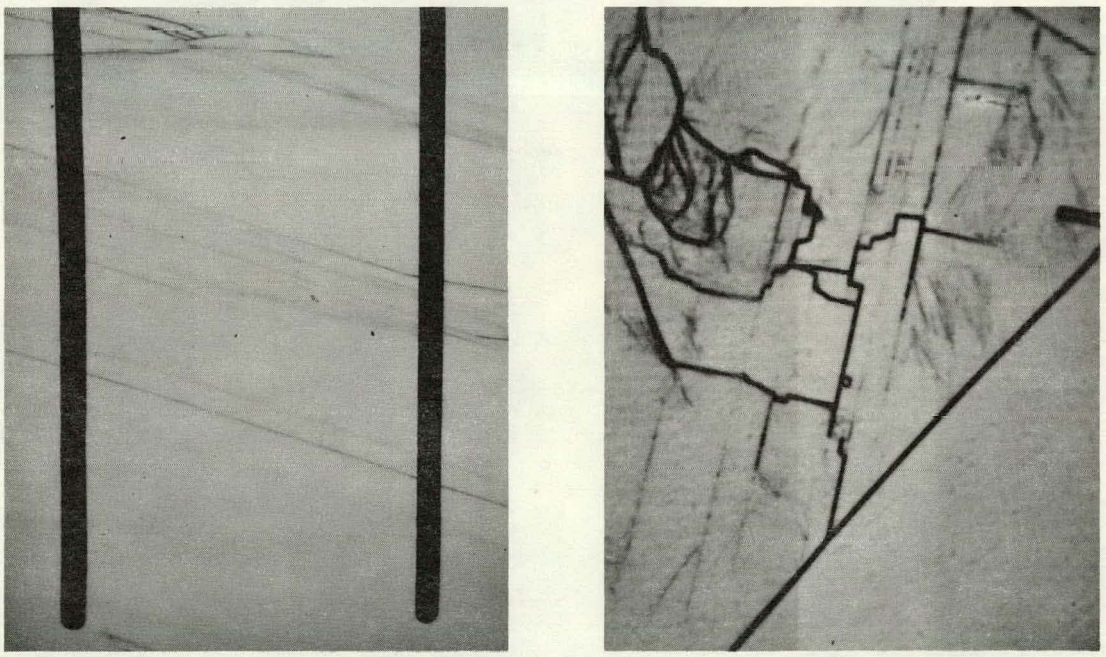

(a) (b)

Fig. 1. Typical EBIC photos of polycrystalline silicon solar cells. (a) is the EFG ribbon cell - the two dark vertical lines are metallization bars. (b) is a cell made of refined metallurgical silicon.

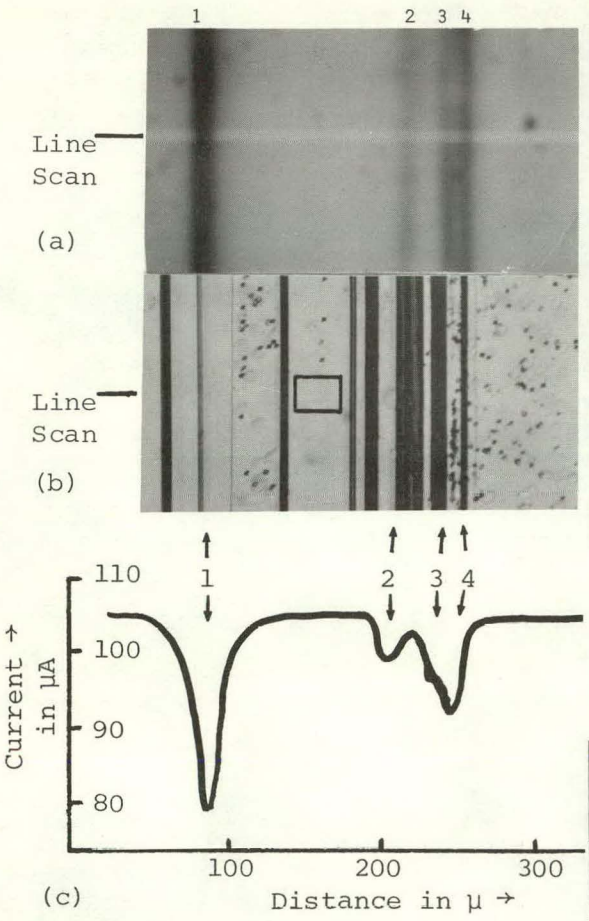

Figure 2

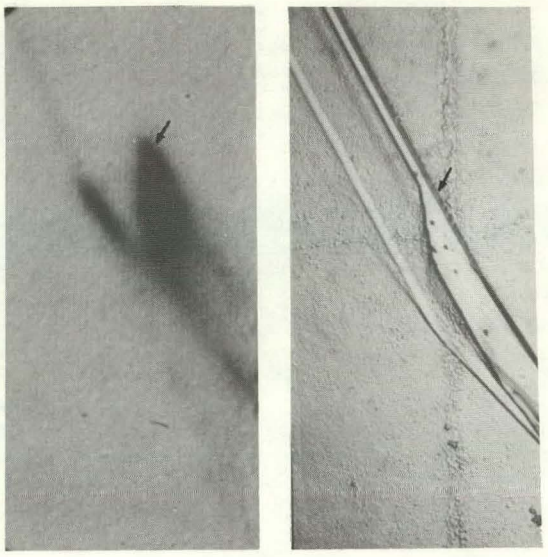

(a) (b)

Figure 3

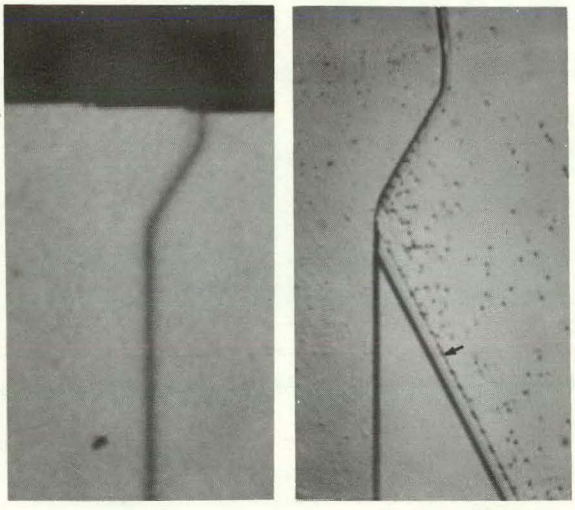

(a) (b)

Figure 4

Captions:

Fig. 2. Example of quantitative EBIC studies. (a) is the EBIC image; (b) is the same region after being Sirtl etched; and (c) is a quantitative line scan of the EBIC image.

Fig. 3. Example of lack of correlation between EBIC contrast and etch pit density. (a) is the EBIC image, and (b) is the same region after Sirtl etching. The arrows refer to similar regions.

Fig. 4. (a) EBIC photo of grain boundary which kinks and which also shows in (b) after Sirtl etching, a grain boundary with dislocation etch pits and no EBIC contrast (arrow). The upper black bar in (a) is the metallization bar.

NOTES

THIS PAGE

WAS INTENTIONALLY

LEFT BLANK

BACKSCATTERING AND TEM STUDIES OF LAYERED STRUCTURES

J. W. Mayer
California Institute of Technology
Pasadena, California 91125

The outer micron of photo-voltaic structures is an important region in solar cells whether it be the junction dopant profile, metallization adhesion, defects in epitaxial layers, or the composition and interdiffusion in thin film structures. In recent years, analytical measurement techniques have been hard pressed to provide sufficient information required for technological applications. For example, an understanding of thin film interdiffusion or interfacial reactions requires the analysis of a layer 10 to 100 atom layers thick that is located some 1000 to 10,000 atom layers below the surface. Extended defects such as twins, stacking faults, and misfit dislocations also play a role in the performance of photo-voltaic devices. This paper reviews two analytical tools that have been utilized in the measurement of thin film and layered structures: Rutherford backscattering spectrometry (RBS) and transmission electron microscopy. Backscattering spectrometry provides depth microscopy the determination of atomic composition as a function of depth[1-3]. When channeling effects are combined with backscattering, one obtains a depth profile of defects. Transmission microscopy then allows identification of the nature of the defects. The techniques are illustrated here by choosing examples of solid-phase epitaxial growth of silicon through Pd silicide as a transport medium.

Rutherford backscattering spectrometry requires a particle accelerator, usually one of the numerous Van de Graaff accelerators, relatively modest target chambers (chamber pressures are usually 10^{-6} to 10^{-7} torr) and nuclear data acquisition electronics. An energetic ion, such as a 2 MeV ^{4}He ion, traversing a solid experiences an energy loss that increases linearly, to a close approximation, with depth. The relatively small fraction of particles that are backscattered, lose energy along their inward and outward tracks. By measuring the energies of particles scattered from the front surface and back surface of a thin film structure, one obtains a measure of the thickness. A rule of thumb for Si or Al is that the energy width is about 100 eV/Å which translates into a depth resolution of about 150 to 200 Å for standard particle detector and amplifer energy resolution of 15 to 20 keV. Near the surface, the depth resolution can be improved to 20 to 40 Å by tilting the target with respect to the beam.

Mass identification is also provided by measurement of the energies of backscattered particles. The energies of 2 MeV ^{4}He ions scattered from Pd and Si atoms at the surface are about 1.5 and 1.1 MeV, respectively. This energy difference allows a clear separation of signals from Pd and silicon atoms in silicide layers a few thousand Angstroms thick. The

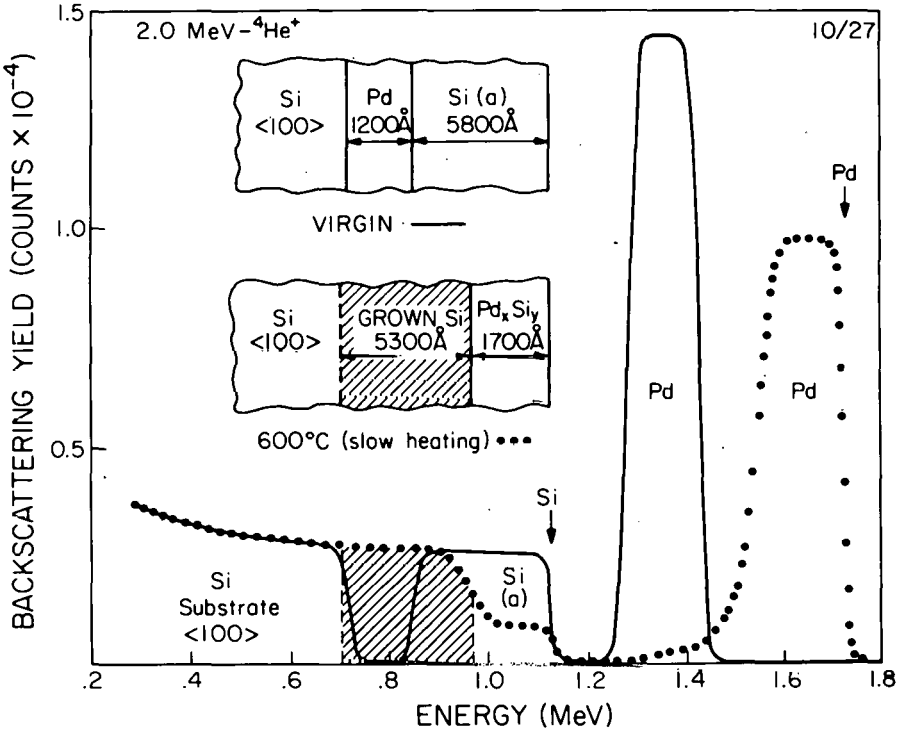

Fig. 1 Backscattering energy spectra for solid-phase epitaxy in the Si<100>/Pd/Si(amorphous) system. (From Lau et al.[6])

composition can be determined by measuring either the total number of particles scattered from Pd and Si atoms (the average composition) or the ratio of the signal heights at equivalent depths (composition as a function of depth).

Channeling measurements depend on alignment of the crystal axis of the sample with the incident particle beam. The yield of backscattered particles drops 30 fold since the majority of the incident ions are steered by the axial or planar channels and do not undergo close-impact collisions with lattice atoms. However, the channeled particles can make direct collisions with atoms displaced away from lattice sites. This provides the basis for extracting disorder profiles from the aligned yield of backscattered particles. Extended defects such as twins[4] or dislocations[5] cause dechanneling of the aligned beam. The dechanneled particles can then make close-impact collisions with lattice atoms which again allows determination of the depth distribution of defects.

The concepts are illustrated in Figs. 1 and 2. For epitaxial growth of Si layers obtained by solid-phase reaction through a silicide layer. The spectrum for the as-deposited sample shows the Pd signal displaced below the surface signal (vertical arrow). The amount of displacement indicates that the thickness of the overlying amorphous Si layer is about 6000 Å.

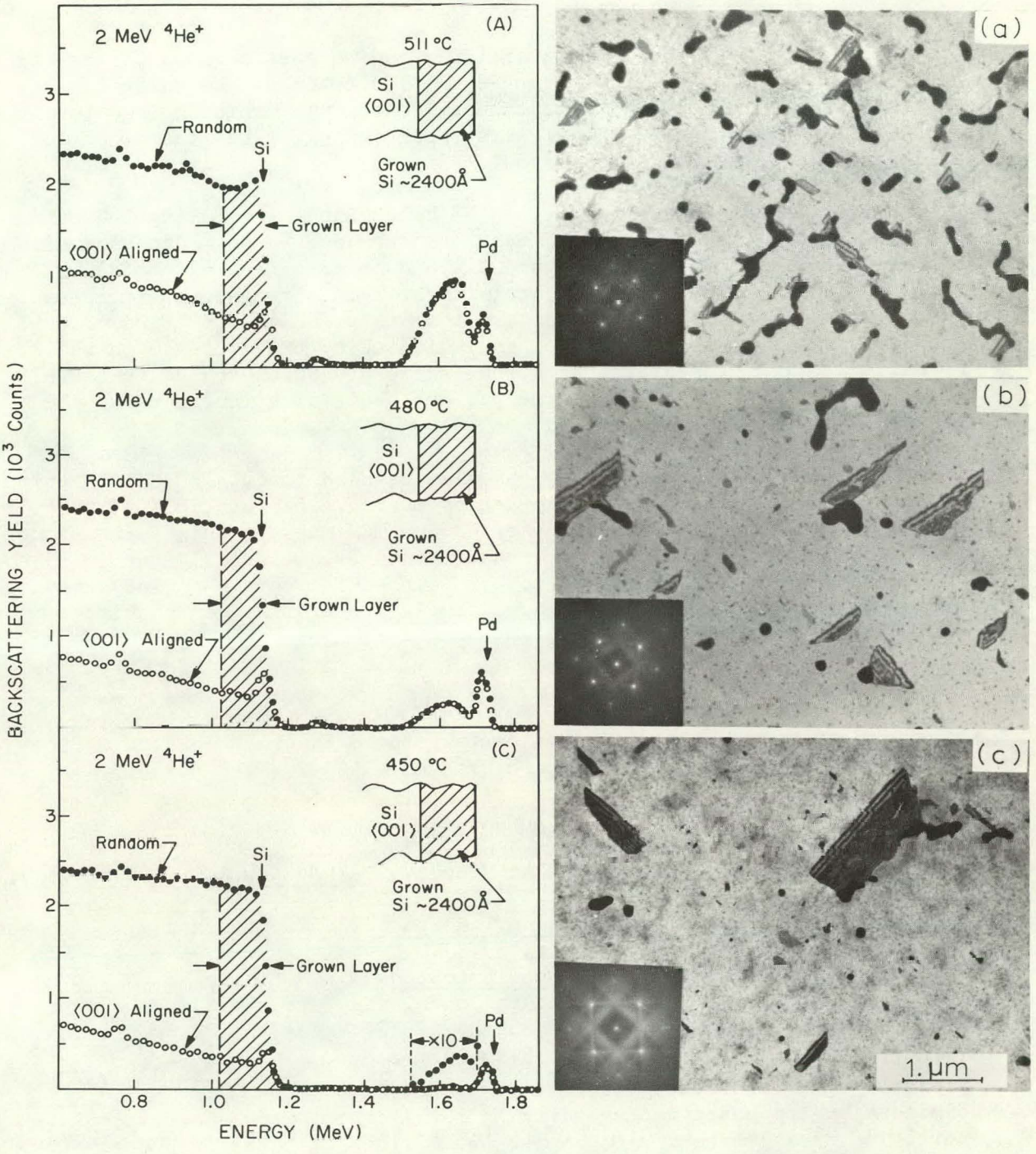

Fig. 2 Channeling spectra (left) and TEM micrographs of epitaxial layers grown in the Si/Pd/Si system. The outer Pd silicide was removed prior to measurement. The Pd signal in the spectra and the dark regions in the micrographs represent Pd inclusions in the grown layer. (From Tseng et al.[7])

After heat treatment, Pd forms a silicide and becomes shifted to the top surface. The shift to the top surface is indicated by the shift in the Pd signal to higher energy. The composition of the silicide is determined by the ratio of the Pd and Si signals (correcting for the factor of 10 difference in scattering cross section) in the surface region.

The quality of the underlying Si can be determined by removing the outer silicide layer. The channeling measurements shown in the left-hand side of Fig. 2 indicate that the aligned yield decreases from 511 to 450°C (Fig. 2A to 2C). This improvement in crystal quality is also indicated in the selected area diffraction pattern inserts. The amount of Pd trapped in the grown layer also decreases as indicated by the decrease in the Pd signal. The TEM micrographs show that there are twins in the epitaxial layer. The number of twins decreases, but their size increases as the process temperature is decreased.

Transmission electron microscopy can also be used to obtain an indication of the depth distribution of disorder by making cross sections of the sample[8,9]. The use of backscattering and TEM measurements form a powerful combination. Backscattering measurements are relatively rapid (15 to 40 min/sample) and allow one to select samples for more detailed measurements with electron microscopy where sample preparation can be time-consuming.

Acknowledgements

Financial support was provided in part by the U.S. Army Research Office under the Joint Services Electronic Program (DAAG-29-77-C-0015).

References

1. W. K. Chu, J. M. Mayer and M-A. Nicolet, Backscattering Spectrometry, (Academic Press, New York, 1978).
2. Material Characterization Using Ion Beams, A. Cachard and J. P. Thomas, Eds., (Plenum Press, New York, 1977).
3. Thin Films - Interdiffusion and Reactions, J. M. Poate, K. N. Tu and J. W. Mayer, Eds., (Wiley Interscience, New York, 1978).
4. G. Foti, L. Csepregi, E. F. Kennedy, J. W. Mayer, P. P. Pronko and M. D. Rechtin, Phil. Mag. A 37, 591 (1978).
5. W. F. Tseng, J. Gyulai, T. Koji, S. S. Lau, J. Roth and J. W. Mayer, Nucl. Instr. Meth. 149, 615 (1978).
6. S. S. Lau, Z. L. Liau, M-A. Nicolet and J. W. Mayer, J. Appl. Phys. 48, 917 (1977).
7. W. F. Tseng, Z. L. Liau, S. S. Lau, M-A. Nicolet and J. W. Mayer, Thin Solid Films 46, 99 (1977).
8. T. T. Sheng and C. C. Chang, IEEE Trans Electron Devices, Ed-23, 531 (1976).
9. B. Y. Tsaur, Z. L. Liau, J. W. Mayer and T. T. Sheng, J. Appl. Phys. (in press, May 1979).

NOTES

THIS PAGE

WAS INTENTIONALLY

LEFT BLANK

79-78

Note: This is a draft of a paper being submitted for publication. Contents of this paper should not be quoted nor referred to without permission of the authors.

NEW TECHNIQUES FOR THE STUDY AND CONTROL OF GRAIN BOUNDARY EFFECTS

R. F. Wood, R. T. Young, R. D. Westbrook, J. Narayan,
W. H. Christie, and J. W. Cleland

THIS PAGE

WAS INTENTIONALLY

LEFT BLANK

NEW TECHNIQUES FOR THE STUDY AND CONTROL OF GRAIN BOUNDARY EFFECTS*

R. F. Wood, R. T. Young, R. D. Westbrook, J. Narayan,
W. H. Christie, and J. W. Cleland
Solid State Division, Oak Ridge National Laboratory
Oak Ridge, Tennessee 37830

A major difficulty in studying grain boundary effects in semiconductors arises because conventional growth and thermal diffusion techniques are thought to cause segregation of the dopant at grain boundaries and are unable to provide control of the fast diffusion which is known to occur along the grain boundaries. In this paper, we discuss several recently-developed doping techniques which should allow these problems of grain boundary segregation and diffusion to be studied and circumvented if desired. These techniques involve transmutation doping and laser-induced melting of the near-surface region of the polycrystalline samples.

According to the model of carrier trapping at grain boundaries developed by Kamins,[1] Seto,[2] and others, a pronounced minimum in the carrier mobility as a function of doping concentration is evidence for free carrier trapping by interface states at the grain boundaries. In fact, given the grain size, the position of the minimum may be taken as a measure of the carrier concentration that is required to saturate the grain boundary traps in polycrystalline material. Seto observed such a mobility minimum in his measurements on fine-grained polycrystalline silicon (polysil) formed by chemical vapor deposition (CVD). He concluded that carrier trapping by grain boundary states is the dominant factor in determining the electrical properties of polysil and that grain boundary segregation of dopants is of little importance. Others,[3] however, have interpreted resistivity data on polysil in terms of grain boundary segregation, which has been demonstrated to occur in metals using, e.g., ion microprobe techniques.[4] Immediately after ion implantation the concentration of dopants at grain boundaries will be the same as that in the bulk of the grains. However, high-temperature, long-term annealing to remove the lattice damage and electrically activate the dopant ions also results in substantial dopant migration and this makes an unambiguous interpretation of Seto's results difficult.

Neutron transmutation doped (NTD) silicon contains an extremely uniform concentration of phosphorus throughout the material, whether it be in single crystal or polycrystalline form. Transmutation doping of silicon is based on the fact that normal silicon contains approximately 3% ^{30}Si which transmutes to ^{31}P after thermal neutron absorption with a half-life of 2.6 hrs. Since ^{30}Si atoms are chemically equivalent to the atoms of all other isotopes of silicon their distribution in normal silicon is completely uniform. The lattice damage introduced by transmutation doping of silicon is annealed[5] by heating at 750°C for 1/2 hr. Because of the extreme uniformity of the doping,

there are no gradients to drive the dopant diffusion and migration of the phosphorus should be negligible during annealing, thus eliminating grain boundary segregation. Figure 1 shows results of mobility measurements on NTD silicon as a function of carrier concentration. The large dips around $10^{15}/cm^3$ in the curves marked with open triangles and circles are what one expects from Seto's development of the carrier trapping model. From this model, one can extract an approximate grain size for this material, and we found it to be $\sim$ 33 μm, which is in very satisfactory agreement with the average grain size of $\sim$ 25 μm obtained from electron microscopy. However, we note that the mobility of the sample thermally diffused with lithium was substantially altered by that treatment which almost certainly resulted in grain boundary segregation of the lithium.

The newly developed techniques of laser annealing[6,7] of ion-implanted samples and laser-induced diffusion[8] offer two other closely related methods for control of dopants at grain boundaries. These two methods rely on the intense radiation from a Q-switched ruby or Nd:YAG laser to melt the near surface region of the sample during times of the order of 50-100 nsecs. In the case of laser annealing, this is enough time to repair the lattice damage and electrically activate the dopant and in the case of laser-induced diffusion it is enough time for dopant atoms deposited in a thin layer on the surface to diffuse into the crystal. Since in both of these techniques the energy of the laser pulse can be chosen such that the near-surface region is melted, grain boundaries can in effect be eliminated during the annealing and diffusion processes. Hence, no grain boundary diffusion or segregation can occur. Of course, the grain boundaries regrow as the material resolidifies but this occurs so rapidly that little or no dopant diffusion can occur after the grains are reformed. Table 1 gives some results of recent experiments on the laser annealing of boron-implanted polysil. The measured surface carrier concentration of these samples is $\sim 5 \times 10^{20}$ cm^{-3}, which is several orders of magnitude greater than the concentration of grain boundary traps estimated by Seto for this type of material. Therefore, no evidence for free carrier trapping is apparent and the mobility is close to that expected for single crystal material. Another series of exeriments at lower implanted doses is now underway. The data in Table 1 indicate that extensive grain growth

Table 1. Electrical Parameters of ^{11}B (35 KeV, 1.1×10^{16} cm^{-2}) Implanted Laser-Annealed Polycrystalline Silicon. n is the carrier concentration, μ the mobility, and ρ the resistivity.

Sample	Grain Size (before) μm	Energy (J/cm^2)	Grain Size (after) μm	n (10^{16} cm^{-2})	μ (cm^2/V sec)	ρ (Ω/□)
1	0.02	0.45	0.5	1.0	16	38
2	0.02	0.88	1.5	1.1	20	28
3	0.02	1.17	-	1.1	17	32
4	25	0.66	-	0.45	21	64
5	25	0.88	-	1.1	25	22

occurs during laser annealing. Figure 2 shows transmission electron microscopy results for samples 1 and 2 of Table 1. Grain growth induced by laser irradiation has already been observed and reported by others. Although of considerable interest in itself, grain growth represents an additional complication in studies of grain boundary trapping and segregation. There is an aspect of laser annealing which is somewhat complementary to those we have just been discussing. If by proper choice of diffusion times and temperatures the grain boundaries can be preferentially doped, then laser-induced melting should be useful in studying both diffusion away from the grain boundaries and grain growth mechanisms.

In our talk, brief reviews of the carrier trapping model of grain boundary effects, transmutation doping of silicon, and laser annealing will first be given. Then the results we have obtained using a variety of experimental techniques, including electrical properties measurements, transmission electron microscopy, secondary ion mass spectroscopy, etc., will be presented. The extent to which these results support the carrier trapping model or point to the need for development of more complex models will be discussed. Finally, our progress in attaining control of ground boundary segregation and diffusion by transmutation doping, ion implantation and laser annealing, and laser-induced diffusion will be assessed.

ACKNOWLEDGMENT

We wish to thank C. W. White for the ion implantation of our samples and J. Y. W. Seto for providing the fine-grained CVD polysil samples.

REFERENCES

*Research sponsored by the Division of Materials Sciences, U. S. Department of Energy under contract W-7405-eng-26 with the Union Carbide Corporation.

1. T. E. Kamins, J. Appl. Phys. 42, 4327 (1971).
2. J. Y. W. Seto, J. Appl. Phys. 46, 5247 (1975).
3. See for example M. E. Cowher and T. O. Sedgewick, J. Electrochem. Soc. 119, 1565 (1972).
4. W. H. Christie, D. H. Smith, and H. Inouye, J. Radioanal. Chem. 32, 85 (1976).
5. R. T. Young, J. W. Cleland, R. F. Wood, and M. M. Abraham, J. Appl. Phys. 49, 4752 (1978).
6. R. T. Young, C. W. White, G. J. Clark, J. Narayan, W. H. Christie, M. Murakami, P. W. King, and S. D. Kramer, Appl. Phys. Lett. 32, 139 (1978).
7. J. C. Wang, R. F. Wood, and P. P. Pronko, Appl. Phys. Lett. 33, 455 (1978).
8. J. Narayan, R. T. Young, R. F. Wood, and W. H. Christie, Appl. Phys. Lett. 33, 338 (1978).

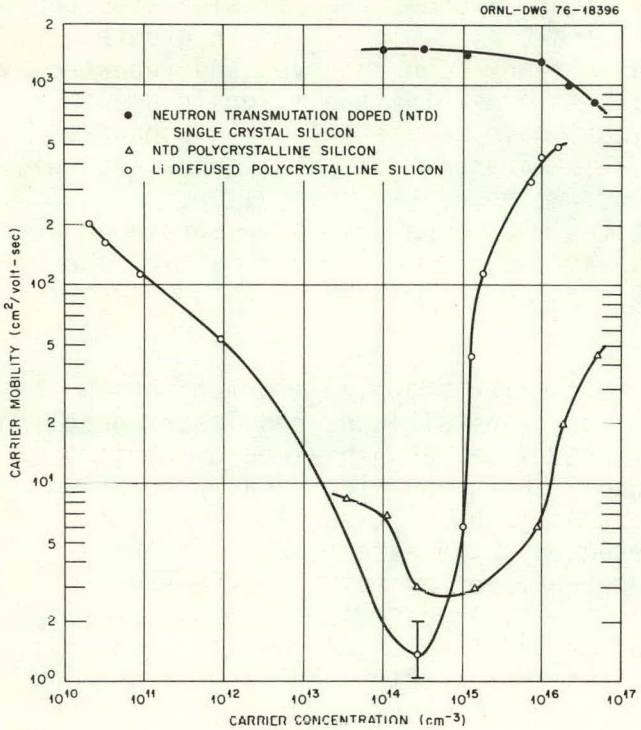

Fig. 1.

Carrier mobility in NTD single crystal and polycrystalline silicon.

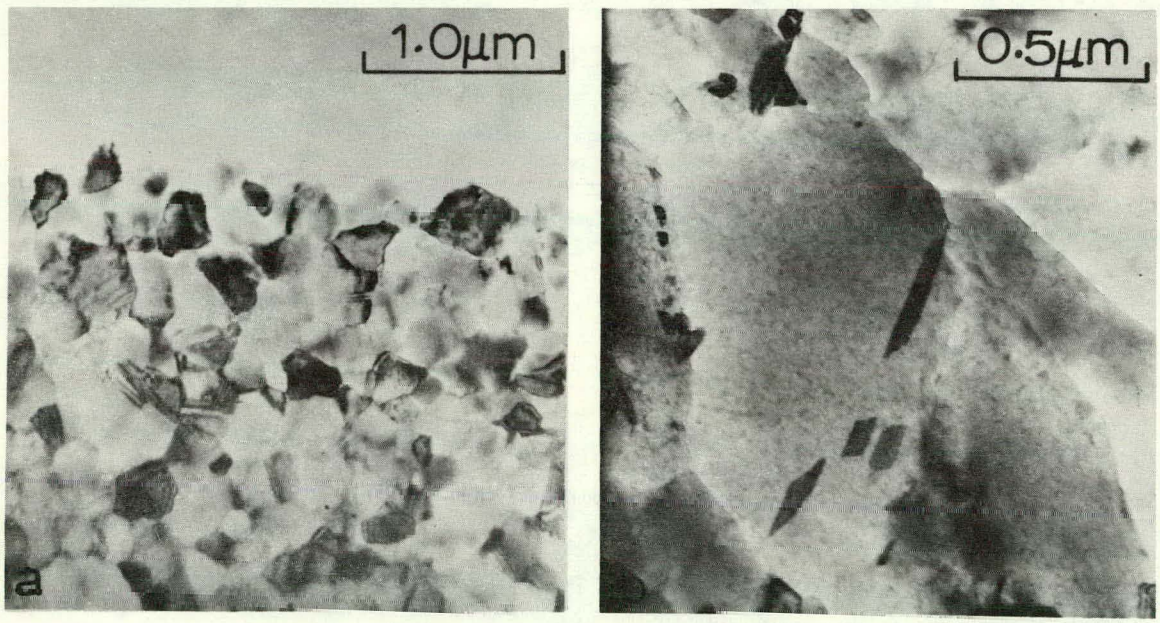

Fig. 2. Transmission electron micrographs of samples 1 (left) and 2 (right) of Table 1. After laser annealing the grain size in sample 1 is ∿ 0.5 μm and in sample 2 it is ∿ 1.5 μm.

NOTES

THIS PAGE

WAS INTENTIONALLY

LEFT BLANK

GRAIN SIZE AND ITS INFLUENCE ON EFFICIENCY IN POLYCRYSTALLINE GaAs SOLAR CELLS

A. E. Blakeslee* and S. M. Vernon
IBM Research Center
Yorktown Heights, NY

*Present Address: Solar Energy Research Institute, Golden, CO

Several studies of GaAs solar cell fabrication have been published recently in which the active material was a layer of polycrystalline GaAs on an inexpensive substrate such as graphite or a metal (1-4). The purpose of these studies was always to reduce the thickness of the GaAs in the layer to a small value and thus reduce the cost of the cell, meanwhile hoping that the efficiency would not fall too seriously below the ∿20% value obtainable with LPE-grown GaAs cells (5).

Johnston and Callahan (1) and Chu, et al. (2) used the well-established chloride transport process for growth of their polycrystalline GaAs, while Blakeslee and Vernon (3) and Dapkus, et al. (4) chose the newer metal-organic system (6) for their work. The rationale for choosing the metal-organic method was that, even though less was known about it, it was thought to possess greater potential for eventually becoming an economically affordable large scale production process. The chloride process work has tended to yield large grain films more readily and has led generally to higher efficiencies. This is understood in terms of the report of GaAs epitaxy on single crystal tungsten by Amick (7), using a chloride transport method, and the fact that the chloride process naturally operates in a state much closer to equilibrium, i.e. with a much lower vapor supersaturation (2,3), than does the metal-organic process. Nevertheless, since the metal-organic process is still generally felt to have greater economic potential, it is necessary to overcome the difficulties involved and optimize the process.

The early thinking regarding thin film GaAs solar cells was essentially that the major problem would be control of grain size; i.e. that if continuous films a few microns thick with grain size several times the minority carrier diffusion length could be produced, then solar cells with efficiencies reasonably comparable to those of single crystal GaAs cells should follow in short order. Several authors have computer-modeled the grain structure and predicted device efficiencies in excess of 10% (8,9).

We have developed several variations of the metal-organic process for growth of polycrystalline GaAs films. The grain size of these films ranges from less than one to several hundred microns, yet the AMO efficiencies of the best Schottky barrier cells made from films grown by each procedure are all about 2%. Clearly enhancement of grain size is not enough, and the roles of contamination and/or process-induced defects must be thoroughly investigated in order to understand and improve the low efficiencies. This paper briefly describes the different film growth modes and examines correlations between the various modes and the resulting grain sizes and cell parameters.

The first process used was simply a direct application of the conditions found to be optimum for growth of reasonably clean and defect-free homoepitaxial GaAs. One ccm of $Ga(CH_3)_3$ and 5 ccm AsH_3 were transported in approximately 2000 ccm H_2. The GaAs films were deposited at 700 C, using RF heating, on polycrystalline, amorphous or in a few cases monocrystalline substrates--including Mo, Ta, W, Si, SiO_2, vitreous carbon and graphite. The nature of the films was very much the same on all substrates except for monocrystalline GaAs, Ge or Al_2O_3, which yielded epitaxial growth. All the other substrates produced films characterized by small (<1 μm) non-columnar grains showing no evidence of preferred orientation. The most severe problem is the continuous renucleation of small GaAs grains one upon the other, which is rather puzzling in view of the readily occurring homoepitaxy for the case of monocrystalline GaAs substrates. It has been suggested (10) that the renucleation may be caused by a "poisoning" effect of reaction products, the accumulation of which is more severe for polycrystalline growth than for single crystal.

In the second process, the two variables temperature and $Ga(CH_3)_3$ flux were adjusted in order to reduce the supersaturation and hence the degree of renucleation. In order to do this within the constraint of obtaining complete coverage of the substrate, a two-step procedure was developed. This consisted of nucleating the film at 600 C for 30 seconds and then continuing the growth for, say, 15 minutes at 850 C under a reduced $Ga(CH_3)_3$ flux. Grains with a 2-5 μm average dimension and a more nearly columnar morphology were obtained in this way, but again there was no evidence of preferred orientation.

The third procedure, termed the gallium pre-coat method, was conceived as an adaptation of the VLS process (11) wherein crystals grow out of a liquid medium fed by a vapor nutrient. Gallium is an obvious choice for the liquid and is easily deposited from $Ga(CH_3)_3$ to a thickness of a micron or so by simply not adding AsH_3. Next the $Ga(CH_3)_3$ is turned off and the AsH_3 turned on, resulting in conversion of the Ga film to GaAs. Finally GaAs is vapor deposited in the normal way upon this base layer. Regions were found having average grain sizes of several microns, but nonuniform morphology exhibited as clumps and spikes was prevalent. Shorting of Schottky barrier solar cells often occurred, although some were obtained with fairly good characteristics. The ability of the Ga film to wet the substrate uniformly is apparently the chief criterion for success with this method. Mo was found to be the most effective substrate for this purpose.

The fourth, and most promising, procedure involved the rapid melting and recrystallization of fine-grained films which had been grown by the unmodified CVD technique. Care had to be taken to prevent excessive loss of As during the melting and cooling. When this was successful, a 5 μm thick layer having ∿0.2 mm grains was formed on a Mo substrate. This layer was highly conductive, and the GaAs-Mo junction was ohmic. The lightly doped layer needed for Schottky barrier solar cells was then formed by the normal CVD process. The final CVD layer epitaxially replicates the large-grained recrystallized layer. Films made in this way have yielded solar cells with efficiencies >4% in terrestrial sunlight.

By using these four processes, we have been able to obtain a series of GaAs thin films covering a factor of several hundred in grain size. Devices made from such a series should be useful to test the theories relating grain size to cell parameters. Schottky barrier solar cells were accordingly fabricated from films grown by each procedure, and the cell parameters of the best film of each type are listed in Table I. The small number of devices processed from each type of film dictates that the data can be considered only as a qualitative guide. Furthermore, results with cells made on single crystals showed low efficiencies compared with published values (12), which indicates that our cell fabrication techniques were not optimized and that perhaps all of our results ought to be somewhat higher. Nevertheless, several conclusions can be drawn from Table I.

The most obvious conclusion is that the efficiencies do not increase as expected when large increases are effected in the grain size. For all but the smallest-grained film, J_{sc} is quite large, in good agreement with prediction (8) and in fact being largest for the next-to-smallest (albeit least well controlled) grain size. This is the most encouraging result. On the other hand, V_{oc} and fill factor are lower in every case but one for the larger grain samples, and it is this tendency toward low V_{oc} and fill factors, already noted in the literature (13), which keeps the efficiency low. We do not mean to imply that this effect is a consequence of larger grains; rather it is likely that the special processing used to increase the grain size above the value for unmodified growth acts detrimentally to the voltage and fill factor by introducing contamination and/or defects to the grain boundaries or to the grains themselves. The high J_{sc} for all cases except unmodified growth suggests that grain boundary recombination is not as serious a problem as previously assumed and that future efforts should be directed more toward uncovering other more subtle recombination mechanisms and understanding the cause of the low V_{oc}.

TABLE I

SOLAR CELL PARAMETERS

Gold Schottky Barriers
AM0 Uncoated

Preparation Method	Grain Size	J_{sc}	V_{oc}	FF	Efficiency
No treatment	.5 μm	6.6 mA/cm^2	.44 V	.505	1.09%
Gallium pre-coat	∿1.5	20.5	.35	.47	2.50
Two temperature	3	15.7	.37	.28	1.20
Recrystallization	200	15.8	.35	.56	2.28

REFERENCES

1. W. D. Johnston, Jr. and W. M. Callahan, Gallium Arsenide and Related Compounds (St. Louis) 1976, (Inst. Phys. Conf. Series 33b, London, 1977) p. 311.
2. S. S. Chu, T. L. Chu, H. T. Yang and K. H. Hong, J. Electrochem. Soc. 125 1668 (1978).
3. A. E. Blakeslee and S. M. Vernon, IBM J. Res. Develop. 22 346 (1978).
4. P. D. Dapkus et al., Conf. Rec. 13th Photo. Spec. Conf. (IEEE, New York, 1978).
5. J. M. Woodall and H. J. Hovel, Appl. Phys. Lett. 30 492 (1977).
6. H. M. Manasevit and W. I. Simpson, J. Electrochem. Soc. 116 1725 (1969).
7. J. A. Amick, RCA Rev. 24 555 (1963).
8. C. Lanza and H. J. Hovel, IEEE Trans. Electron Devices ED-24 392 (1977).
9. H. C. Card and E. Yang, IEEE Trans. Electron Devices ED-24 397 (1977).
10. A. A. Chernov, Inst. of Crystallography, Moscow, private communication.
11. R. S. Wagner and W. C. Ellis, Appl. Phys. Lett. 4 89 (1964).
12. R. J. Stirn and Y. C. M. Yeh, IEEE Trans. Electron Devices ED-24 476 (1977).
13. L. L. Kazmerski, Solid-State Electronics 21 1545 (1978).

NOTES

THIS PAGE

WAS INTENTIONALLY

LEFT BLANK

CHARACTERIZATION OF EFG SILICON RIBBONS BY ION BEAM TECHNIQUES

M. Hage-Ali, R. Stuck, M. Toulemonde, P. Siffert

Centre de Recherches Nucléaires
Groupe de Physique et Applications des Semiconducteurs
(PHASE)
67037 STRASBOURG-CEDEX (FRANCE)

ABSTRACT

Secondary Ion Mass Spectrometry (SIMS) combined to Rutherford Backscattering (RBS) and specific nuclear reactions have been used to investigate the nature, concentration and distribution of the impurities existing in EFG silicon ribbons grown from the melt with a graphite die. The relative features of these methods are discussed.

INTRODUCTION

To reach the cost reduction needed for large scale use of terrestrial solar cells, new approaches are necessary. Edge defined silicon ribbon growth (EFG) constitutes one of the promising methods to prepare directly the low cost silicon sheets. Characterization of this material, especially of the impurities, plays an important role. The goal of this paper is to show the possibilities given by a combination of three different ion beam techniques to determine the nature of these impurities, their concentration, location and also to give information of the crystal quality.

I. EXPERIMENTAL TECHNIQUES

1) Rutherford Backscattering in and without channelling conditions was used to analyze both the surface damage and the impurities within the ribbon. The principle of this method is well known [1] : a beam of ions from an accelerator in the MeV range hits the sample mounted on a three axes goniometer, which allows an eventual aligment of the beam with respect to one of the major axes of the crystal. By measuring the energy of the backscattering it is possible to identify the mass and depth location of the atom which collided with the projectile and to give their absolute concentration.

Here 2 MeV α-particles have been employed, the backscattered particles being detected either with a solid state detector or with a high depth resolution electrostatic analyzer [2]. A typical spectrum is shown on Fig. 1 both for random and channelling conditions. Besides C and O several other impurities are present, they are reported together with their concentration on Table I.

2) Secondary ion mass spectrometry (SIMS).

By performing mass analysis of both positive and negative ions sputtered off the substrate under low energy argon bombardment, it is possible to further determine the composition of the target. Our [3] system can work in two modes either under a low current ion beam to remove only a thin layer (≈20 Å) of the target during the full mass scale analysis, or in the dynamic mode, with a 100 times stronger current in order to profile in depth selected elements. Figs. 2 and 3 show a surface and a 1000 Å deep spectrum of the positive ions, whereas Fig. 4 gives the profile of the most important impurities. The depth of their penetration is also reported on Table I.

3) Nuclear reactions

Rutherford backscattering is not useful for impurities having masses lighter than that of the substrate, the background, even under chanelling conditions being too important. To overcome this difficulty we used specific nuclear reactions [4]. As an example, we investigated the presence of carbon, which can be introduced during the growing process, the die giving the shape being made on graphite.
We have chosen the resonance at 2.47 MeV [5] of the $^{12}C(^{3}He, ^{1}H)^{14}N$ reaction and detected the produced protons for different excitation levels of the residual nucleus (fig. 5). The width of the resonance (80keV) allows the measurement of the location of the carbon nuclei with a depth resolution of 4000 Å by progressively increasing the projectile energy. In this case calibration is obtained with known layers of graphite.

II. DISCUSSION

The three techniques used here allowed the determination of several impurities present in the material. The origin of most of them can be established from growth conditions and starting material. Rather than discussing this point, it seemed to us more interesting to focus our attention to the possibilities of these ion beam techniques in thin film characterization. Even if they are not the most sensitive (for example, activation analysis can detect down to 10 E12 cmE-3 of specific elements) they give the nature of the chemical element as well as the depth from the surface and from this point of view, these methods are unique.
Furthermore, backscattering gives information on the crystal quality when channelling is used, as well as on surface damage over a depth which is much greater than normal X-ray analysis.
The relative merits of the 3 methods have been summarized on Table II.
It seems to us that each method, when used alone, is not sufficient for silicon analysis, but their combination gives a powerful investigation method. For example, Sims alone has a good sensitivity but no absolute depth and concentration calibration, if associated with RBS this calibration is obtained in absolute scale.

REFERENCES.

1. W. K. CHU et al in "Backscattering Spectrometry (1978) Academic Pres
2. M. HAGE-ALI et al submitted to 4th Conf. on Ion Beam Analysis.
3. H. W. WERNER Vacuum 24 (1974) 493.
4. see for ex. J. MAYER et al. Ion Beam Surface Layer Analysis edited by Elsevier (1974)
5. Hsin - Min KUAN et al Nucl. Phys. 51 (1964) 481.

TABLE I ANALYSIS EFG SILICON RIBBONS

IMPURITY	CONCENTRATION (either volume or layer)	DEPTH DISTRIBUTION	POSITION IN MATRIX
C	1.10^{22} cm^{-3} from RBS $8.5.10^{21}$ from N.R.	400 – 800 Å	not substitutional
Na	$\simeq 1.10^{21}$ cm^{-3}	$\gg$ 1000 Å	?
P	close to sensitivity limit $\simeq$ some 10^{16} cm^{-3}	$\gg$ 1000 Å	substitutional
S	1×10^{13} cm^{-2}	300 Å	Interstitial ?
Cl	6×10^{14} cm^{-2}	100 Å	Interstitial
Ar	7×10^{19} cm^{-3}	$\gg$ 1000 Å	substitutional
K	3×10^{19} cm^{-3}	$\gg$ 1000 Å	substitutional
Tl	1×10^{13} cm^{-2}	300 Å	Interstitial
Cr	1×10^{18} cm^{-3}	$\gg$ 1000 Å	substitutional
Fe	4×10^{18} cm^{-3}	400 Å	substitutional
Ni	1.5×10^{13} cm^{-2}	300 Å	Interstitial ?
Cu	1×10^{19} cm^{-3}	800 Å	substitutional
Zn	3×10^{12} cm^{-2}	150 Å	Interstitial
Sr	5×10^{17} cm^{-3}	1000 Å	substitutional
Mo	6×10^{11} cm^{-2}	300 Å	Interstitial ?
Al, Ca	has not been analyzed.		

TABLE II

SILICON ANALYSIS BY ION BEAM TECHNIQUES

	SIMS	RBS	Nuclear Reactions
Range of elements which can be investigated.	> H	In general, heavier than target matrix	Z from 1-30 approx. with classical Van de Graaffs.
Quantitative analysis	not directly	Yes	Yes, with calibrations
Average detection lim	10^{16} cm^{-3}	5×10^{17} for the heavier elements	10^{17}–10^{19} cm^{-3}, depends strongly on reaction
Depth resolution	5 – 20 Å	20 Å if electrostatic analyser, glancing angle is used	depends strongly from resonance width.
Calibration in depth	No	Yes	Yes, if standards
Lattice location in the crystal	No	Yes	Yes
Lateral resolution	depends on system from cm^2 to μ2	0.5 mm, but with micro beams down to a few μ	Idem as for RBS
Size of samples	from cm^2 to mm^2 depends on system	mm^2	mm^2
Compound information	not directly	No	No
Destructiveness	Yes	No	No
Main advantages	1. Sensitivity 2. Full mass scale 3. Imaging possible 4. Depth profiling	1. Absolute calibration in both depth and concentration 2. Sensitivity for heavier elements 3. Profiles 4. Atom location in latice	1. Specific to selected element 2. Sensitive to light elem 3. Atom location
Limitations	1. Complex spectra, many interferences 2. Strong enhancement effects by impurities is possible 3. Sputtering yiel varies by several orders of magnitude from elem. to element and for different matrix. 4. Edge effects.	1. Small sensitivity for light elements	1. Detect only one isotop at a time 2. Standards required 3. Generally time consuming.

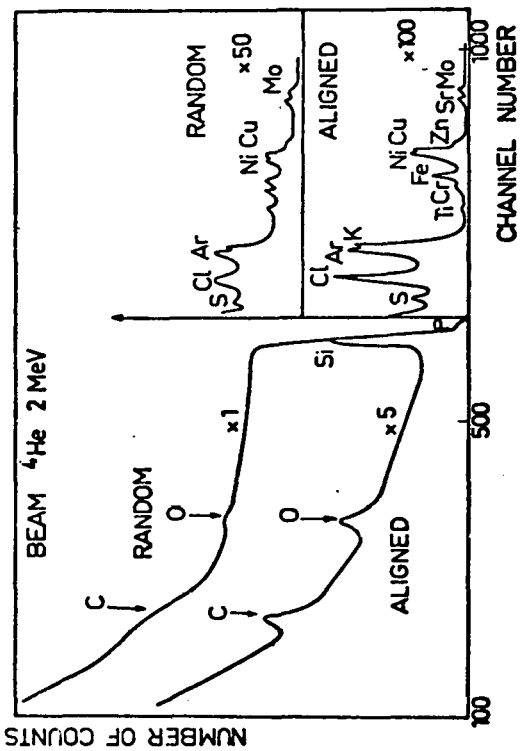

FIG. 1

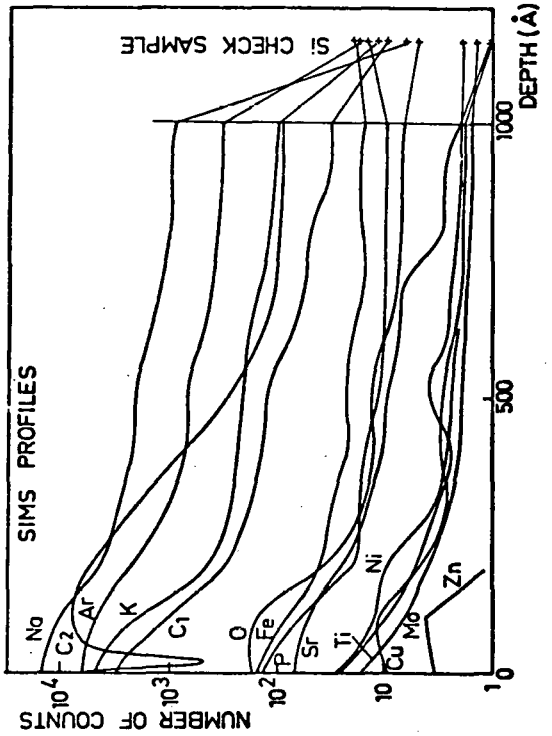

FIG. 4

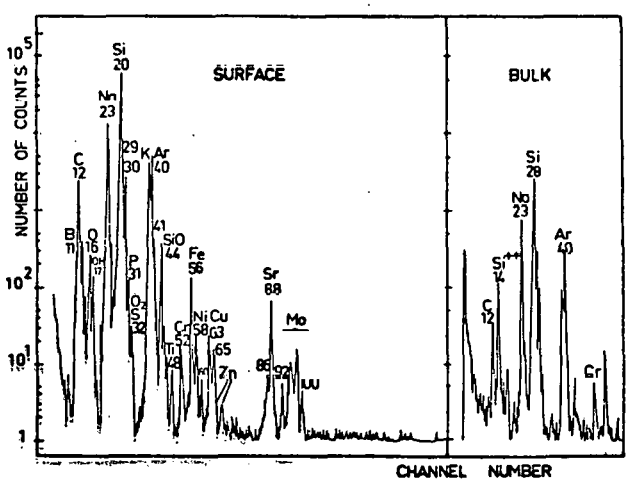

FIGS 2 and 3

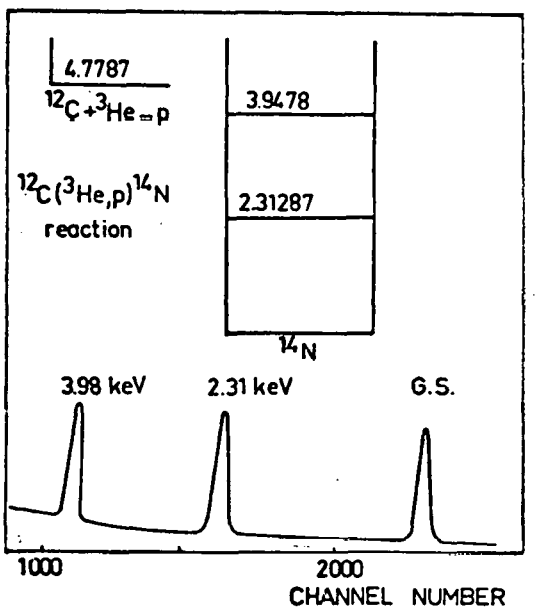

FIG. 5

NOTES

THIS PAGE

WAS INTENTIONALLY

LEFT BLANK

COMPOSITION ANALYSIS OF Cu_2S/(Zn,Cd)S THIN FILM SOLAR CELLS BY MEANS OF ELECTRON SPECTROSCOPY

L. C. Burton and D. W. Dwight
Departments of Electrical & Materials Engineering
Virginia Polytechnic Institute and State University
Blacksburg, VA 24061

M. V. Zeller
Physical Electronics Division
Perkin-Elmer Corporation
Eden Prairie, MN 55344

INTRODUCTION

The photocurrent for Cu_2S/CdS and Cu_2S/(Zn,Cd)S solar cells is generated in the Cu_2S layer. A large number of investigations of properties of Cu_2S as formed on CdS by means of ion-exchange have been reported.[1] Even though some "tails" of Cd have been reported to extend from the interface into the Cu_2S[2], Cd concentrations in the Cu_2S bulk are apparently low[3] (if not zero), and are not thought to bear adversely on cell response.

It has been verified that replacing the CdS with a CdS-ZnS alloy results in increased V_{oc} values.[4] However, a problem with the Cu_2S/(Zn,Cd)S cell has been reduced short circuit current density. Possible mechanisms for this can be related to the Cu_2S, (Zn,Cd)S and the interface. The retention in or near the Cu_2S layer of Zn that did not participate in the ion-exchange could conceivably have an adverse effect on the resulting cell.

We have therefore chosen to study the composition of Cu_2S as formed on (Zn,Cd)S via ion-exchange. Three types of electron beam analyses were performed to elucidate composition profiles for Cu_2S/(Zn,Cd)S junctions. The objective was to compare atomic profiles (Zn and Cd in particular) through the Cu_2S into the (Cd,Zn)S base, with Zn content of the base as a parameter. To evaluate the convolution of beam effects with actual atomic profiles, angle-resolved x-ray photoemission as well as ion-milling with both AES and ESCA (XPS) analysis were carried out on several samples types. In addition, atomic absorption spectrometry (AAS) measurements were made on cuprous ion barrier solutions, and on solutions of dissolved Cu_2S and (Zn,Cd)S.

EXPERIMENTAL

A combined ESCA/SAM instrument (PHI Model 550)[5] with a double pass Cylindrical Mirror Analyzer (CMA) was used. Profiling was accomplished with 5 KV Ar^+ ions, rastered across 10 x 10 mm of sample for ESCA profiles or ~ 2 mm dia. for AES profiles.

The atomic absorption measurements were made using a Perkin-Elmer mod. 403 spectrophotometer.

Cu_2S layers were formed via ion-exchange on (Zn,Cd)S films of several compositions (for the electron beam measurements) and on both films and

powders (for the AAS work). Other sample information is noted below.

RESULTS

As seen in Figures 1-3, the Zn and Cd profiles are distinctly different through the outer structure, until the bulk of the base material is reached. (The Cu_2S for these samples was formed by dry solid state reaction and were not rinsed following the reaction). For each analysis, as the profile proceeds into the Cu_2S (using the Cu profile as a base), an anomalously high Zn concentration appears in amounts roughly proportional to the Zn content of the base layer. The Zn to Cd ratio is apparently larger than unity over a large fraction of the Cu_2S. This is illustrated in Figure 1. The decrease in Cd during the initial part of the ion etch is due to the $CdCl_2$ on the surface, and is similar for 0 and 36 atomic percent Zn. However, for the 36% Zn sample, the Zn concentration exceeds Cd over a substantial distance (hatched region of Figure 1). Similar sub-surface segregation of zinc is apparent in the ESCA profile of Figure 2 (hatched region in particular). The peak positions in the ESCA spectra indicate that Cu^+, Cd^{++} and Zn^{++} are the cations present. The sulfur is mostly sulfide, with some sulfate present on the outer surface. The latter was determined by grazing angle ESCA, which also confirmed the sub-surface excess of zinc.

These results indicate that Zn^{++} diffuses out more slowly during the ion-exchange reaction. This slower reaction of Zn is expected from the higher stability of ZnS bonds, and is also indicated by the reduced rate of Cu_2S formation in wet barrier solution as the base Zn content is increased.

This slower out-diffusion of Zn during ion-exchange has been corroborated by the atomic absorption measurements. Zn and Cd concentrations were measured in the following solutions: a) cuprous chloride barrier, b) Cu_2S etched in 0.1 M KCN and c) (Zn,Cd)S etched in HCl. The Zn/Cd ratios measured for a nominal 15% zinc sample are shown in Table 1 (averages of five separate runs).

Table 1
Zinc to Cadmium Ratios Measured by AAS for the Three Solutions Described Above

Solution	Zn/Cd Ratio
Barrier	0.143
KCN	0.418
HCl	0.161

Separate tests have verified that the high Zn/Cd ratios for the KCN solutions are not due to the dissolution of the mixed sulfide base material by KCN.

CONCLUSIONS

These measurements verify that a lower fraction of zinc is participating

in the ion-exchange reaction than exists in the (Zn,Cd)S base material. This is evident in the AES and ESCA profiles, and in the AAS measurements, and results in the retention of a correspondingly larger amount of Zn in the Cu_2S layer. A more complete report is planned for similar measurements made on these and other samples.

REFERENCES

1. R. Hill, "Thin Film Solar Cells," Chapter 10 of Active and Passive Thin Film Devices, T. J. Coutts ed., Academic Press (1978).

2. J. D. Meakin, International Workshop on Cadmium Sulfide Solar Cells and Other Abrupt Heterojunctions, University of Delaware, 1975 (Proceedings, p. 75); A. E. vanAerschodt et al., IEEE Trans. Electron Devices ED-18, 471 (1971).

3. Final Report, NSF/RANN/AER72-03478A04, Institute of Energy Conversion, University of Delaware, p. 13 (1977).

4. W. Palz et al., Proc. 10th IEEE Photovoltaic Specialists Conference, Palo Alto, CA (1973); L. C. Burton and T. L. Hench, Appl. Phys. Lett. 29, 612 (1976).

5. Physical Electronics Div., Perkin-Elmer Corp., Eden Prairie, MN.

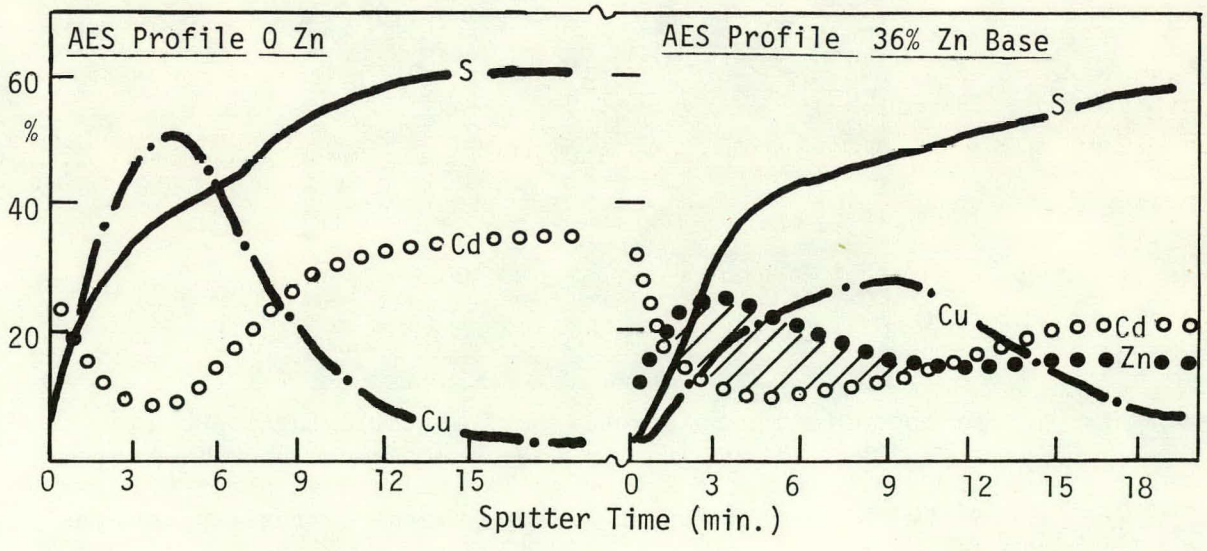

Figure 1. Composition profiles employing Auger (AES) analysis for Cu_2S/CdS (left) and $Cu_2S/Zn_{.36}Cd_{.64}S$ (right) junctions. The hatched area corresponds to Zn/Cd concentration ratio > 1.

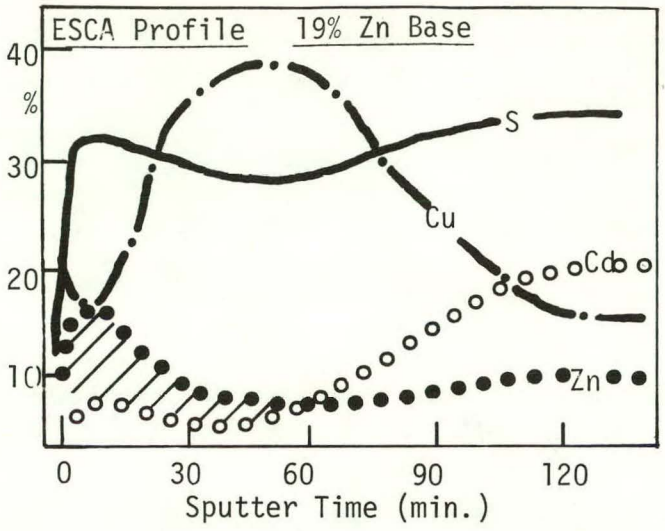

Figure 2. Composition profile employing ESCA (XPS) of a $Cu_2S/Zn_{.19}Cd_{.81}S$ junction.

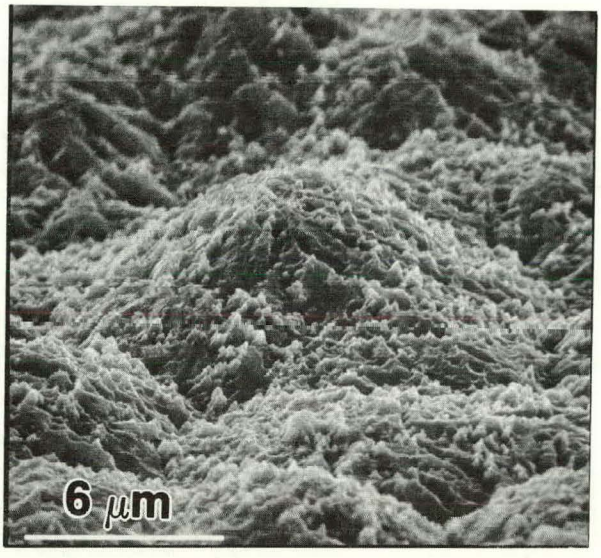

Figure 3. SEM photomicrograph of cell surface following ion-beam profiling. The basic grain shape at about 10 μm is preserved. However, a roughness is produced at about 0.5 μm by the beam which may contribute to the diffuse appearance of the interfaces.

NOTES

THIS PAGE

WAS INTENTIONALLY

LEFT BLANK

SCANNING LIGHT SPOT ANALYSIS OF FAULTY SOLAR CELLS*

K. Lehovec and A. Fedotowsky
University of Southern California
Los Angeles, CA 90007

Current output patterns for solar cell panels exposed to a scanning light spot are computed on the basis of a distributed network model. Patterns of fault-free panels are compared with those of faulty cells having either cracks which expose the junction and cause leakage current, or else point shorts in series with spreading resistances. The computed data can be used to evaluate experimental results obtained by D. Sawyer and co-workers[1,2].

The equivalence of output patterns generated by the scanning light spot and those generated by a line of illumination parallel to the finger electrodes allows the use of simple one-dimensional current flow in computing output patterns. Computations are facilitated by assuming uniform attenuation of the photoelectrically generated current on its path from the illuminated spot to the collecting electrodes. Uniform attenuation lengths of from 1/4 to 1/2 the typical electrode spacing are optimal for fault resolution, and can be obtained by modulating the light intensity at frequencies in the low MHz range. Figure 1 shows the output current for various attenuation lengths of the photoelectrically generated current in a fault-free cell. The full lines pertain to attenuation by conductive flow over the junction, while the dotted lines pertain to capacitive current flow over the junction as obtained by high frequency intensity modulation. Figures 2 and 3 show output patterns for cells cracked at various distances from the finger electrodes. Figure 2 refers to a crack with no leakage flow across the exposed junction, while such a leakage current is assumed in the case of Figure 3. The crack is revealed by an abrupt change of the panel output as the light spot moves from one side of the crack to the other side. Leakage conductance across the exposed junction at the crack is indicated by a change of panel output with distance of the light spot from the crack in close vicinity of the crack. A tilt of the crack with respect to the direction of the finger electrodes causes only a second order effect; therefore the output pattern can be obtained by combination of patterns with cracks at different distances from and parallel to the finger electrodes. Figure 4 shows the reduction of the output current for a cell having a partial short of the

*supported by the U.S. Department of Commerce, National Bureau of Standards contract P.O. 809453 under Department of Energy Contract EA-77-A-01-6010

photovoltaic junction at a position half-way between the finger electrodes (dotted lines), compared to that of a fault-free cell (full lines).

References

1. D.E. Sawyer, "A Technique for Using an Optical Scanner to Reveal Solar Cell Defects," Conference Record of the 13th IEEE Photovoltaic Specialists Conference, p. 1249, Washington, D.C. June 5-8, 1978.

2. D.E. Sawyer and S.W. Berning, "Laser Scanning of Active Semiconductor Devices," National Bureau of Standard Special Publication, pp. 400-427, February 1976.

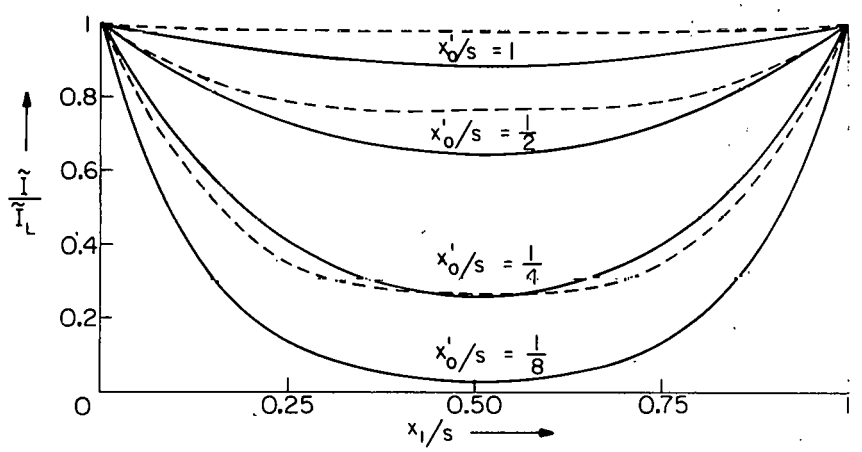

Fig. 1: Dependence of current collected by the electrodes of a fault free cell on the position x_1 of illumination. Parameters are finger electrode spacing s and the attenuation length x_o'. Dotted lines: modulated light so that $x_o'' = x_o' = x_o/\sqrt{2}$; Solid lines: unmodulated light, $x_o'' = 0$. Response to modulated and unmodulated light of $x_o'/s = 1/8$ coincides closely.

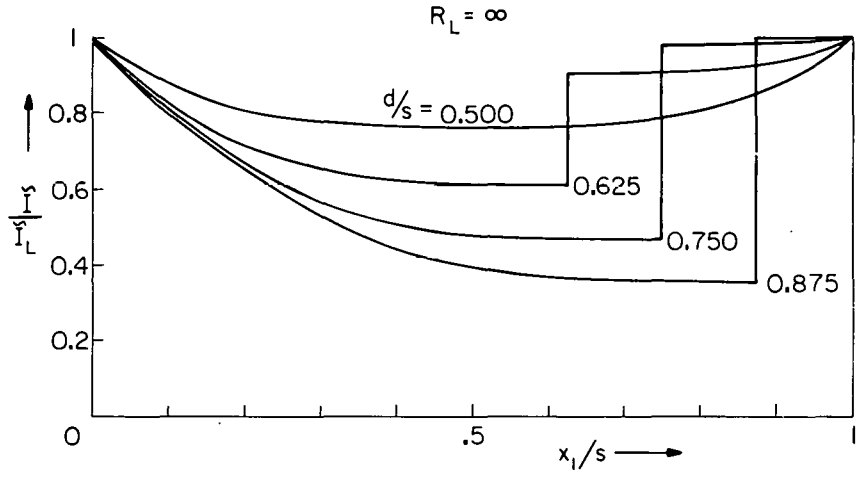

Fig. 2: Response of cell cracked at x = d to modulated illumination at $x = x_1$ with no leakage resistance over the exposed junction.

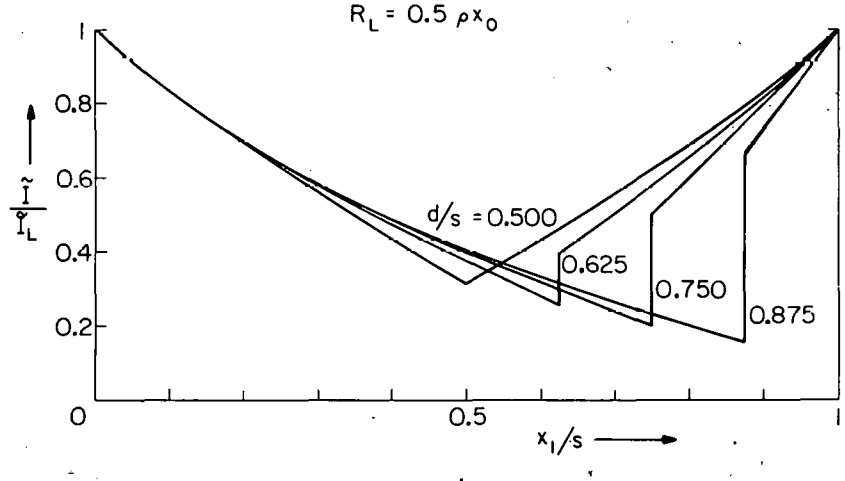

Fig. 3: As in Fig. 2 but with finite leakage resistance over the exposed junction at the crack. [Sheet resistance ρ and attenuation length $x_o = s/\sqrt{2}$]

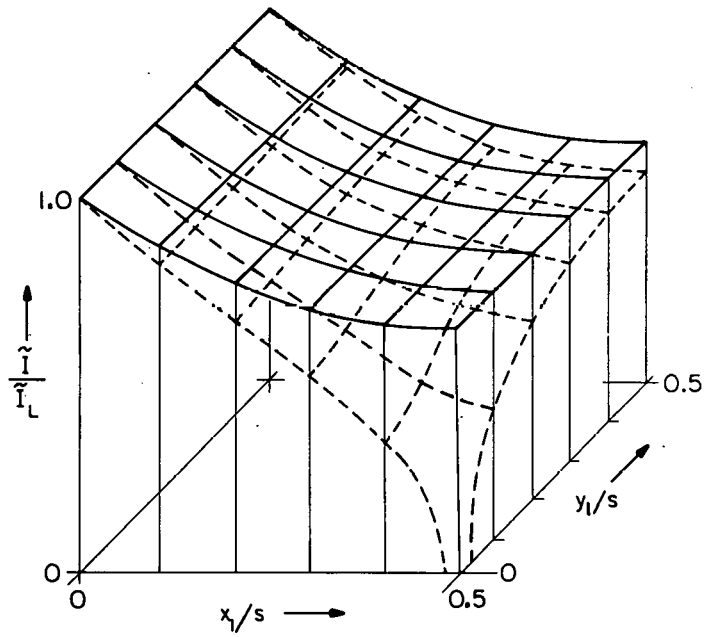

Fig. 4: Currents collected by a fault-free cell (solid lines) and those collected by a faulty cell (dotted lines) having a point short $R_{sh} = \rho/2$ located midway between the electrodes, for various locations x_1 of the illuminated spot ($x_o' = s/2$ and $x_o'' = 0$).

NOTES

THIS PAGE

WAS INTENTIONALLY

LEFT BLANK

Optical/Electro-optical Session

PHOTOCONDUCTIVITY AS A PROBE OF POLYCRYSTALLINE FILMS

R. H. Bube

Department of Materials Science and Engineering
Stanford University
Stanford, California 94305

Photoconductivity measurements can provide information about the properties of polycrystalline films through a variety of direct and indirect effects. If the dark conductivity of a material is controlled by carriers of one type,

$$\sigma_o = n_o q \mu_o \tag{1}$$

photoexcitation can produce a change in conductivity $\Delta\sigma$ by causing a change in carrier density Δn or a change in carrier mobility $\Delta\mu$:

$$\Delta\sigma = \Delta n \; q \; \mu_o + (n_o + \Delta n) \; q \; \Delta\mu \tag{2}$$

The wavelengths of light effective in making these changes, i.e., the spectral response for photoconductivity, depend upon the localized states present in the bandgap as well as being associated with transitions across the bandgap itself. The change in mobility $\Delta\mu$ caused by photoexcitation could have a small contribution due to changes in bulk mobility through alteration of the density of charged imperfection scattering centers by illumination, but in polycrystalline films is usually associated primarily with a change in intergrain barrier height and depletion layer width caused by illumination. Since carrier transport past intergrain barriers may occur either by thermal excitation over the barrier or by tunneling through the barrier with or without thermal assistance, photoexcitation producing $\Delta\mu$ may also involve a change in the dominant mode of barrier transport. The temperature dependence of photoconductivity, as interpreted via several models, may also give significant clues as to the nature of the imperfection states and their distribution. The temperature dependence of photoconductivity decay, or its associated phenomenon of thermally stimulated conductivity, may be used to obtain information and evaluate parameters of imperfections. Finally a variety of photoinduced chemisorption phenomena may occur at the surface of a thin polycrystalline film exposed to different ambients, which may dominate the electrical properties of the film.

Because it is usually not possible to tell from photoconductivity measurements alone whether the effect of photoexcitation is to alter carrier density, carrier mobility, or both, it proves extremely helpful to be able to make measurements that allow separation of density and mobility effects. The two approaches most commonly used have been photo-Hall and photothermoelectric effects. Since the magnitude of carrier mobilities in thin polycrystalline films is frequently quite small, the photothermoelectric effect technique generally proves to be the more convenient of the two; since the thermoelectric power can be directly correlated with the carrier

density, the mobility can be calculated from a simultaneous measurement of conductivity. If a Schottky barrier can be formed on the polycrystalline film, photocapacitance measurements can also be used to separate carrier density and mobility effects in the measured conductivity.

Taking an n-type semiconductor as a frame of reference, the height of the intergrain barrier, ϕ, is determined by an equality of charge on the intergrain interface states and of charge in the depletion layers surrounding the intergrain region. The charge on the interface states is given by

$$Q_{int} = q\, N_i \{E_G - (E_c - E_F) - \phi\} \tag{3}$$

and the charge in the depletion layers is given by

$$Q_{dep} = q\, N_D\, (2d) = (8\, q\, N_D\, \varepsilon\, \phi)^{\frac{1}{2}} \tag{4}$$

where N_i is the interface state density, E_G is the bandgap, $(E_c - E_F)$ is the distance of the Fermi level below the conduction band, N_D is the ionized donor density, d is the depletion layer width, and ε is the dielectric constant of the material. The value of ϕ is given by setting $Q_{int} = Q_{dep}$. For such an n-type semiconductor, the effect of photoexcitation will be to provide holes for capture by the negatively charged interface states, thus reducing Q_{int} and ϕ, which results also in a decrease in depletion layer width. Since depletion layer width may be a critical variable in determining whether barrier transport is by tunneling, photoexcitation may shift the transport mechanism toward tunneling and provide a different temperature dependence for the measured mobility.

A model proposed by Petritz (1) provides a useful framework within which to consider these barrier modulation effects with photoexcitation. If the mean free path for scattering is appreciably less than the grain size in the polycrystalline film, the measured mobility may be expressed as

$$\mu_o = \mu_g \exp(-\phi/kT) \tag{5}$$

where μ_g is the mobility determined by processes within the grain. The effect of photoexcitation is then to provide a change in mobility $\Delta\mu$ given by

$$\Delta\mu = -\frac{\Delta\phi}{kT}\, \mu_g \exp(-\phi/kT) \tag{6}$$

The fact that photoexcitation may cause a Δn as well as a $\Delta\mu$ can be conveniently expressed through a quantity B that expresses the relative effect of barrier modulation compared to the change in carrier density:

$$B = (\Delta\mu/\mu_o)/(\Delta n/n) \tag{7}$$

so that the photoconductivity is given by

$$\Delta\sigma = q\, \mu_o\, (1 + B)\, \Delta n \tag{8}$$

Although historically there was a long debate about whether photoexcitation caused primarily a change in density or a change in mobility

in Pb-salt infrared detectors, in general it is found that materials with a lower dark conductivity have a value of B approaching zero, whereas materials with a high density of thermal equilibrium carriers are more likely to show larger values of B - except, of course, in the limit of very high dark carrier densities when the depletion widths become so small that tunneling between grains is essentially unlimited by the intergrain barriers.

A further consideration must be included in materials exhibiting what has come to be known as "sensitized" photoconductivity. In these materials the bulk photoconductivity in the grains, associated with the lifetime of majority carriers, is greatly increased by the presence of specific "sensitizing centers" that have a large capture cross section for photoexcited minority carriers and then a subsequently very small cross section (10^{-20} cm^2 or less) for photoexcited majority carriers (2).

In any case it is convenient to describe the Δn component of photoconductivity in terms of a carrier lifetime,

$$\Delta n = f \tau_n \tag{9}$$

where f is the photoexcitation rate per unit volume per unit time. Specific expressions for τ_n then depend on the specific recombination model used, and in real situations τ_n may be a function of excitation intensity, temperature, imperfection density and type, and location of the equilibrium Fermi level. The basic dependence of τ_n on other variables for a model in which a single recombination center controls the lifetime has been worked out by Shockley and Read (3) and extended by others (4).

The significance of some of the above comments can best be illustrated by considering two specific examples involving polycrystalline films of CdS and PbS. The polycrystalline films of CdS were deposited by spray pyrolysis and are strongly n-type with dark electron densities in the 10^{16} to 10^{17} cm^{-3} range. Dark electron mobilities at room temperature are of the order of 0.1 cm^2/V-sec, compared to a bulk CdS electron mobility of about 300 cm^2/V-sec (5). The polycrystalline films of PbS were deposited by a chemical method and are p-type with dark hole densities between 10^{15} and 10^{17} cm^{-3}. Dark hole mobilities at room temperature are of the order of 5 cm^2/V-sec, compared to a bulk PbS hole mobility of about 500 cm^2/V-sec (6). For both types of film the dark mobility is thermally activated as described by Eq. (5), with ϕ = 0.2 - 0.5 eV for the CdS films, and ϕ = 0.08 eV for the PbS films. Photoexcitation produces very small changes in the electron density in CdS films, but reduces ϕ and accentuates a temperature independent range of μ associated with tunneling through the intergrain barriers. In one specific instance, photoexcitation reduced the barrier height from 0.46 eV to 0.22 eV, while increasing the mobility in the tunneling regime from 0.015 to 1.5 cm^2/V-sec. If the dark electron density in these CdS films is reduced by incorporation of Cu acceptors, the contribution of Δn to $\Delta\sigma$, relative to that of $\Delta\mu$, becomes larger, but even when n_o is reduced to 10^{15} cm^{-3} or less, both

Δn and $\Delta \mu$ make major contributions to $\Delta \sigma$. In the PbS films, on the other hand the contribution of Δn to $\Delta \sigma$ is always much greater than that of $\Delta \mu$. In fact, unless the conductivity of the PbS films has been deliberately reduced by a heat treatment in vacuum, there is almost no affect of photoexcitation on the hole mobility at all except for a small low-temperature effect in what appears to be the tunneling regime. Although the actual intergrain barrier height in the CdS films varies widely with preparation conditions, as well as photoexcitation, the apparent intergrain barrier height in the PbS films is virtually independent of the details of the method of chemical deposition or of the nature of the substrate on which the films are deposited (7). This result suggests a specific chemical identity to the intergranular regions in the PbS, probably associated with oxide formation.

The adsorption of a gas on the surface of a semiconductor film with exchange of charge with the film is commonly called chemisorption. Such a process of chemisorption can either remove majority carriers or supply majority carriers, and photoexcitation may be effective in causing either adsorption (by increasing the density of carriers to be involved in chemisorption) or desorption (by increasing the density of opposite-type carriers). Oxygen chemisorption on n-type CdS decreases the conductivity, whereas oxygen chemisorption on p-type PbS increases the conductivity. A variety of effects is distinguishable depending on whether the adsorbed oxygen interacts primarily with the grains, or whether the adsorbed oxygen also changes the properties of the intergrain barriers.

The temperature dependence of photoconductivity yields the temperature dependence of the carrier lifetime. Characteristic behavior can be identified with specific types of imperfections. Photoconductivity measurements on polycrystalline PbS show that τ_p is controlled by sensitizing centers lying 0.22 eV below the conduction band. Similar measurements on polycrystalline Si suggest a high density of states in the forbidden gap, lying both above and below the Fermi level, giving a behavior similar to that found in amorphous semiconductors (8,9).

REFERENCES

1. R.L.Petritz, Phys.Rev. 104, 1508 (1956)
2. R.H.Bube, Photoconductivity of Solids, Wiley & Sons, N.Y. (1960); R.E.Krieger, Huntington, N.Y. (1978)
3. W.Shockley and W.T.Read, Phys.Rev. 87, 835 (1952)
4. J.S.Blakemore, Semiconductor Statistics, Pergamon, Elmsford, N.Y. (1962)
5. C.Wu and R.H.Bube, J.Appl.Phys. 45, 648 (1974)
6. S.Espevik, C.Wu and R.H.Bube, J.Appl.Phys. 42, 3513 (1971)
7. E.Lee and R.H.Bube, J.Appl.Phys. 43, 4259 (1972)
8. M.Hirose, M.Taniguchi and Y.Osaka, J.Appl.Phys. 50, 377 (1979)
9. T.C.Arnoldussen, R.H.Bube, E.A.Fagen and S.Holmberg, J.Appl.Phys. 43, 1798 (1972)

NOTES

THIS PAGE

WAS INTENTIONALLY

LEFT BLANK

OPTICAL PROPERTIES OF POLYCRYSTALLINE SEMICONDUCTOR FILMS

A. H. Clark
University of Maine at Orono
Orono, Maine 04469

Abstract

Techniques for the determination of optical constants will be reviewed, with emphasis on polycrystalline semiconductor films important for photovoltaic applications. Artifacts produced by surface roughness will be discussed. The principle features of the optical constants of ideal single crystal semiconductors will be reviewed and used as a basis for discussing effects due to grain boundaries. Two models of grain boundary effects - amorphous and single crystal mixtures, and electric field broadening of the absorption edge - will be discussed.

The semiconductor literature contains hundreds of papers detailing optical properties of polycrystalline semiconductor films. In the vast majority of these papers, the effects of grain boundaries are neglected in the assumption (usually justified) that such effects upon the optical properties are small. In this presentation, I shall restrict myself to studies of optical constants of polycrystalline semiconductor films which specifically address the effects of grain boundaries. This eliminates most of the literature.

I. Experimental Techniques for Determining Optical Constants

A. Transmission and Reflectance at Normal Incidence

Assuming $n_{substrate}$ to be real and known, the wavelength λ and the film thickness d to be known, one may use measurements of T and R to determine n and k. (See ref. 1, 2, 3 for details).

B. Ellipsometry

Spectroscopic ellipsometry is becoming an increasingly important tool for precise determination of optical constants. See ref. 4, 5 for reviews. In particular the high accuracy obtainable is applicable for study of small effects due to grain boundaries.

C. Surface Roughness and Inhomogeneities

Most determinations of thin film properties reported in the literature assume a perfectly smooth film on a perfectly smooth substrate. In fact, surface roughness is probably the dominant contributor to the uncertainty in most determinations of optical constants. For example, surface roughness the order of 10 A can lead to 0.1%

inaccuracies in optical constants (ref. 6). Surface roughness the order of 1000 A is not unusual in semiconductor thin films produced by certain techniques (ref. 2).

Spatial fluctuations of the optical constants in the bulk of a material can also lead to anomalous transmission and reflectance values. In a polycrystalline semiconductor, the presence of grain boundaries, stoichiometry deviations, voids, and other imperfections may be expected to lead to such fluctuations. Recently progress has been made in characterizing such inhomogeneities using precise ellipsometric determination of optical constants at large photon energies (well above the fundamental absorption edge) (ref. 7).

Surface roughness may be taken into account in transmission and reflectance measurements (ref. 2), ellipsometric measurements, or by direct determination of total diffuse reflectance. Bragagnolo and Fagen will discuss this latter technique during the following session of this workshop.

II. Models of the Optical Properties of a Polycrystalline Semiconductor

A. Amorphous - Single Crystal Mixtures

In general one would not expect a grain boundary region to be composed of amorphous material. The optical constants of grain boundaries, however, may sufficiently resemble those of an amorphous material that the optical properties of the total material may be viewed as due to an amorphous - single crystal mixture. The absorption edge of polycrystalline InAs films has been reasonably modeled in this way (ref. 2). In addition the optical constants of polycrystalline silicon produced by low pressure chemical vapor deposition have been accounted for as due to a mixture of crystalline Si, amorphous Si, and voids (ref. 7).

B. Dow - Redfield Model

Excess absorption on the low energy side of the absorption edge of a polycrystalline semiconductor may be due to a Franz-Keldysh effect from electric fields arising from the grain boundaries. Attempts to model the absorption edge of CdS (ref. 8) and ZnS (ref. 9) polycrystalline films based on this effect have been made with some success. Unfortunately the materials were not sufficiently well characterized to rule out other sources of edge broadening.

III. Conclusions

Progress to date in understanding optical properties of polycrystalline semiconductors has been rather meager. Effects due strictly to grain

boundaries are often inseparable from those due to other defects and impurities. Furthermore most optical measurements have not adequately accounted for surface and substrate roughness effects.

The arrival of high precision spectroscopic ellipsometry promises to improve the accuracy of optical constants measured on these materials. In addition improved techniques for materials preparation and characterization should enable investigators to fabricate polycrystalline films of sufficient quality in order to better understand their optical properties.

References

1.) O. S. Heavens, Optical Properties of Thin Solid Films (Butterworths, London; 1955).

2.) J. Szczyrbowski and A. Czapla, Thin Solid Films 46, 127 (1977).

3.) J. C. Manifacier, J. Gasiot, and J. P. Fillard, J. Phys. E. 9, 1002 (1976).

4.) D. E. Aspnes, Optical Properties of Solids - New Developments, B. O. Seraphin, Ed. (North Holland, Amsterdam; 1976) pp 799-846.

5.) N. M. Bashara and S. C. Azzam, Eds. Ellipsometry (North Holland, Amsterdam; 1976) pp 37-48.

6.) H. E. Bennett and J. M. Bennett, Physics of Thin Films, G. Haas and R. E. Thun, Eds. (Academic Press, N.Y.; 1967) Vol. 4.

7.) B. G. Bagley, D. E. Aspnes, and C. J. Mogab, Bull. Am. Phys. Soc. 24, 363 (1979).

8.) M. Bujatti and F. Marcelja, Thin Solid Films 11, 249 (1972).

9.) P. Bugnet, Rev. Phys. Appl. (France) 9, 447 (1974).

NOTES

ELECTRON DIFFUSION LENGTHS IN THE Cu_xS/CdS CELL FROM SPECTRAL RESPONSE MEASUREMENTS

C. Moses
SUNY at Canton
Canton, N.Y. 13676

D. Wasserman
Department of Engineering Physics
Cornell University
Ithaca, N.Y.

Abstract We have determined the recombination diffusion length of electrons in Cu_xS generated by light in standard wet-dip Cu_xS/CdS solar cells. The recombination diffusion lengths were determined from measurements of the relative variation in short circuit current with wavelength. For cells with a copper sulfide thickness of .2μ to .3μ, diffusion lengths have ranged from .08 to .26μ. No significant changes in diffusion length have been measured after various cell heat treatments in air and hydrogen even when large changes in the short circuit current occured.

Introduction The recombination diffusion length of electrons in Cu_xS is of considerable importance since it is this length which determines how many electrons reach the charge separating interface and consequently what photocurrent is generated in the cell. This length has been previously determined from spectral response measurements (1)(2) and from junction scans with a light spot (3) and an electron beam (4). All of these techniques except (4) have given diffusion lengths characteristic of single crystal Cu_xS/CdS cells or of Cu_xS evaporated on single crystals of CdS. We have chosen to apply the method of reference (1) to ordinary wet-dip cells in order to measure diffusion lengths characteristic of optically generated electrons in a polycrystalline Cu_xS/CdS cell and in order to follow changes in the diffusion length as the cell is subjected to post-fabrication heat treatments in air and hydrogen.

Theory A schematic diagram of a Cu_xS/CdS cell is shown in figure 1.

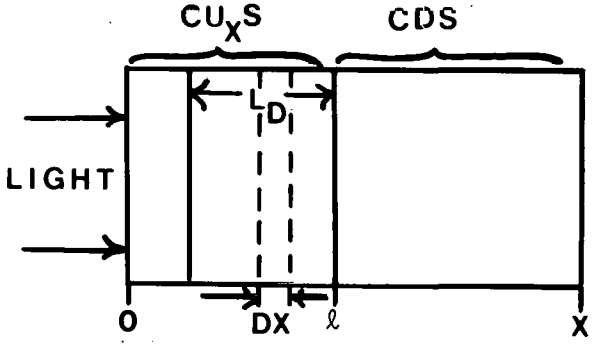

ℓ = Cu_xS thickness
L_D = electron diffusion length

FIGURE 1

The number of hole-electron pairs generated in the slab dx at a given wavelength is proportional to $I_o e^{-Kx} \cdot K$ where I_o is the intensity at x=o and K is the absorption constant of Cu_2S. If one assumes that only those carriers within L_D of the interface contribute to the current one can sum the contributions from the slabs dx as follows:

$$i_{sc}(\lambda) \propto e(1-\beta)\ I\{\ell-L_D\} \int_{x=\ell-L_D}^{\ell} Ke^{-Kx}\ dx$$

where $i_{sc}(\lambda)$ is the short circuit current at λ, e is the electronic charge, β is a factor representing bulk and interface recombination, $I\{\ell-L_D\}$ is the intensity at $\ell-L_D=(1-R(\lambda))\ I(\lambda)\ e^{-K(\ell-L_D)}$ where $R(\lambda)$ is is the fraction of the incident intensity reflected at the plastic $-Cu_2S$ boundary and $I(\lambda)$ is the incident intensity of the light source.

The spectral response, which we define as the number of amps per watt generated by the cell, is then given by the following expression

$$S.R. = \frac{i_{sc}(\lambda)}{I(\lambda)} \propto e\ (1-\beta)(1-R(\lambda))e^{-K(\ell-L_D)} \int_{\ell-L_D}^{\ell} Ke^{-Kx}\ dx$$

At any wavelength this formula predicts an increased S.R. for an increase in L_D provided that β is constant with wavelength. In order to eliminate β from the calculations, β is assumed to be a slowly varying function of λ, and the ratio of S.R.'s at adjacent wavelengths are taken. Taking ratios of the spectral response at adjacent wavelengths also compensates for changes in the junction electric field. In addition a bias light source was used to provide a stable junction electric field. If the ratio of S.R.'s at two adjacent wavelengths is taken, one obtains the following expression.

$$\frac{S.R._1\ (1-R_2)\ e^{2K_1\ell}}{S.R._2\ (1-R_1)\ e^{2K_2\ell}} = e^{(K_1-K_2)L_D}\ \frac{(eK_1L_D-1)}{(eK_2L_D-1)}$$

where S.R. means the spectral response at λ_1 and the other quantities are similarly defined. Thus L_D can be determined by a simple program if ℓ, K, R, and S.R. values at different wavelengths are known. We have measured ℓ and S.R. and used Shiozawa's results (5) for K and R.

In applying this model to experiment the following assumptions were made:

(a) A Cu_2S thickness greater than or equal to the diffusion length. This is in general agreement with most other measurements on the thin film Cu_2S/CdS cell.
(b) A well defined planar slab of Cu_2S of thickness ℓ. This is the most uncertain assumption in this work. In defense of it we point out that ℓ is a chemically determined average thickness which has shown good reproducibility in repeated trials. Also very little Cd has been found in the digested Cu_2S layer indicating a rather abrupt transition from Cu_2S to CdS.
(c) Carrier generation only in the Cu_2S. This is insured by analyzing data at wavelengths longer than that corresponding to the CdS band gap (510 nm).
(d) A single light pass through the Cu_2S. This is a plausible assumption since most of our measurements were made in the visible range where the absorption is high.

Table 1

Comments on Cell	Wavelengths in nm at which S.R. ratios were computed	L_D in μ
Clevite Cell, #262C2 $\ell_{Cu_2S}=(.34\pm.03)\mu$ pre-heat treatment a 10% change in ℓ produces a 30% change in L_D for fixed SR ratios.	550/650 600/700 650/750 700/800 750/850 850/950 900/1000	.28 .26 .24 .21 .12* .24 .28 $\overline{L}_D=(.252\pm.03)\mu$
Cell #262C2, same ℓ, 1 hr. heat treat in air at 75°C; cell showed a 25% increase in SR	same	$\overline{L}_D=(.255\pm.02)\mu$
Cell #262C2, same ℓ, 1 hr. additional heat treat in air at 160°C; cell showed a 20% decrease in SR	same	$\overline{L}_D=(.235\pm.03)\mu$

Comments on Cell	Wavelengths in nm at which S.R. ratios were calculated	L_D in μ
651 B_{1-2}, made at IEC, $\ell_{Cu_2S}=(.24\pm.02)\mu$ no heat treatment	same	$\overline{L}_D=.082\mu\pm.05\mu$
468-M_2, made at IEC, $\ell_{Cu_2S}=(.18\pm.03)\mu$, pre-heat treatment. I-V curve showed I_{sc} = 18.75mA, V_{oc}=.505V, Efficiency = 4.0%	same	$\overline{L}_D=(.101\pm.04)\mu$
468-M_2, same ℓ, after 12 hours in H_2·Argon mixture at 150°C. I-V curve showed I_{sc}=26.10 ma, V_{oc}= .520V, Efficiency=5.4%, cell showed a 25% increase in S.R.	same	$\overline{L}_D=(.091\pm.02)\mu$

Experimental Set-Up The experimental apparatus consisted of a voltage stabilized tungsten-iodide light source, focussing lenses, a light chopper and reference cell, various long-pass filters, a monochromator, a white bias light, and a sample holder all mounted on an optical bench.

The solar cell under study was short-circuited through a 1.0Ω metal film resistor and the voltage across the resistor fed into a lock-in amplifier. The general procedure was to measure the intensity at the cell's position in μwatts/cm^2 with a calibrated silicon cell, measure the short circuit current density in μamps/cm^2 for a Cu_2S/CdS cell, and divide the two measurements to find the S.R. of the cell in μamps/μwatt. The thickness of the Cu_xS layer was determined by measuring the copper concentration with an atomic absorption spectrophotometer and by assuming a planar Cu_2S layer.

Results The electron diffusion lengths measured for cells ranging in Cu_2S thickness from .34 to .18μ ranged from .26 to .082μ. Even though significant changes in IV and spectral response curves were seen after heat treatments, no appreciable changes in diffusion length were measured. Full results are shown in Table 1.

The uncertainties in the Cu_2S thickness are upper bounds; they were arrived at by compounding the errors in the quantities used to determine ℓ. The uncertainty in ℓ is critical since small changes in ℓ can produce large changes in L_D as noted in Table 1. The uncertainties in L_D are standard deviations. The values of L_D listed in Table 1 compare favorably to those measured with the SEM by Partain, Oakes, and Greenfield (4) on polycrystalline Cu_2S/CdS cells. They found L_D values of .11 to .57μ for Cu_2S thicknesses of 0.2 to 1.0μ. Our results also agree with the single crystal results of Gill and Bube (3) who found diffusion lengths of .1 to .4μ by means of a light spot scan of bevelled junctions. We do not find good agreement with the single crystal results of Mulder (2) who found L_D=.030 to .035μ and Pavelets et al (1) who found L_D=.025μ in films of Cu_2S evaporated onto single crystals of CdS.

The most unexpected result of this work is the constant diffusion length found in situations where a reducing heat treatment had increased the short circuit current by about 25% at all wavelengths. This is not expected if the main effect of an H_2 heat treatment is to reduce the copper oxide present in the cell, hence raise the stoichiometry of Cu_xS and thereby reduce the hole concentration, p. In this case L_D should increase because $L_D \propto \sqrt{\tau}$ and $\tau \propto 1/p$ where τ is the recombination life time for electrons in Cu_xS. Thus we conclude that a reducing heat treatment has little effect on charge movement through the Cu_xS volume but somehow profoundly influences the ability of the junction to collect charge. A possible mechanism could be an increase in junction electric field perhaps produced by the reduction of Cu_xO and the subsequent diffusion of copper into the CdS.

Acknowledgements The authors wish to thank Dr. Raymond Serway of Clarkson College of Technology for helpful discussions and for the use of laboratory facilities.

References

(1) S. Yu. Pavelets, G.A. Fedorus, and Ya. F. Kononets, Soviet Phys.-Semicond. 4, 282 (1970).
(2) B.J. Mulder, phys. stat. sol. (a) 13, 569 (1972).
(3) W.D. Gill and R.H. Bube, J. Appl. Phys. 41, 1694 (1970).
(4) L.D. Partain, J.J. Oakes, & I.G. Greenfield, 11th IEEE Photovoltaic Specialists Conference 1975, Scottsdale, Ariz. p. 454.
(5) L.R. Shiozawa, Clevite Final Report, ARL 69-0155, Oct. 1969.

NOTES

THIS PAGE

WAS INTENTIONALLY

LEFT BLANK

THE DESIGN AND UTILIZATION OF A MICROPROCESSOR-CONTROLLED ABSOLUTE SPECTRAL RESPONSE SYSTEM

L.M. Kilgren, N.C. Wyeth, and W.E. Devaney*
Institute of Energy Conversion
University of Delaware
Newark, DE 19711

1. Introduction

A fully automated system has been assembled which permits the direct monitoring of solar cell output under varying conditions of illumination and bias voltage. The primary system components are a chopped monochromatic light source of continuously variable wavelength, a lock-in amplifier, and a microprocessor. Analogue-to-digital and digital-to-analogue conversion allows the microprocessor to be used to control data acquisition and to perform data conditioning and output.

2. System Description

The system is shown schematically in Figure 1. A grating monochromator is driven by a stepping motor under control of the microprocessor. The monochromatic beam is focused on the surface of a silvered light-chopping blade placed at 45° to the path of the incoming light beam. The transmitted beam illuminates the cell under test through an appropriate lens system. The beam reflected from the chopper is monitored to give a continuous measurement of the primary beam intensity. The light-chopper control provides the reference signal for a lock-in amplifier which is used to measure the AC output of the cell. An ELH tungsten-iodide lamp driven by a stabilized DC supply provides the bias light. The cell under test is mounted on a thermoelectric temperature-controlled block with electrical connections for application of a bias voltage and measurement of cell output. A flat pyroelectric detector can be substituted for the cell block and the intensity-wavelength curve of the monochromatic beam stored in the microprocessor as the monochromator is stepped through the wavelength range of 400 nm to 1600 nm (a grating change is made at 800 nm). The microprocessor uses the stored reference intensity curve to compute the collection versus wavelength performance of the cell under test and then either prints out the digital data or displays the analogue information on a video terminal or provides hard copy on an x-y plotter.

*Present address: SES, Inc. Newark, DE 19711

3. Applications

A major advantage of the present system is the ability to measure the spectral response of the cell while under normal operating conditions of both illumination and voltage bias. This feature is essential for cells such as CdS/Cu_2S in which the total illumination strongly influences the collection efficiency (1).

3.1 Spectral response under normal operating conditions

The quantum efficiency of a cell or the number of current carriers collected per incident photon is measured as a function of wavelength with the cell at zero bias (short circuit current). In addition to measuring the collection efficiency of photo-generated minority carriers, this data can also provide information on the optical absorption properties of the active layers of cells. The system can be used with the chopped monochromatic beam only; alternatively the spectral response can be measured while the cell is illuminated with either a broad band white light or with a second continuous (DC) monochromatic bias beam.

3.2 Minority carrier diffusion length

For certain ranges of absorber/generator layer thickness and minority carrier diffusion length, the spectral response of a photovoltaic cell can be analyzed to set a lower limit to the diffusion length without needing a detailed knowledge of the absorption behavior of the active semiconductors (2). The diffusion length in turn can then be used to determine the wavelength dependence of the absorption coefficient from the spectral response curve. Measurements of this type have been made on polycrystalline Cu_2S and will be reported.

3.3 Internal photoelectric emission

When the photon energy of the incident beam is reduced below the smallest bandgap in a junction device, the current due to internal photoelectric emission of carriers over junction barriers less than the band gap can be detected. The microprocessor is programmed to generate a plot of the square root of the normalized response versus photon energy which by linear extrapolation to the energy axis gives the barrier height (3). Measurements will be reported on both semiconductor heterojunctions and metal/semiconductor Schottky contacts.

3.4 Interface recombination and junction field studies.

The use of phase-sensitive detection to measure the cell response to a modulated light source superposed on a DC bias light also makes it possible to measure the light-generated current as a function of the junction bias voltage. Measurements on CdS/Cu_2S cells show that the light-generated current can vary with applied voltage. The sensitivity to bias voltage is found to be strongly influenced by the intensity and spectral content of the applied bias light and the structure and history of the cell under test. This technique which reveals cell

current collection performance at the maximum power point has major advantages over more traditional procedures which are confined to the vicinity of the short-circuit current.

References

(1) A. Rothwarf, J. Phillips, N.C. Wyeth, Thirteenth IEEE Photovoltaic Specialists Conference - 1978(IEEE, New York, 1978) p. 399.
(2) N.C. Wyeth and A. Catalano, J. Appl. Phys. 50, 1304 (1979).
(3) J.I. Pankove, "Optical Processes in Semiconductors" (Dover, New York, 1975) pp. 314-319.

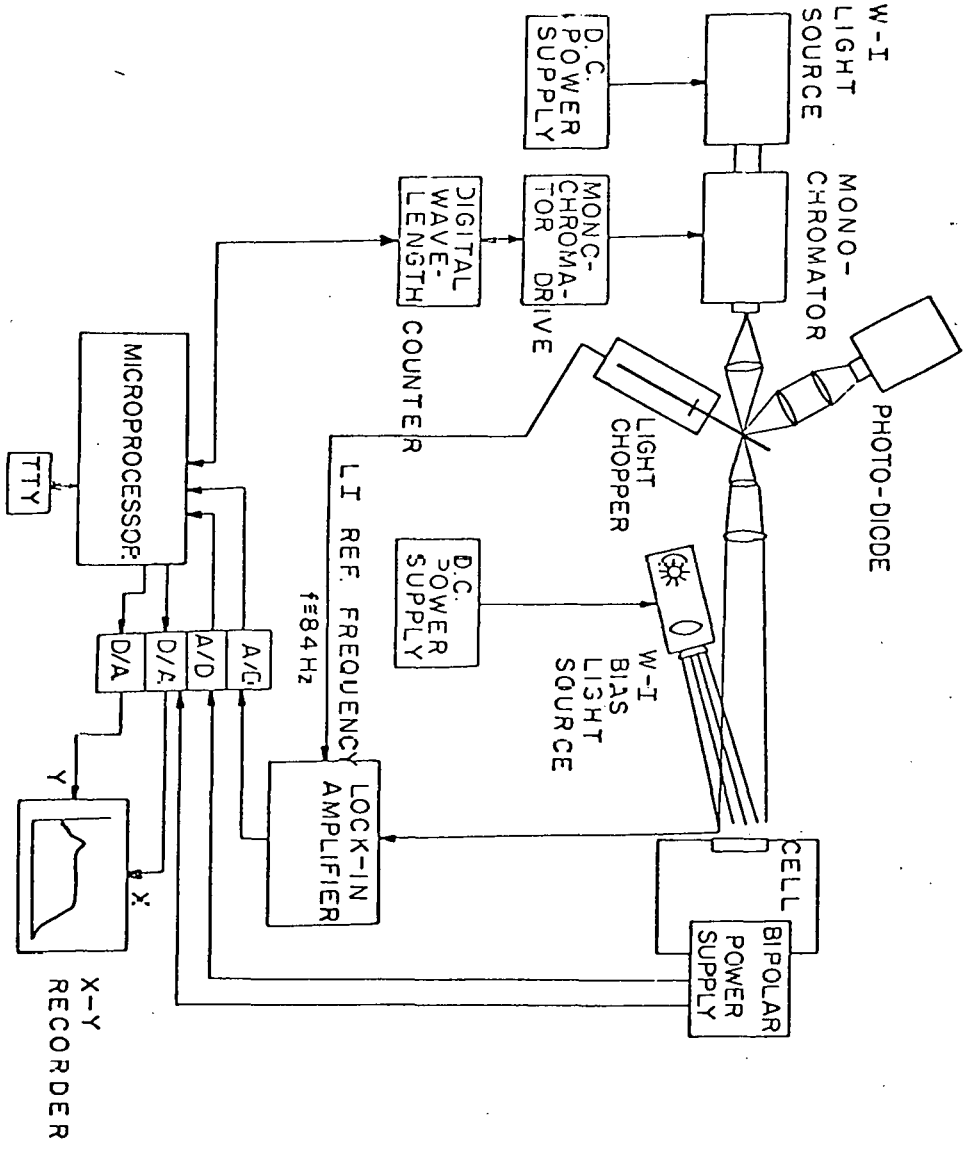

Fig. 1. Experimental System

NOTES

EFFECTIVE DIFFUSION LENGTH IN POLYCRYSTALLINE SEMICONDUCTOR THIN FILMS*

T. L. Chu, E. D. Stokes, and S. S. Chu
Southern Methodist University
Dallas, Texas 75275

I. Introduction

Minority carrier diffusion length is an important property of a semiconductor, affecting the operation of most of its devices. In a semiconductor under thermal equilibrium, the product of hole and electron densities is a constant at a given temperature. However, external perturbations, such as optical excitation, can produce carriers in excess of the thermal equilibrium values. The excess carriers tend to recombine to re-establish the equilibrium conditions; and the average distance a minority carrier diffuses before recombining is referred to as "minority carrier diffusion length". Its magnitude is determined predominately by the mechanism of carrier recombination. In direct-gap semiconductors, direct electron-hole pair annihilation dominates; energy and momentum can be conserved by emission of a photon with band-gap energy and characteristically small momentum. This direct recombination mechanism is characterized by intrinsically short diffusion length (a few micrometers, for example). In indirect-gap semiconductors, energy and momentum conservation cannot be satisfied in most electron-hole encounters, and carrier recombination occurs through an intermediate energy state utilizing a massive third entity, such as an impurity atom. This mechanism is characterized by relatively long diffusion length (a few hundred micrometers, for example) depending on the concentration of recombination centers, and energy and momentum are released in consecutive nearly-equal quanta of thermal vibration. In addition, trapping also plays a role in indirect-gap semiconductors so that conservation requirements are most easily satisfied by electron or hole localization on a "trap" rather than by a larger energy transition.

Numerous methods have been developed for the direct and indirect measurement of minority carrier diffusion lengths in single crystalline semiconductors. In most methods, the measurement provides only the average value over a relatively large volume. However, diffusion length

*Prepared for the Division of Solar Technology, Department of Energy Under Contract No. EY-76-C-03-1285.

inhomogeneities in single crystalline semiconductors have been observed due to recombination centers associated with localized chemical and structural defects. In polycrystalline thin films, large spatial variations in diffusion lengths are expected since most grain boundaries act as recombination centers. The measured values may thus be referred to as "effective diffusion length". Polycrystalline semiconductor films for photovoltaic applications are usually supported on conducting substrates, and this configuration precludes the use of techniques involving conductivity modulation. In this paper, two methods for the measurement of effective diffusion length in polycrystalline films of significant photovoltaic materials are reviewed: the surface photovoltage method for silicon films and the scanned electron beam method for gallium arsenide films.

II. The Surface Photovoltage Method

The steady-state surface photovoltage method is most convenient for the direct, high resolution measurements of diffusion length in polycrystalline silicon films. In this mehtod, the surface of a semiconductor crystal is illuminated with chopped monochromatic radiation of energy slightly greater than the band-gap of the semiconductor. The electron-hole pairs produced diffuse to the surface where they are separated by the electric field of the depletion region to produce a surface photovoltage. When $t \ll L$, $d \gg L$, $\alpha t \ll 1$, $\alpha d \gg 1$ (where t is the depletion layer thickness at the surface, d is the specimen thickness, L is the diffusion length, and α is the optical absorption coefficient), and the carrier injection is at a low level, then the incident light intensity required to produce a given surface photovoltage is a linear function of the reciprocal absorption coefficient. The extrapolation of the incident light intensity versus the reciprocal absorption coefficient plot to zero intensity yields "diffusion length" as the negative intercept.

The surface photovoltage method has been extended to shallow junction devices, such as solar cells. When the junction depth is considerably smaller than the diffusion length, short-circuit current may be used instead of the surface photovoltage for the measurement of diffusion length in the base region of the device. Thus, the diffusion length may be obtained by measuring the incident light intensity required to produce a given short-circuit current as a function of wavelength and extrapolating the intensity versus the reciprocal absorption coefficient plot.

The minority carrier diffusion lengths in cast semiconductor-grade polycrystalline silicon and silicon films deposited on polycrystalline metallurgical silicon substrates have been measured by the surface photovoltage method. The results were compared with those obtained by the short-circuit current collection method using Schottky barriers from the cast material and shallow p-n junctions deposited on metallurgical silicon substrates. Diffusion length profiles in these devices were also measured using a light beam of about 0.02 cm^2 area and compared with the diffusion length inhomogeneities in single crystalline silicon solar cells.

III. The Scanned Electron beam Method

The use of the steady-state surface photovoltage method for the determination of minority carrier diffusion length in direct-gap semiconductors is difficult because a high degree of monochromaticity of the incident light is required due to the rapid variation of optical absorption coefficients with wavelengths. The scanned electron beam induced current method with Schottky barrier collectors has been most successful for the direct determination of minority carrier diffusion length in single crystalline gallium arsenide.

In this work, the hole diffusion length in n-type polycrystalline gallium arsenide films has been measured on a Au-GaAs Schottky barrier structure with a scanned electron beam for carrier injection. This method requires no high temperature processing and optical absorption data, and is capable of measuring the diffusion length in single grains. An ETEC Autoscan electron microscope was used to inject carriers and to provide simultaneous measurement of beam position and the response of the Schottky barrier. A single grain at the edge of the Schottky barrier structure was selected on the basis of size and surface topography. The magnification was increased to 10,000X to 20,000X, and the grain positioned on the viewing screen. The signal from the beam-induced current was then switched from Z-axis modulation to Y-axis modulation producing an oscilloscope type trace. The system was then placed in a linear scan mode to suppress Y-axis roaster, and an area selected with an apparent exponential shape for the current versus position display. This signal was then recorded photographically for digitizing and analysis. A plot of the logarithm of the relative current versus distance from the barrier was then used to calculate the diffusion length in a single grain. These results were compared with the hole diffusion length measured in epitaxial gallium arsenide films.

NOTES

EBIC AND SCANNING LIGHT SPOT TECHNIQUE FOR INVESTIGATING THE RESPONSE OF POLYCRYSTALLINE SOLAR CELLS

N. Inoue, S. M. Goodnick and C. W. Wilmsen
Colorado State University
Fort Collins, Colorado 80523

Introduction

Solar cells fabricated with polycrystalline silicon can have large photoresponse variation across the cell area as a result of grain boundaries and defects which act as sinks for photogenerated carriers. We have applied the EBIC and scanning light spot (SLS) techniques to the investigation of photoresponse variations in ITO/polysilicon solar cells.[1] For this present work the polycrystalline substrates were cut from a float zone refined bule provided by Monsanto. The paper discusses the resolution of the EBIC and SLS techniques, compares the results obtained by the two techniques and reports on observations of grain boundaries and defects as seen by EBIC.

Resolution of EBIC and SLS

In using EBIC, the electron beam can be focused to a small spot on the surface of the cell (in our case 0.1 μm). However, these electrons lose energy over an interaction volume which is much larger than the spot size as shown in figure 1a. The diameter of this volume, R, depends on the atomic number of the material and the energy of the incident electrons. The diameter has been calculated to be 2.8 μm for a 15 KeV beam and 6.5 μm for a 25 KeV beam for Si. In order to estimate the resolution of our EBIC analysis, several different experiments were performed. Figure 1b illustrates the first experiment which measures the current as a function of position for a single scan of the electron beam across the surface of a cleaved single crystal cell. The current response for 15 and 25 KeV electrons is plotted in figure 1c. The 90% of maximum current for the two energies occurs at 3 and 6 μm which corresponds closely with the theoretical values of 2.8 and 6.5 μm.

In another experiment single electron beam sweeps across various locations of a "V" formed by the intersection of two grain boundaries were recorded (Fig. 2). For a 15 KeV beam the two grain boundaries could be resolved with a 3 μm separation, which is again the theoretical electron range. Using the intensity modulated mode, the grain boundaries appear to be approximately R/2 in width.

The difference in resolving surface and bulk defects can also be seen in figure 2. The surface debris is seen in clear focus and are resolved to the approximate spot size (0.1 μm). The bulk defects are convolved with the electron interaction volume and thus appear smeared out. In the case of SLS, although there is no interaction volume difficulty as with EBIC, the spot size is usually much larger than this volume. In our system, the scanning mirrors were normally placed between the final lens and the solar cell. This allowed scanning over a 0.4 x 0.4 cm area, but the spot size was approximately 20 μm diameter. By placing a 10X, f = 5 mm microscope objective lens between the scanning mirrors and the cell, a 5 μm spot size was obtained with a field of view of approximately 200 square microns. By using single scans of the laser it was observed that the spot size to a large extent determined the resolution of the SLS technique. By using a high enough magnification final lens, the resolution of SLS can approach that of EBIC, however the field of view is much smaller and it is difficult (it not impossible) to determine the location on the cell.

Comparison of EBIC and SLS

Intensity modulated mode EBIC and SLS photographs of the same 0.31 cm diameter ITO/Si solar cell are shown in Fig. 3. The major features are very much the same in both photographs except the EBIC has better resolution. This leads to the important conclusion that the EBIC and photoresponse are the same and thus the EBIC technique can be used to analyze the photoresponse of a solar cell.

EBIC Results

The EBIC analysis of an ITO/silicon solar cell fabricated with Monsanto float zone refined polysilicon is shown in Fig. 3b. The EBIC photograph shows many grain boundaries not shown in the secondary mode SEM photo of Fig. 4. The EBIC also shows areas of intermediate darkness, dark and light. The gray and dark area indicate reduced I_{sc}. The contrast between these areas can be controlled by a number of factors: pre amp gain, emission current and the brightness control. A close up of a dark, gray and light area reveals that all areas contain approximately the same density of defect clusters (Fig. 5). The reason for the difference in the average response in the various areas is not known, however the defects could be more effective at certain locations or the large defects seen by EBIC do not effect the response as much as point defects which would not be observed by EBIC.

Conclusions

1. The resolution of SLS is determined by the size of the light spot while the resolution of EBIC is determined by the electron range.

2. With high magnification, the resolution of SLS can be improved but the field of view is greatly reduced.

3. The response seen by SLS and EBIC are the same and therefore it appears that the EBIC yields a realistic photoresponse map.

4. Grain boundaries reduce I_{sc} over only a short range.

5. There are many defect clusters in the Monsanto poly.

References

1. G. Cheek, N. Inoue, S. Goodnick, A. Genis, C. Wilmsen, and J. B. DuBow, Appl. Phys. Lett. 33, 643 (1978).

2. K. Kanaya and S. Okayama, J. Phys. D. Appl. Phys., 5, 43 (1972).

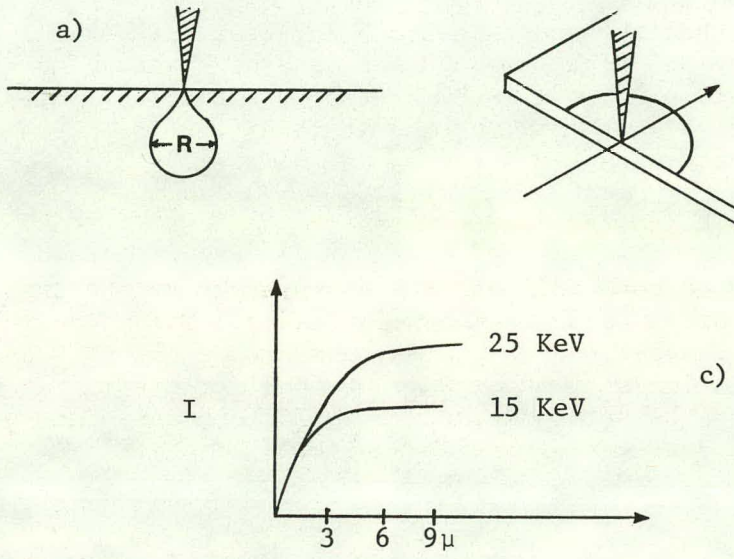

Figure 1

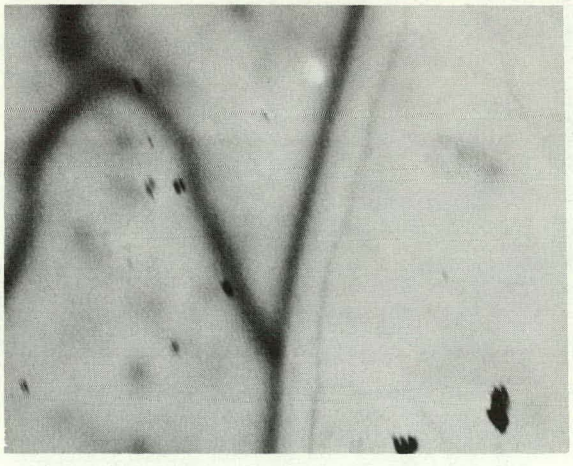

EBIC of "V" 1300X

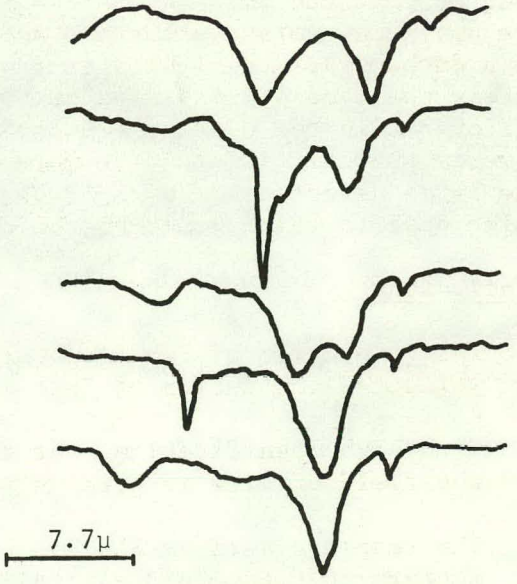

Figure 2

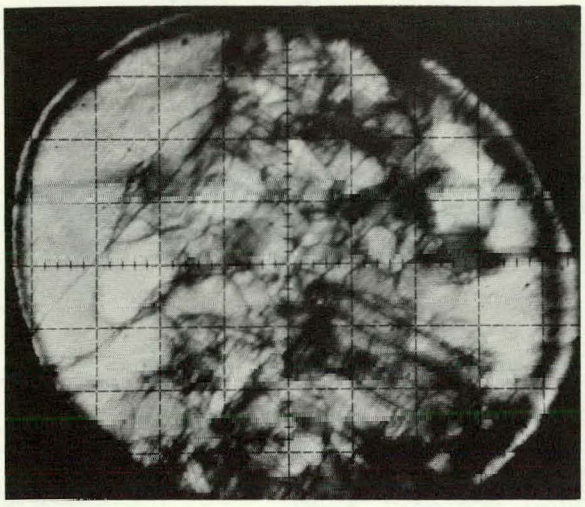

a) SLS, 25X

b) EBIC, 30X

Figure 3

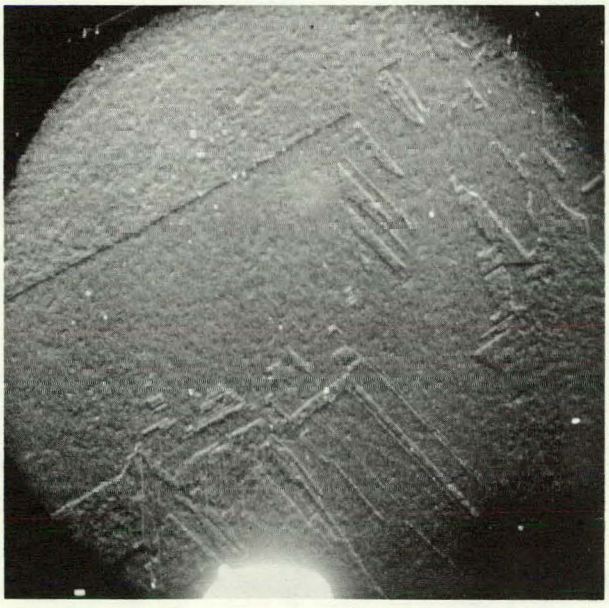

Secondary Electron Mode, 30X

Figure 4

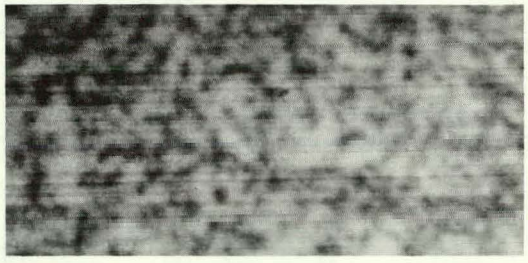

Light

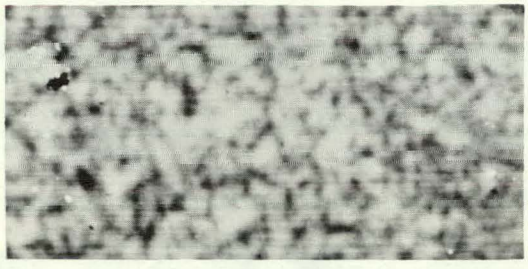

Gray

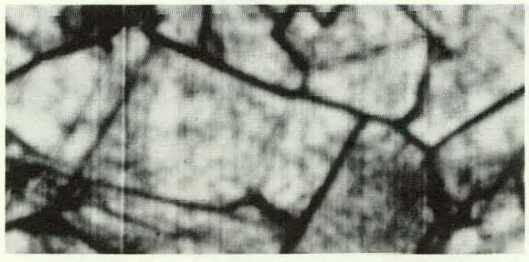

Dark

EBIC, 210X

Figure 5

NOTES

THIS PAGE

WAS INTENTIONALLY

LEFT BLANK

SOME INVESTIGATIONS ON THE INFLUENCE OF DEFECTS/GRAIN BOUNDARIES ON PHOTOVOLTAIC MECHANISMS IN POLY-CRYSTALLINE SILICON FILMS*

B. L. Sopori and A. Baghdadi
Motorola, Inc., Solar Energy R & D Department
Phoenix, Arizona 85005

Photovoltaic mechanisms in single crystal silicon are known to be sensitive to defects and impurities which may be present in the starting material and/or introduced during Solar Cell processing. In the case of poly-crystalline films, the presence of grain boundaries (GB) can also exert profound influences on photovoltaic mechanism via increased carrier generation-recombination, impurity segregation, and alterations in barrier height. Consequently there are strong spatial variations in photoresponse of polycrystalline solar cells, and it is common experience that solar cell characteristics like V_{oc} and I_{sc} are not well related to the "average" diffusion length, L (or lifetime, τ).

This paper will describe the results of a continuing study which is aimed at: (i) Influences of defects and grain boundaries on the local values of L (ii) relationships between local values of L and the local photoresponse, and (iii) definition and measurement of an average value of L, $\langle L \rangle$, in a polycrystalline cell, which can be well related to solar cell characteristics. We have utilized several non-destructive methods which can measure local parameters like L, τ and photoresponse with high spatial resolution. These include:

(i) The surface photo-voltage(SPV)method for measurement of L. This technique can be used on as-grown or partially processed films or solar cells. The method consists of determining the spectral dependence of the photo-signal generated due to the presence of a depletion type region at the surface of unprocessed films or at the p-n junction for processed cells ($0.8\ \mu m \leq \lambda \leq 1.0 \mu m$). A plot of the light intensity I_λ transmitted into the film vs. reciprocal absorption coefficient, α^{-1}, is a straight line whose intercept with the α^{-1} axis is the diffusion length. To increase the spatial resolution ($\sim$10L) the conventional method is modified by using a focussed optical beam (diameter = d). However, this necessitates some corrections being made (depending on d/L) to determine the diffusion length.

(ii) The current phase-shift (CPS) technique. This method is based on the fact that when a modulated light source illuminates a semiconductor, the carriers generated exhibit a phase-shift ϕ, with respect to the incident light. This phase-shift is related to the carrier lifetime, τ, by the relation $\tan \phi = \omega\tau/2$. By using a schottky barrier to collect the carrier, the phase difference between the short circuit current and the indident light can be measured. Measurements can be made using a Hg contact or a p-n junction.

(iii) A focussed laser scanner (FLS) with a beam size $\sim$5μm (multi-wavelength option) to measure the spatial variation in photo-response

(iv) The SEM/EBIC technique to directly evaluate (qualitatively) the electrical activity of a particular defect.

Investigations were carried out on laser-grown polycrystalline films (thicknesses 4-10 mils). These films exhibit varied defects including grain boundaries, twin planes and "twin bundles", stacking faults, and dislocations. Dislocations (within a grain) range from relatively low densities ($10^4/cm^2$) to high densities ($4 \times 10^6/cm^2$). Results obtained to date have shown:

1. Local variations in L are well related to variations in the dislocation density. Films with a dislocation density of $\sim 5 \times 10^5$ cm^{-2} exhibit typical diffusion lengths of about 50 μm. Presence of GB's and impurity segregates can degrade diffusion lengths further.

2. Photo-response, both current and voltage, measured at long wavelength (λ= 1.15 μm) operation of FLS show good correlation with the diffusion length. However, at short wavelengths (λ = 0.63L8 μm) only L vs. I_{sc} shows a good correlation; an anti-correlation is observed for L vs. V_{oc}. This behavior is particularly useful for characterizing the nature of a GB. A typical dependence of short wavelengths photoresponse on the diffusion length is shown in figure 1.

3. Twins and low angle GB's have very little influence on L. This, in general, is in agreement with our results from EBIC studies indicating the lack of EBIC response at a majority of twin boundaries. However, we have also observed that some "twin-bundles" can exhibit fairly strong electrical activity. Figure 2 shows EBIC pictures of two diodes (1mm in size) fabricated on RTR ribbons. The diode in Figure 2a has a high density of twins and some GB (as seen under an optical microscope). It is seen that only about 30% of the twins are active. In contrast, a majority of twins in diode 2(b) exhibit electrical activity. Although several speculative arguments can be presented to explain this behavior, further investigations are needed.

4. Large angle GB's can cause significant changes in the photoresponse and can exert influence upto a few mm away from the GB. Figure 3a shows diffusion length mapping in the vicinity of a large angle GB. Corresponding variations in the short and long wavelengths FLS current responses are shown in Figures 3b and 3c respectively. It is clear that the influence of a GB extends farther when the carrier generation is due to long wavelength excitation.

5. Inhomogenieties in silicon ribbons may be divided into two groups.

(a) Regions of varying diffusion length but homogeneous in other material properties. In this case the overall cell may be regarded as constituted by small individual cells, and the measured diffusion length will average out the good and the bad areas. Figure 4 shows the results of an experiment carried out using two cells. Curve #1 was obtained on a low diffusion length cell, and curve #2 on a 50 micron diffusion length cell. The average value for the diffusion length would then be given by: $$\langle L \rangle = k \left(L_1 A_1 + L_2 A_2 \right) . A^{-1}$$

where<L>represents the average value for the two cells; L_i, A_i are the diffusion lengths and the areas, respectively of the cells (i = 1,2). $A = A_1 + A_2$ is the total area, and k is a constant determined by the experimental conditions . Curve #3 was obtained by measuring the total response from both cells illuminated simultaneously. Thus the diffusion length measured by curve #3 falls between the values measured on individual cells, shown in curves #1 and #2.

(b) The presence of a transverse field associated with certain GB's can result in considereable internal carrier transport between the inhomogeneous regions. In such a case the "average" values measured by SPV, and CPS can be in significant error.

6. FLS long wavelengths response, in conjunction with one-point SPV calibration, can be used to determine <L>. <L> measured in this way shows an excellent correlation with I_{sc}.

7. In some cases measured values of L are light intensity dependent - higher intensity resulting in lower values of L. This effect is believed to be caused by the inhomogenieties of type 6b.

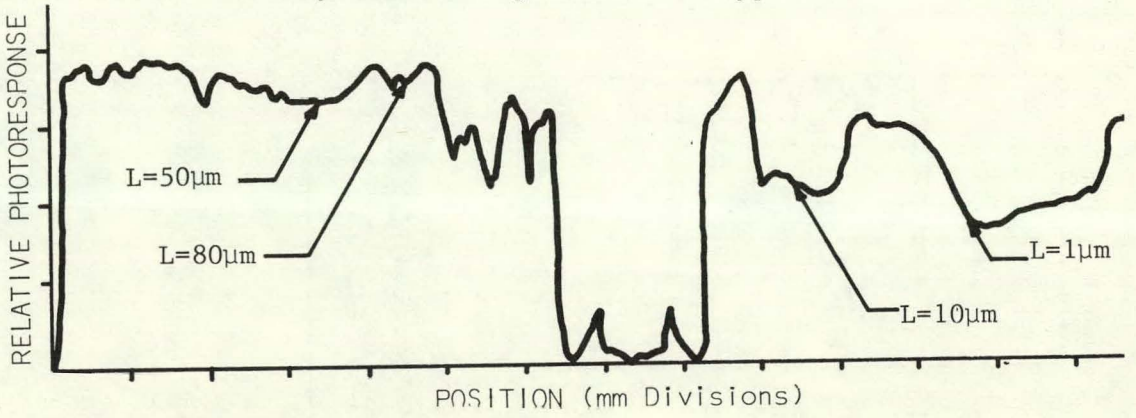

Figure 1. Line-Scan Measurements of the Variation in Photoresponse.

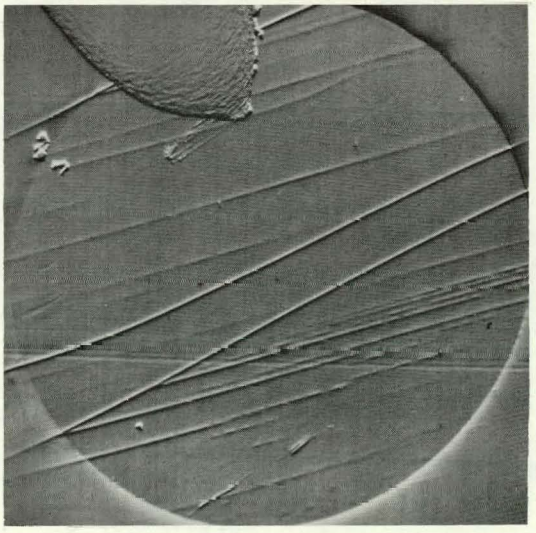

Fig.2a

G.B's

TWINS

Fig.2b

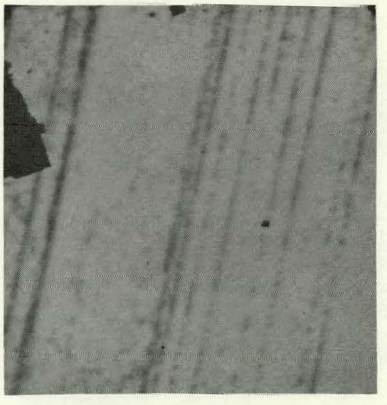

EBIC Pictures of Diodes 1 and 2

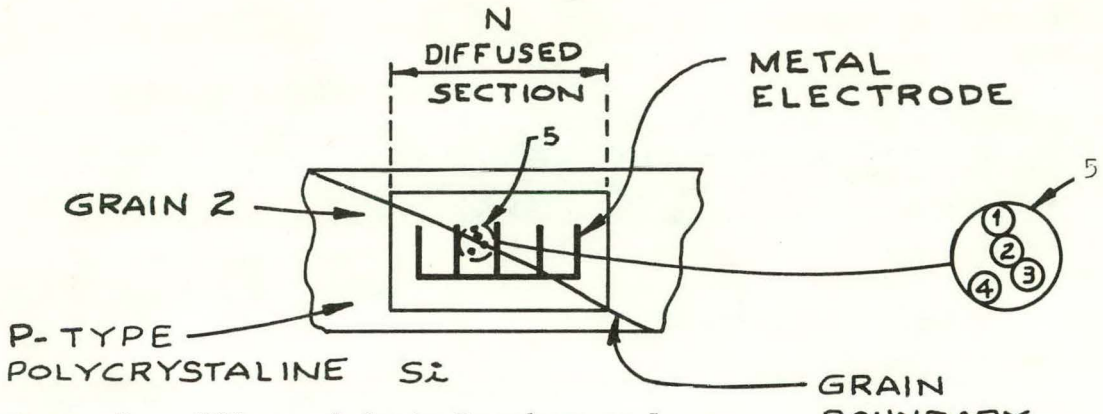

Figure 3a: Effect of Grain Boundary on L.
L_1=125μm, L_2=80μm, L_3=70μm, L_4=140μm, L_5=<L>=95μm, 0≃1mm Diameter Spot Size

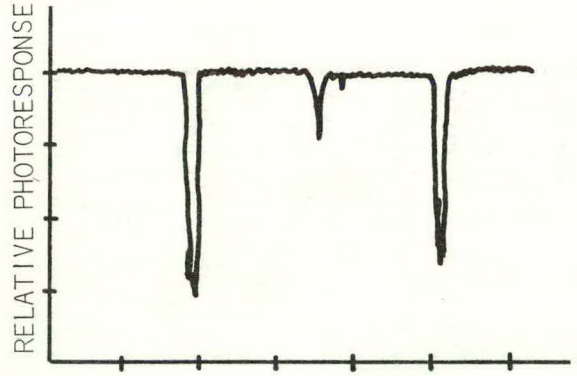

Fig.3b: FLS line scan, λ=0.6328 μm

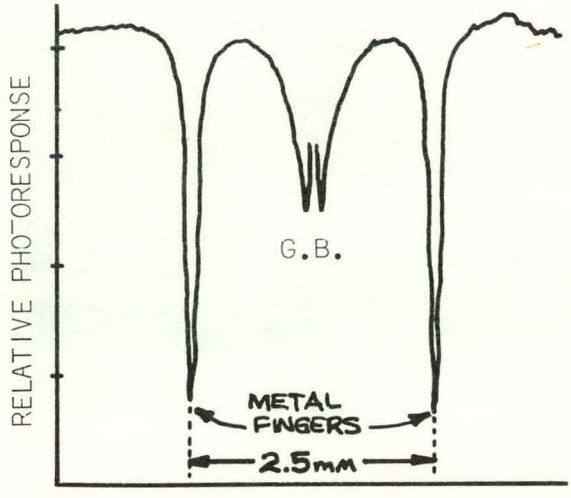

Fig.3c: FLS line scan, λ=1.15 μm

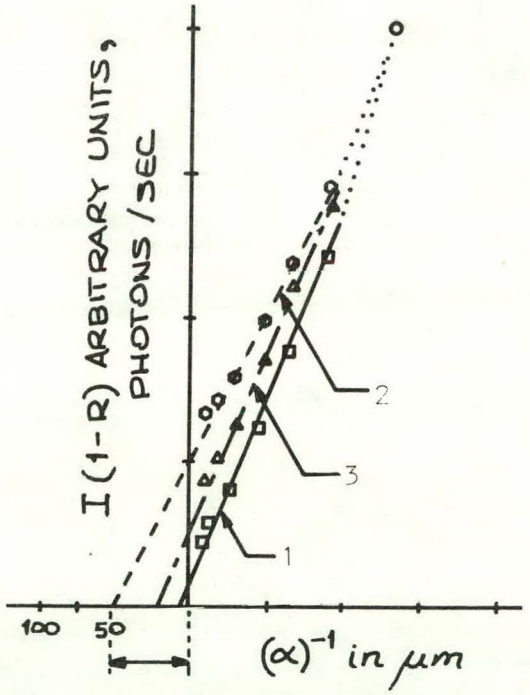

Fig. 4: SPV measurements on inhomogeneous cell.

NOTES

THIS PAGE
WAS INTENTIONALLY
LEFT BLANK

SCANNED LASER RESPONSE STUDIES OF CURRENT TRANSPORT IN POLYCRYSTALLINE CZOCHRALSKI AND DENDRITIC WEB SILICON MIS SOLAR CELLS

J. R. Szedon, T. A. Temofonte and T. W. O'Keeffe
Westinghouse Research and Development Center
Pittsburgh, PA 15235

To date, most considerations of polycrystalline silicon for solar cell applications have been based on the assumption that grain boundaries should act as surfaces of very high recombination velocity. Cell performance is expected to fall off as grain size is reduced, due to photocarrier loss by recombination at the boundaries and to increased diode opposing current associated with the grain boundaries. (1,2) It has been recognized that grain boundary behavior may be more complex than that just described, depending on details of the field conditions near the boundary. (3) Controlled diffusion producing collecting barriers at grain boundaries which contact that produced on the top surface has been reported. (4) Similar treatment to reduce the effective recombination velocity at grain boundaries might alleviate the performance degradation expected for very small grain sizes. Up to the present time, practical cell work on polycrystalline silicon has focussed on using materials with large grains (>200 μm), which behave as single crystal material of comparable diffusion length. (5,6)

A year ago work began at Westinghouse to investigate MIS solar cells on silicon material of good basic quality encompassing a range of grain sizes and distributions. Initially the approach was to determine if the grain size effects on short circuit current density and open circiut voltage were consistent with grain boundaries having very high surface recombination velocities. MIS cells were chosen since their processing can be done at low temperatures having less effect on grain boundary properties than, for example, the conditions associated with forming diffused junction barriers. Czochralski material grown using a polycrystalline seed was used for the initial work. A polishing etch procedure, adequate for removing saw damage in single crystal material (∿50 μm), produced preferential etching of the surface. Irregular features delineated by this etch were assumed to be grain boundaries.

The cells were evaluated in terms of their open circuit voltage vs. logarithm of short circuit current density. A range of irradiance values (50 to 1000 mW/cm^2) was produced by varying the distance between the cell under test and a quartz halogen lamp. For five small area (∿0.01 sq. cm) baseline cells having few or no discernible etch features, the characteristics were similar, with little spread in behavior. At irradiance values below 230 mW/cm^2, diode ideality (n) factor values were about 1.1. The spread in open circuit voltage values indicated about 30% higher opposing current in the poorest cell as compared with the best. For a similar cell with a high density of surface etch features, a somewhat larger n-factor value (1.5) was obtained and the diode opposing current was inferred to be about 90% higher than for the cell with the lowest V_{oc} value in the baseline group. For a larger cell with a comparable density of etch features a higher n-factor value (3.0) and a much lower value of V_{oc} were obtained for AM1 conditions. Ordinarily such results might be taken to support the

degrading effect of grain boundaries on cell performance. This would have been a premature conclusion for the experiments described. A second cell of 0.1 cm^2 size with a surface feature density comparable to that described above exhibited V_{oc} vs. log J_{sc} behavior nearly co-incident with that of the best base-line cell.

A second line of study was begun using scanned laser spot photocurrent response of selected MIS cells. (7) With this method, the electrical activity of grain boundaries can be observed directly, e.g. as shown in Fig. 1b. Comparison with a reflection image (Fig. 1a) produced by the same apparatus, reveals that many surface features have no direct correspondence with the grain boundaries of reduced photocurrent response. Many of the parallel features in the right hand portion of Fig. 1b are thought to be twin lines with no electrical activity. These results demonstrate that detailed studies of polycrystalline silicon require careful and definitive identification of electrically active grain boundaries. The scanned light spot apparatus handles this problem well and can provide additional information useful in analyzing material and cell behavior.

Figure 2 shows the region below the upper electrode finger in Fig. 1 at higher magnification, with emphasis on the portion involving a number of vertical, suspected twin lines (Fig. 2a). The terminuses of these lines lie along the upper branches of the "Y" shown in Fig. 2b. Figure 2c shows the effects of grain boundaries on the photocurrent amplitude along the horizintal line "B" in Fig. 2b. The response cusps in Fig. 2c indicate a maximum local photocurrent loss of 30 to 40% for the grain boundaries shown. The higher figure is typical of the darkest features in Fig. 1b.

From Fig. 1b, the length of the grain boundaries giving lower photocurrent response is estimated to be about 4.53×10^3 μm. In treating the grain boundary photocurrent response, an effective width of 16 μm is estimated for the region of reduced response from Fig. 2c. Thus, over the entire cell the affected area is about 7.2×10^4 μm^2. With the nominal cell area of about 8.6×10^5 μm^2, the grain boundary area of reduced current response is about 8% of the total. Since the maximum reduction in amplitude of response is estimated to be 40% locally, this implies that the overall short circuit response of the cell to light of the laser wavelength would be about 3% lower for the cell in question in comparison to one free of grain boundaries. Somewhat larger influences might be expected for longer wavelength excitation. Short circuit current for this cell was about 8% lower, under simulated AM1 illumination, than for similar cells free of grain boundaries.

An estimate of the expected effect in the cell of interest of the grain boundaries on open circuit voltage can be made. The length of grain boundary walls (assumed to penetrate through the wafer thickness of about 250 μm thickness) is 4.53×10^3 μm. Since both sides of the wall are expected to affect diode opposing current, the net area of the grain boundary walls is 2.3×10^6 μm^2. The overall area of the cell, including the grid, is 1.0×10^6 μm^2. For the observed reduction in V_{oc}, this cell requires an opposing current 1.9 to 2.3 times larger than in the monocrystalline cells on the same wafer. Thus, the density of opposing current from the grain boundary walls should be 40 to 60% of that for the

monocrystalline case, if opposing current from the planar areas is the same in both cases.

Similar studies were made on cells prepared in polycrystalline dendritic web silicon. This form of the material results under very particular growth conditions. For solar cell work it has the advantage of being composed of crystallites with the same basic orientation. Use of this material presents the opportunity to investigate grain boundary effects on solar cells in material of less complex polycrystalline nature than the Czochralski grown silicon. In particular, X-ray topography can be used to identify grain boundaries. Studies of photovoltaic behavior and of scanned light spot response for small MIS solar cells in the dendritic web material gave similar results to those for the Czochralski material.

This preliminary report is intended to highlight some of the problems in identifying electrically active features in polycrystalline silicon solar cells. The use of high resolution, scanned light photoresponse and reflection behavior are very usefull tools for this purpose. Using these for detailed analysis of polycrystalline material, we expect to elucidate influences of various heating and ambient treatments associated with annealing or cell fabrication. Such studies should establish the roles played by material grain size, purity and preparation and by cell processing in limiting solar cell performance.

This work was supported in part by U.S. Department of Energy Contract No. EY-76-C-03-1282. The authors are grateful to Dr. R. G. Seidensticker of the Westinghouse R&D Center for providing the polycrystalline dendritic web silicon.

REFERENCES

1. H. J. Hovel, Semiconductors and Semimetals Vol. II: Solar Cells, p. 103 ff, Academic Press, New York, N. Y. (1975).
2. S. I. Soclof and P. A. Iles, Proc. 11th IEEE Photovoltaic Specialists Conf., IEEE Cat. No. 75CH0948-OED, 56 (1975).
3. L. M. Fraas, J. Appl. Phys. 49:871 (1978).
4. T. H. DiStefano and J. J. Cuomo, Appl. Phys. Lett. 30:351 (1977).
5. H. Fischer and W. Pschunder, Proc. 12th IEEE Photovoltaic Specialists Conf., IEEE Cat. No. 76CH1142-9ED, 86 (1976).
6. J. Lindmayer, Proc. 13th IEEE Photovoltaic Specialists Conf., IEEE Cat. No. 78CH1319-3, 1096 (1978).
7. J. R. Szedon, T. W. O'Keeffe and T. A. Temofonte, ibid. p. 774.

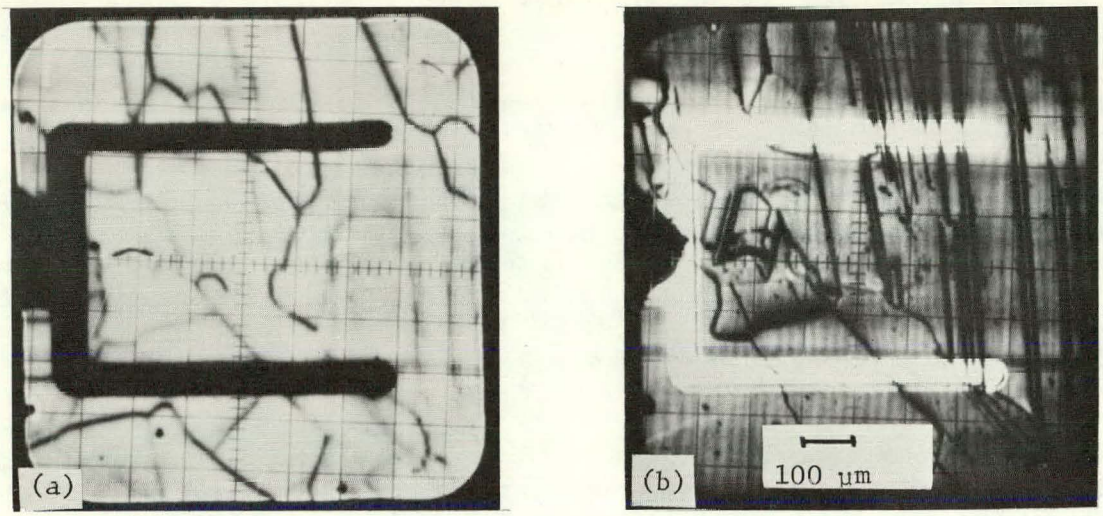

Figure 1. (a) Reflection and (b) photocurrent images of a laser (6330 Å) scanned, Al-SiO_2-pSi solar cell produced in polycrystalline Czochralski Si.

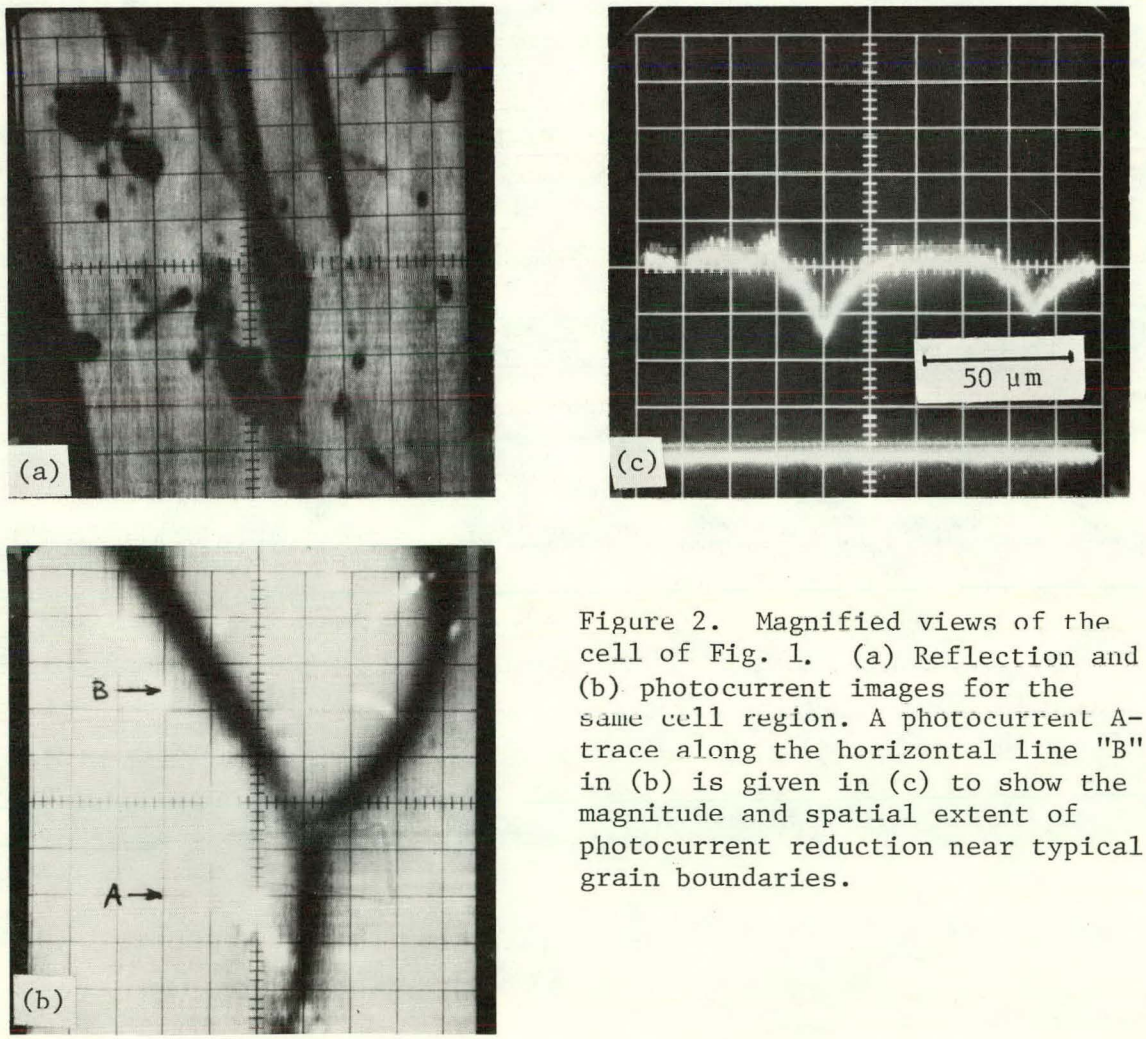

Figure 2. Magnified views of the cell of Fig. 1. (a) Reflection and (b) photocurrent images for the same cell region. A photocurrent A-trace along the horizontal line "B" in (b) is given in (c) to show the magnitude and spatial extent of photocurrent reduction near typical grain boundaries.

NOTES

THIS PAGE
WAS INTENTIONALLY
LEFT BLANK

INFRARED ELECTROLUMINESCENCE AS A DIAGNOSTIC TOOL FOR POLYCRYSTALLINE GaAs SOLAR CELLS*

G. W. Turner, J. C. C. Fan and J. P. Salerno
Lincoln Laboratory, Massachusetts Institute of Technology
Lexington, Massachusetts 02173

We have found that infrared electroluminescence is an effective diagnostic tool for characterizing polycrystalline GaAs solar cells. Initial experiments on single-crystal GaAs shallow homojunction cells, which utilize an $n^+/p/p^+$ structure with electroplated contact metallization and an anodized antireflection coating, showed that increased intensity and uniformity of the electroluminescent emission from forward biased cells is correlated with improved photovoltaic response. Such a correlation has also been reported for single-crystal GaAlAs-GaAs heteroface solar cells[1]. We have extended the electroluminescence technique to the study of cells with the same $n^+/p/p^+$ shallow-homojunction structure that are fabricated on polycrystalline GaAs layers grown by chemical vapor deposition (CVD) on large-grained substrates of either GaAs or Ge. Two cell configurations have been used. In the first, small (0.002 cm^2) circular cells are fabricated in a dense, regular pattern that yields devices located on single and multiple grain boundaries as well as on areas free from grain boundaries. The second configuration utilizes larger (0.063 cm^2) rectangular cells having four contact fingers, permitting the observation of devices extending over multiple grains. For both configurations, electroluminescence from individual cells is excited by using a curve tracer and either observed with an infrared microscope sensitive to wavelengths between 0.8 and 1.2 μm or spectrally analyzed with a grating spectrometer. As in the case of single-crystal cells, the intensity and uniformity of the electroluminescence from the polycrystalline cells correlates with the photovoltaic response. The information that can be obtained by this method includes: observation of grain boundaries, including those not detected by optical microscopy; differentiation of "active" and "passive" grain boundaries; observation of metallization imperfections due to abrupt surface morphology of the CVD layers; and the detection of junction inhomogeneities due to uneven growth, crystallographic defects, etc. A typical photomicrograph obtained by the electroluminescence technique for one of the larger cells is shown in Fig. 1, together with a photomicrograph of the same cell obtained by the EBIC technique. Each of these techniques has specific advantages and disadvantages in the analysis of the cell response. Further development of the electroluminescence technique, including the fabrication of polycrystalline cells with transparent electrodes in order to permit observation of transmitted infrared radiation, is in progress.

1. S. Kamath and G. Wolff, final technical report AFAPL-TR-78-76, Jan. 1979.

*This work was sponsored by the Department of Energy and the Department of the Air Force.

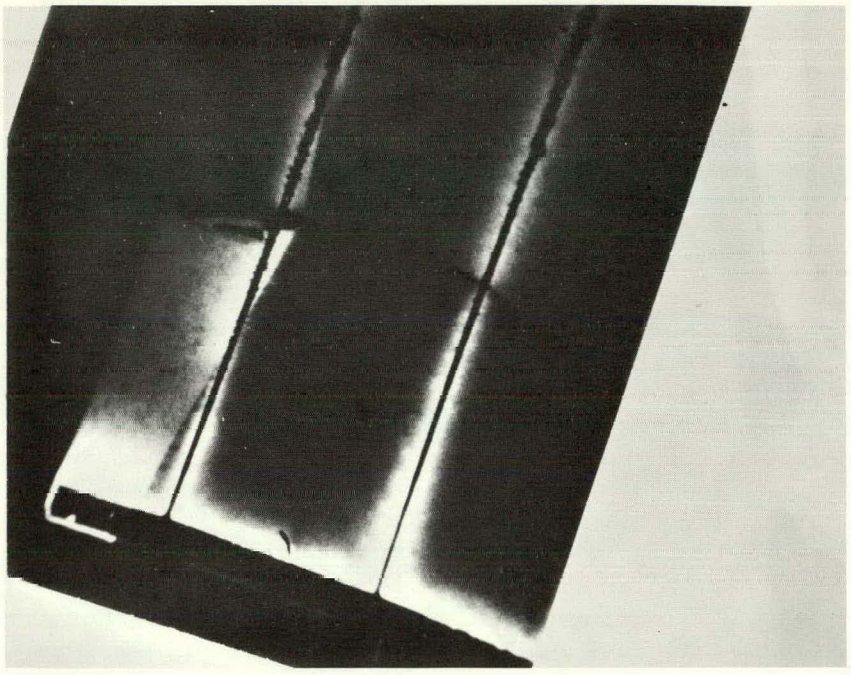

(A)

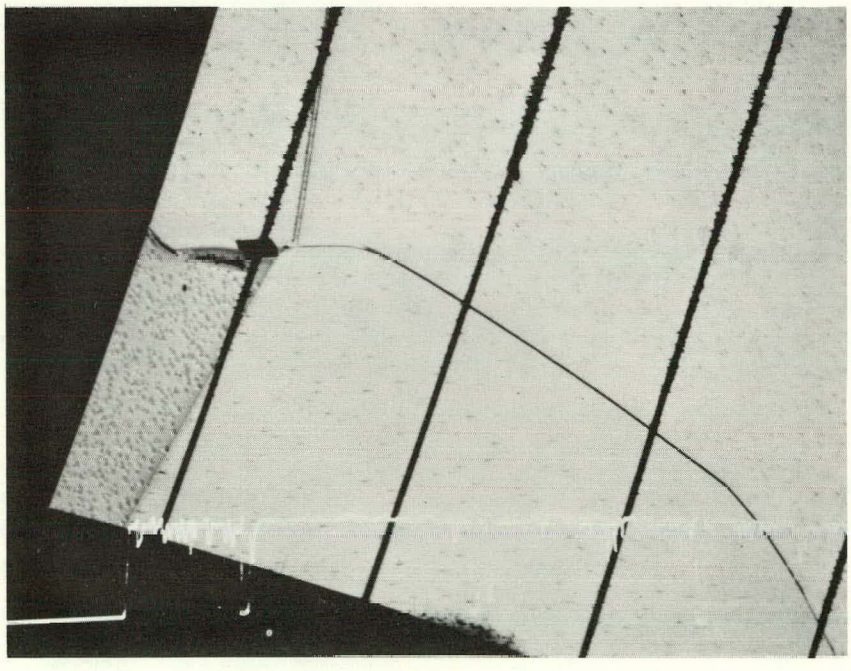

(B)

Fig. 1. (A) Infrared Electroluminescence
(B) E. B. I. C. (with Amplitude Trace)

The views and conclusions contained in this document are those of the contractor and should not be interpreted as necessarily representing the official policies, either expressed or implied, of the United States Government.

NOTES

STUDY OF GRAIN BOUNDARIES IN GaAs BY SCANNING LIGHT MICROSCOPY

R. Fletcher, D.K. Wagner, & J.M. Ballantyne
School of Electrical Engineering
Cornell University
Ithaca, N.Y. 14853

Scanning Light Microscopy (SLM) is a useful tool for investigating the electronic structure of grain boundaries in polycrystalline semiconductors. It reveals directly the presence or absence of electric fields associated with the grain boundary and can be used to measure localized values of the minority carrier diffusion length in its immediate vicinity.

The technique consists of measuring one of a number of specimen properties as a focussed light spot is raster-scanned over a small area of the specimen surface by means of suitably controlled orthogonal mirrors in the beam path.[1,2] In our system a HeNe laser (633 nm) is used as the light source and the spot diameter is 1 μm. Of special interest are measurements of the dc short-circuit photocurrent, since these can be used to reveal directly the presence of lateral internal fields in the semiconductor. When the light spot scans such a region, photogenerated electron-hole pairs are separated by the field causing current to flow in an external short circuit. Similarly, under open-circuit conditions a photovoltage is registered as the photogenerated charges are separated by the internal fields. It is also possible to measure short-circuit photocurrent under voltage bias; this enables one to follow the rearrangement of the internal fields with bias.

We have studied a number of grain boundaries via SLM in GaAs bicrystals prepared from unintentionally doped (n-type) polycrystalline source material. We have also investigated epitaxial layers (n-type) grown by LPE and MBE on semiinsulating bicrystal substrates, but the results tend to be more complex; consequently, we shall report here principally the results on bulk bicrystals.

The grain boundaries fall into two categories: those with internal fields and those with none. In all cases we have measured, those specimens with internal fields detected by SLM exhibit a highly nonohmic current-voltage (I-V) relationship across the grain boundary. Such specimens block current up to approximately ± 10V, then conduct precipitously. In contrast, specimens with no internal fields behave ohmically.

The nonohmic behavior is similar to that observed previously in Ge,[3]

and can be explained on the basis of negatively charged states at the grain boundary, which results in the formation of a space-charge region on both sides of the boundary. This model, which has been analyzed in detail by Taylor, Odell, and Fan,[3] predicts blocking action up to a bias voltage of $\pm 4\phi/q$ as long as the charge at the interface remains fixed with bias. (ϕ is the zero-bias barrier height at the grain boundary and q is the electronic charge.) Our measurement of the zero-bias conductance as a function of temperature indicates that the barrier height ϕ is substantial, i.e., $\phi = 0.8$ eV. Evidently, the interface charge increases with bias because the observed onset of conduction at 10V exceeds $4\phi/q$ by approximately a factor of three.

In most cases the detailed structure of the photocurrent as a function of distance of the spot from the grain boundary can be understood in terms of the Taylor, Odell, and Fan model. The photocurrent changes sign abruptly at the grain boundary, then decays smoothly to zero on either side. The change in sign reflects the discontinuity of the electric field at the grain boundary, while the decay is caused by the diffusion of holes to the depletion edge and varies as $\exp(-|x|/L_p)$, where x is the distance of the light spot from the grain boundary and L_p is the diffusion length for holes. Exponential fits to the decay yield values of L_p between 1 and 2 μm.

The structure of the photovoltage is very similar to that of the photocurrent, but as a rule the decay away from the depletion edge is less rapid and varies markedly from specimen to specimen. The decay can be made nearly as rapid as that in the photocurrent by flooding the specimen with white light. (Flooding with light does not alter the structure of the photocurrent.) This observation suggests that the ambient concentration of holes at the normally depleted surface is influencing the photovoltage.

By biasing the specimen and measuring short-circuit photocurrent, the shift in fields from one side of the grain boundary to the other can be observed. The shift occurs at very low bias levels of approximately 30-50 mV and appears at first to be inconsistent with a barrier height of 0.8 eV. However, it must be remembered that the light is absorbed very close to the surface (within ~1/4 μm), and photogenerated holes are swept to the surface by the fields associated with the depleted surface. There the energy of the holes (with respect to the top of the valence band in the bulk) is comparable to the barrier height. Thus, the two results are in fact consistent.

This work was supported through a subcontract with the Rockwell International Science Center in a program supported by the U.S. Department of Energy (Contract No. EG-77-C-03-1712) and administered by the Solar Energy Research Institute.

1. T. H. DiStefano, NBS Special Publication 400-23, 197 (1976).

2. C. N. Potter & D. E. Sawyer, Rev. Sci. Instrum. 39, 180 (1968).

3. W. E. Taylor, N. H. Odell, & H. Y. Fan, Phys. Rev. 88, 867 (1952).

NOTES

THIS PAGE

WAS INTENTIONALLY

LEFT BLANK

Charge Transport Session

BARRIER HEIGHTS AND PASSIVATION OF GRAIN BOUNDARIES IN POLYCRYSTALLINE SILICON*

C. H. Seager and D. S. Ginley
Sandia Laboratories,† Albuquerque, New Mexico 87185

A simple, frequently presented model for the electronic structure of a grain boundary in an n-type semiconductor is shown in Fig. 1. We have recently completed an extensive series of transport measurements on single grain boundaries in neutron transmutation doped polysilicon with the intent of investigating the applicability of this model. If thermal emission of electrons over the barrier predominates, the zero-bias conductance, G_o, across such a barrier will be proportional to $e^{-\phi_B/kT}$ and the observed activation energy, E_{ACT}, of this quantity will be $\left[\phi_B - \frac{T\partial\phi_B}{\partial T}\right]$. Seager and Castner[1] observed such an Arrenhius behavior for G_o above 270 K for large mismatch angle barriers in silicon; a plot of their activation energies versus dopant density is shown in Fig. 2. If ϕ_B is linear in temperature (as simple theory would suggest), E_{ACT} is $\simeq \phi_B$ (T = 0), hence the vertical scale of Fig. 2 can be interprcted as the low temperature barrier height. The general N_d dependence of these data is in accord with expectations. As the donor density decreases an increasingly smaller amount of excess negative charge is transferred to the boundary (for a fixed value of φ_B). This leaves the Fermi energy in the barrier near its value in the neutral condition (E_{FB} in Fig. 1).

Fig. 1

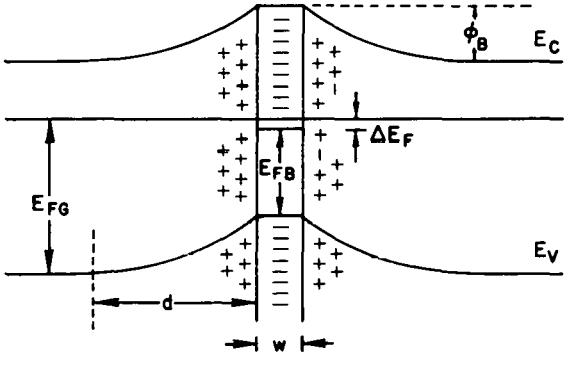

Fig. 2

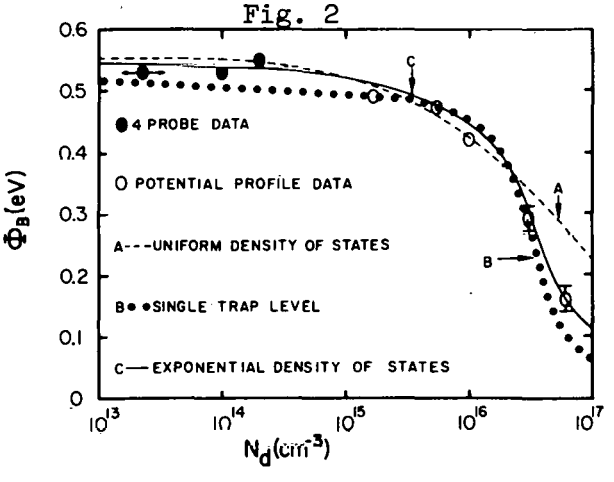

Thus, the barrier height in this "saturated regime" should be constant and equal to $E_{FG} - E_{FB}$; if E_{FB} is temperature independent, this implies a constant value of E_{ACT} (as observed) equal to $E_C - E_{FB}$.

We have made more extensive measurements of G_o on samples lying in this saturation regime; measurements of the zero-bias barrier capacitance, C_o, have also been completed--these latter data give direct information about ϕ_B since:

$$C_o(\text{per m}^2) = \left(\frac{eN_d \epsilon \epsilon_o}{8\phi_B}\right)^{1/2} . \qquad (1)$$

Figure 3 shows the values of ϕ_B deduced from 4 probe capacitance measurements on several samples having a donor density of 1.43×10^{15} cm^{-3}. In agreement with our simple picture, ϕ_B appears to have a temperature dependence very close to that of E_{FG}; furthermore, the deduced value of E_{ACT}, ~ 0.6 ev, is close to that observed by Seager and Castner[1] in this regime.

Measurements of G_o over a wide temperature range for these samples reveal that the situation is not without complications, however (Fig. 4). In the range where most of the capacitance values could be determined with sufficient accuracy very substantial deviations of the slope of G_o towards lower values are evident. The extent of this non-Arrenhius regime varies substantially from sample to sample, as shown, while the capacitance behavior of all samples is virtually identical from 200 to

Fig. 3

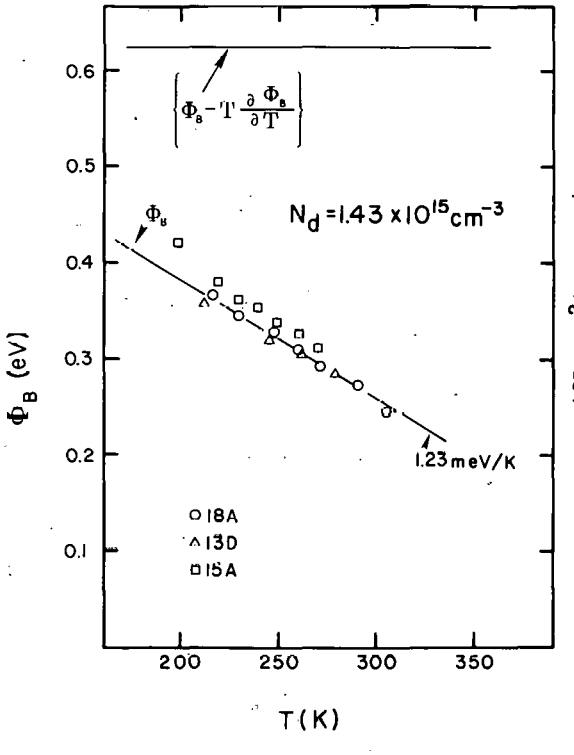

Fig. 4

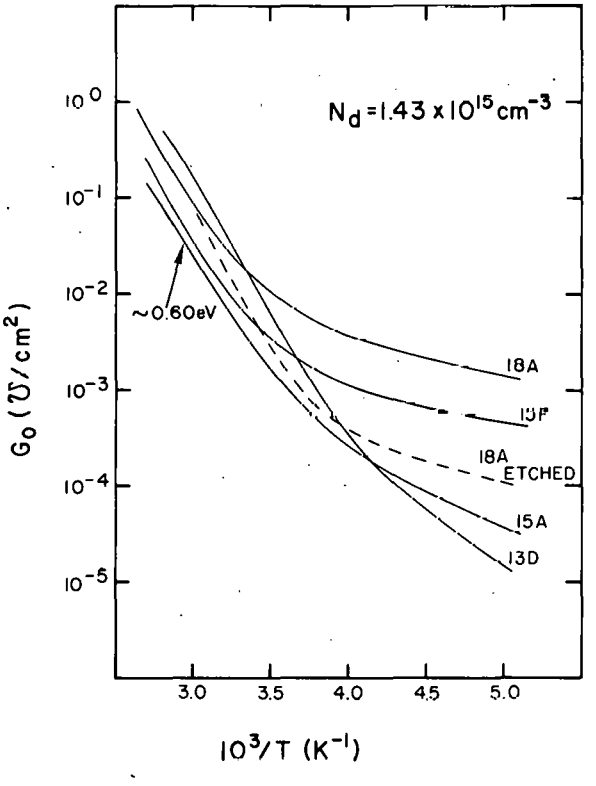

300 K. A clue as to how this behavior can be understood can be obtained by examining the data for sample 18A. After etching off about 5-10 μm from the surface of the specimen bar, the low temperature conductance decreased more than a decade while the capacitance changed only by the few percent expected from the reduction in barrier cross-sectional area. This etch undoubtedly removed a considerable amount of the damage introduced while sawing the sample to size, and this observation suggests that dislocations and stacking faults crossing the grain boundary can lead to substantial current shunting at low temperatures. Such shunts would not be expected to affect measurements of the parallel equivalent capacitance. We thus suggest that the high temperature Arrenhius regime in the G_o data reflects the "intrinsic" behavior of the grain boundary barrier. More data on samples doped to higher phosphorous concentrations are presently being obtained to check these conclusions.

Further information about the electronic structure of grain boundaries can be obtained by measuring the bias dependence of grain boundary barrier conductance and capacitance. Recent theoretical work by Pike and Seager[2] has resulted in a model for the bias dependence of G; they show that data of this type can be used to unfold the density of grain boundary electronic states above the zero-bias Fermi level (for n-type grains). We will discuss data of this type obtained on single boundaries. The importance of the effects of current shunting via defects will be emphasized and some suggestions will be made concerning modifications of the original theoretical assumptions made by Pike and Seager.[2]

Given the modest degree of understanding of grain boundary properties discussed above, several facts concerning their effects on the operation of polycrystalline photovoltaic devices become clear. The first is that the substantial depletion regions present near grain boundaries at doping levels in the 10^{15} - 10^{17} cm^{-3} range will act as very effective minority carrier traps. Secondly, it is also the very states causing these depletion layers which are likely to be the most effective recombination sites

Fig. 5

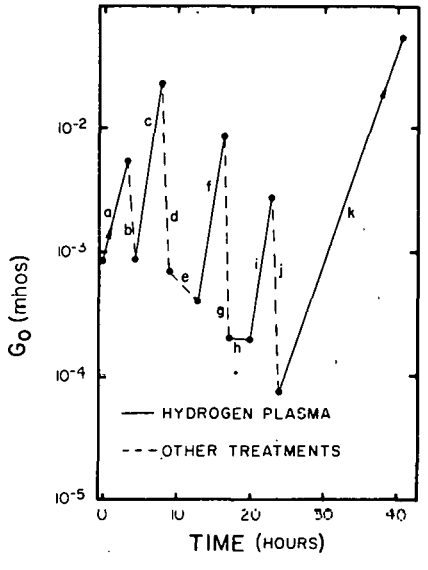

Fig. 6

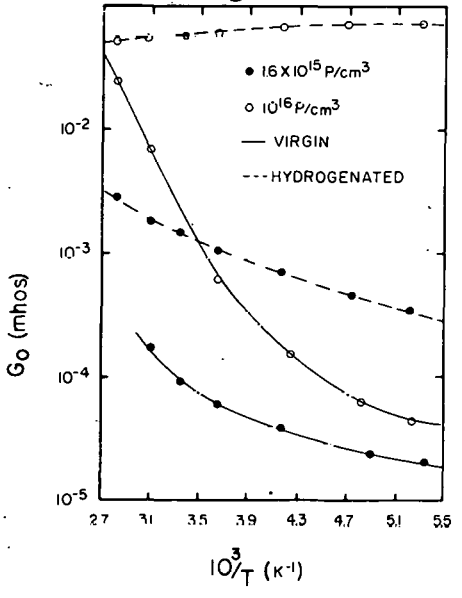

for trapped minority carriers. Prior work on the energy levels associated with the dangling bonds at edge dislocations makes these specific defects a likely choice for the near midgap states inferred from grain boundary measurements.

Recent experiments at Sandia Laboratories[3] and at IBM[4] suggest that the electronic character of these grain boundary states can be markedly changed via in-diffusion of monatonic hydrogen at elevated temperatures. Figure 5 shows the results of a series of such treatments on the conductance of a single boundary (of ~ 1 mm^2 area) in silicon. The hydrogen plasma treatments (ambient ~ 320-380°C) are seen to markedly increase the boundary conductance while the other types of treatments (heating in vacuum at ~ 600°C) designed to drive out the hydrogen, return the boundary to a lower conductance state. Because of the relationship between G_o and ϕ_B, we expect that the marked increases in G_o seen after hydrogen exposure reflect a substantial lowering of ϕ_B--implying a removal of many of the defect states caused by the grain-to-grain mismatch. The data in Fig. 6 reinforces the explanation of barrier height lowering by showing that hydrogenation causes substantial decreases of E_{ACT} relative to the virgin state. Further work has shown that the effects of these hydrogen treatments only extend some 25-100 μm into our bulk polysilicon samples. This suggests that even larger conductance changes could be effected by the treatment of thin films of fine grained silicon. We have recently obtained data that bears out these expectations. Discussions of the kinetics of this process will also be presented.

Finally, we will discuss the results of hydrogenation of some primitive polysilicon photovoltaic devices. Substantial improvements in device efficiencies, fill factors, minority carrier lifetimes, and long wavelength spectral response have been seen following these treatments. The implications of these data suggest that hydrogenation may be a viable treatment for the passivation of silicon grain boundaries, enhancing the prospects for the production of cheaper, more efficient thin film silicon solar cells.

*This work sponsored by the U.S. Department of Energy under Contract DE-AC04-76-DP00789.
†A U.S. Department of Energy facility.

REFERENCES

1. C. H. Seager and T. F. Castner, J. Appl. Phys. 49, 3879 (1978).

2. G. E. Pike and C. H. Seager, J. Appl. Phys., in press.

3. C. H. Seager and D. S. Ginley, Appl. Phys. Lett. 34, 337 (1979).

4. D. R. Campbell, M. H. Brodsky, C. M. Hwang, R. E. Robinson, and M. Albert, Bull. Am. Phys. Soc. 24, Abstract JK8, p. 435 (1979).

NOTES

THIS PAGE

WAS INTENTIONALLY

LEFT BLANK

ELECTRICAL TRANSPORT PROPERTIES IN INHOMOGENEOUS MEDIA

R. Landauer
IBM Thomas J. Watson Research Center
P. O. Box 218, Yorktown Heights, New York 10598

The oral version of this paper contained selected subsections of a recently published review.[1] The abstract of the earlier review follows:

The history of this field is reviewed, with emphasis on the relationship to the development of molecular field concepts in dielectric theory, in the last century, and with emphasis on the relationship to the study of disordered structures, in recent decades. A few of the many methods for calculating effective conductivities will be presented and discussed. One of these is based on the direct macroscopic application of the Clausius-Mossotti relationship. In that connection we emphasize the shortcomings of the commonly accepted Lorentz derivation for the internal field and restate a less well known existing alternative derivation. The symmetrical and unsymmetrical effective medium theories of Bruggeman are presented. Connection is made to transport in randomly chosen resistor networks, to percolation threshold problems, and to transport in magnetic fields in the presence of inhomogeneities. Two more specialized topics are also discussed. One of these is the variability in field effect transistor thresholds arising from the limited size of the samples in which threshold is determined by the onset of percolation. The other specialized topic: The occurrence of strong spatial inhomogeneities in fields and currents in metals, in the presence of lattice defects, even though the mean free path is large compared to the extent of the defect.

[1] Electrical Transport and Optical Properties of Inhomogeneous Media, J. C. Garland, D. B. Tanner, eds. (American Institute of Physics, New York, 1978)pp. 2-45.

NOTES

GRAIN BOUNDARY RESISTANCE MEASUREMENTS IN POLYCRYSTALLINE GaAs

M. J. Cohen, J. S. Harris, Jr. and J. R. Waldrop
Rockwell International Science Center
Thousand Oaks, California 91360

The electronic transport processes in polycrystalline materials which dominate their behavior and determine their application to solar cells are: (i) majority carrier flow via drift perpendicular to grain boundaries, and (ii) minority carrier flow by diffusion both perpendicular and parallel to the grains. These processes are influenced by scattering, trapping and recombination, as well as by potential barriers along grain boundaries which result from lattice distortions, dangling bonds, or an accumulation of impurity atoms.

Increased photocarrier recombination at grain boundaries competes with minority carrier diffusion to the junction and reduces the short circuit current of solar cells. The open circuit voltage is reduced through leakage currents due to grain boundaries which traverse the junction. The added series resistance due to the reflection of majority carriers by the potential barrier at grain boundaries further reduces the power which can be extracted from polycrystalline solar cells.

Until the carrier transport properties in polycrystalline materials are understood, it will be impossible to develop accurate models of polycrystalline solar cell performance. The models are essential to provide a sound basis for optimized polycrystalline cell design. We have used Auger Electron Spectroscopy to perform the first measurements of the resistivity of a single grain boundary in polycrystalline GaAs and discuss the implications to solar cell performance.

The measurements described in this talk were performed on both unintentionally doped bulk GaAs and on layers of n-GaAs (Sn doped) grown on semi-insulating GaAs substrates by Molecular Beam Epitaxy (MBE). The samples all contained a relatively long single grain boundary oriented perpendicular to the surface. Ohmic contacts were applied which either spanned the grain boundary or were located entirely within a single crystal region.

The samples were mounted on TO5 headers and loaded in a Science Center designed and built Scanning Auger Microscope which is essentially an ultra high vacuum scanning electron microscope (all metal seals, 7×10^{-9} Torr without baking) which contains a miniaturized cylindrical mirror Auger analyzer.

In the Auger process, a high energy electron (20 KeV in our case) strikes an atom and the interaction results in the ionization of one of its core electrons. The atom relaxes to its ground state by the ionization of an electron whose kinetic energy is characteristic of the transition involved and the atom from which it was emitted. As the escape depth of an Auger electron is relatively short (10-20Å), Auger analysis is a useful surface chemical analysis tool and when performed in a SAM, chemical information

from an area <1μm can be obtained.

An important subtlety is that the emitted electron has a characteristic energy relative to the potential of the host atom while the Auger analyzer is always referenced to laboratory ground. When a sample is biased away from ground, the entire Auger spectrum is shifted by an energy proportional to the bias voltage. This effect is demonstrated in Fig. 1 where the 272 eV carbon line is shown under various bias conditions. In the Auger potential profiling experiment, a voltage is applied between the two ohmic contacts and the potential profile across the sample is determined by using the energy shift of the 272 eV line as a spatially resolved contactless voltmeter.

Figures 2a and 2b show the results of the Auger potential profiling experiment performed on a lightly doped MBE sample ($n = 2 \times 10^{15} cm^{-3}$) without and with a grain boundary, respectively. A potential of 4V was applied across the sample without the grain boundary. As observed in Fig. 2a, the two ohmic contacts are at equipotentials (oV and 4V) and the voltage increases linearly between the contacts. This linear behavior indicates a spatially homogeneous conductivity throughout the sample. The electric field observed of $E = 2 \times 10^{3} V/cm$ and the measured current of $4.8 \times 10^{-4} A$ agrees with the measured mobility (6450 $cm^2/V\text{-sec}$) and net carrier concentration ($2 \times 10^{15} cm^{-3}$).

Figure 2b shows the results of the same experiment performed on a lightly doped sample containing a grain boundary. In this case 6V was applied across the sample with a resulting current of $6.2 \times 10^{-4} A$. Starting from the left ohmic contact, the voltage increases linearly across the sample with a slope of $2.4 \times 10^{3} V/cm$. In the vicinity of the grain boundary, the voltage increases more rapidly and eventually straightens to approximately the same electric field as on the left side of the grain boundary. The voltage drop across the grain boundary (the displacement of the two straight lines shown in the figure) is 1.6 V. The electric field strength in the single crystal region on either side of the grain boundary together with the measured current again are in agreement with the carrier concentration and mobility determined by Hall measurements.

The data can be understood in terms of a simple model in which the existance of localized band gap interface states at the grain boundary pin the fermi levels in the single crystal regions on either side resulting in a double depletion region (Fig. 3). Using this model, the potential profile data can be used to determine the potential barrier to majority carrier transport due to the grain boundary.

In order to further explore the implications of this model, we have performed I-V, C-V and EBIC measurements as well as Auger Potential Profiling measurements on unintentionally doped bulk material. These data will be presented and their implication to polycrystal solar cell performance will be discussed.

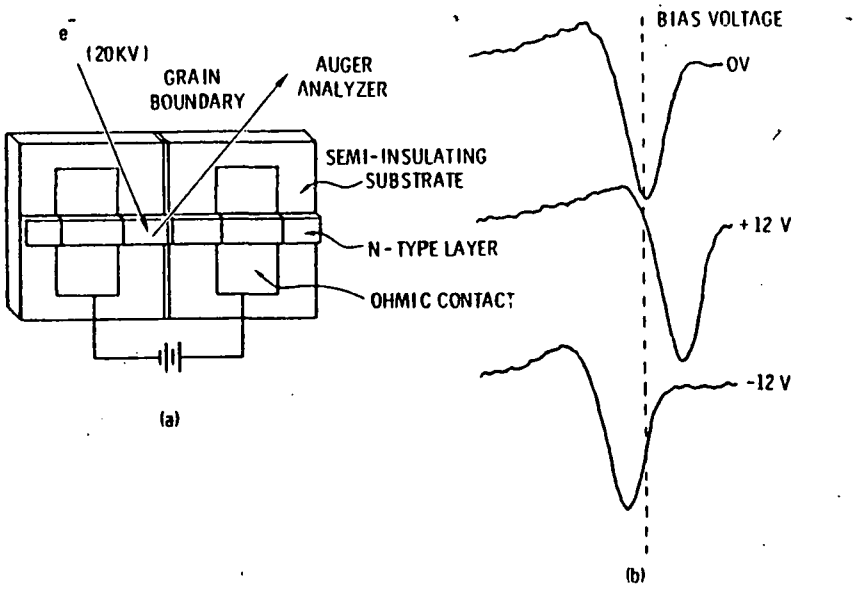

Fig. 1. (a) Schematic of Auger Potential Profiling experiment. (b) Carbon 272 eV Auger line under various bias conditions.

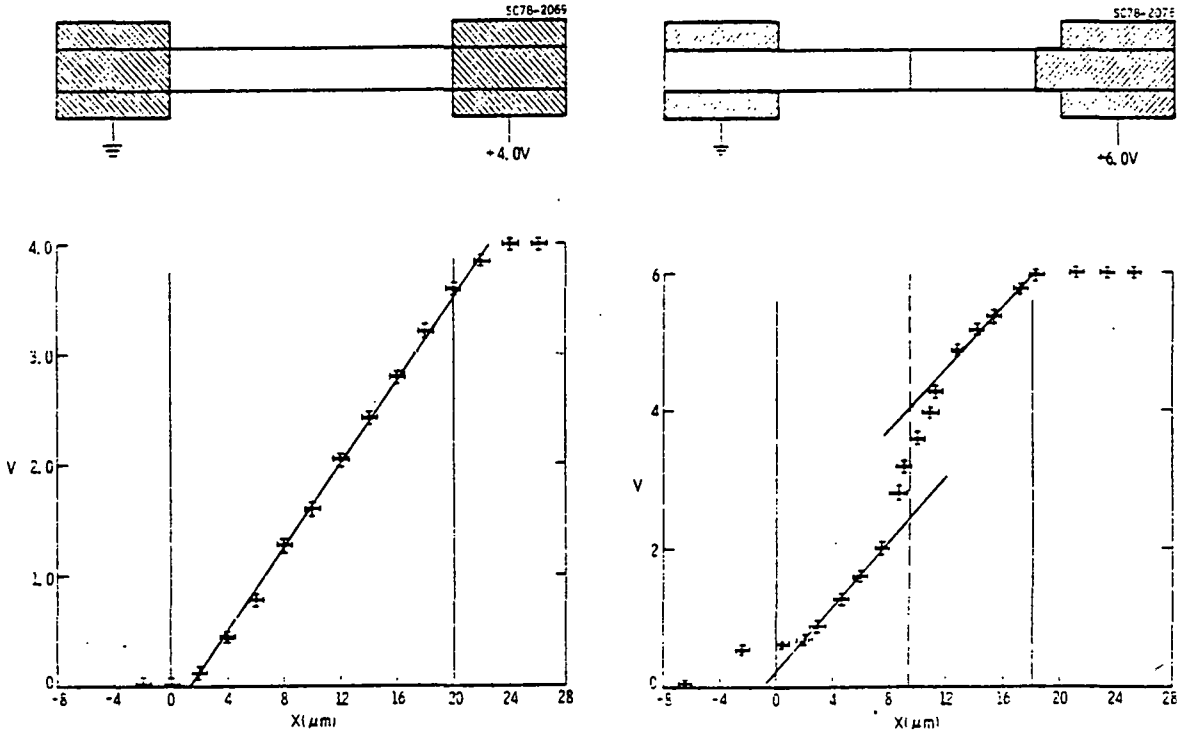

(a) (b)

Fig. 2. (a) Potential profile of single crystal MBE sample. (b) Potential profile of bicrystal MBE sample (see text).

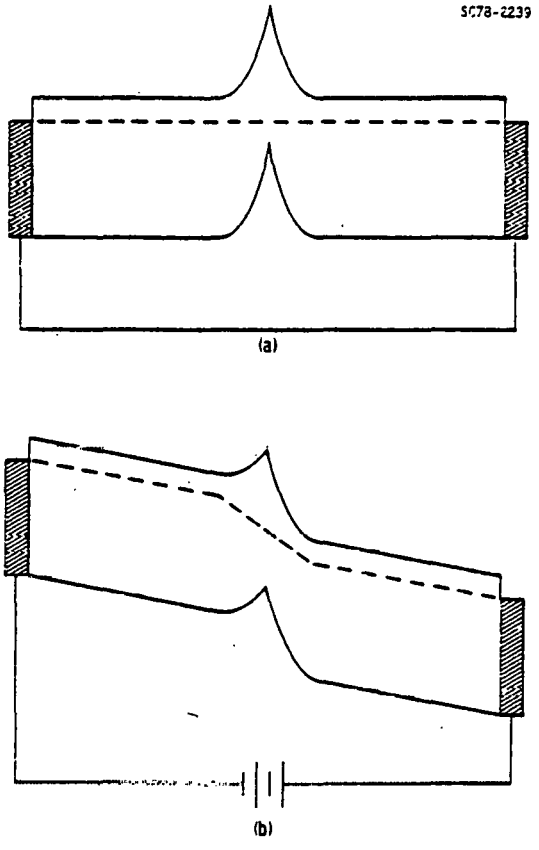

Fig. 3. Band structure in vicinity of grain boundary for sample (a) in equilibrium and (b) under bias (see text).

NOTES

THIS PAGE

WAS INTENTIONALLY

LEFT BLANK

EFFECT OF INTERFACE RECOMBINATION AT p-n JUNCTION PERIMETERS ON PHOTOLUMINESCENCE AND CURRENT

C. H. HENRY
Bell Laboratories
Murray Hill, New Jersey 07974

The interfaces forming the perimeters of $Al_xGa_{1-x}As$ p-n junctions, such as cleaved surfaces or etched surfaces are regions of intense nonradiative recombination. Almost all of the p-n junction 2kT current is due to recombination at these nonradiative perimeters. When an uncontacted sample is studied in photoluminescence, these interfaces produce broad nonradiative regions known as large dark spots. The rate of interface recombination can be quantitatively evaluated from measurement of either the 2kT current or the large dark spot line shape. The 2kT current is usually explained in terms of the Sah, Noyce, and Shockley model of p-n depletion layer recombination. We develop an alternative model in which we show that recombination at a depleted surface will have 2kT character.[1,2] The rate of surface recombination is $R = s_o(np)^{1/2} = s_o n_i \exp(eV/2kT)$ where $s_o \approx 4\times10^5$ cms^{-1} for x = 0.08 active layers with etched surfaces. This form of the recombination rate follows naturally from the requirement that the interface remain neutral. This model should be applicable to describing the effect of other defects cutting across p-n junctions, such as grain boundaries or dislocations.

1. C. H. Henry, R. A. Logan and F. R. Merritt, J. Appl. Phys. 49, 3530 (1978).

2. C. H. Henry and R. A. Logan, J. Vac. Sci. Technol. 15, 1471 (1978).

NOTES

GRAIN BOUNDARY EFFECTS AND CONDUCTION MECHANISM STUDIES IN CR-MIS SOLAR CELLS ON POLYCRYSTALLINE SILICON*

W. A. Anderson, S. L. Hyland,** A. E. Delahoy,**, and K. Rajkanan
State University of New York at Buffalo
Electrical Engineering Department
4232 Ridge Lea Road
Amherst, New York 14226

Introduction

Studies of photovoltaic processes in polycrystalline silicon are being conducted to evaluate the use of this material as a potential low-cost replacement of the more costly single crystal silicon cell. The MIS structure is selected because of the ease of fabrication and adaptability to a future low-cost process. The Cr-MIS design has produced a 12.2% efficiency [1] on single crystal silicon using a process applicable to the polycrystalline silicon material. Wacker "Silso" silicon was selected for study because of its availability and proven performance in p-n junction formation. The object of this study was to gain some initial insight into the effect of grain boundaries on photovoltaic and dark response of polycrystalline solar cells. Data on photovoltaic response, spectral response, laser scan studies, conduction mechanisms, and surface states will be considered herein.

Summary

Wacker "Silso" silicon samples were chemically polished to present a suitable surface for a MIS solar cell. The Si. was etched in CP4A, rinsed in deionized water, heated in O_2 at 950° C to grow an oxide, and finally rinsed in HF and then deionized water to remove the oxide prior to fabrication [1]. A Cr-MIS solar cell was fabricated by thermal evaporation to produce a 5 Å Cr/50 Å Cu/30 Å Cr/20 Å oxide/ Si structure [1]. A peak AM1 photovoltaic response of V_{oc} = 0.50 V, J_{sc} = 24.2 mA/Cm^2, FF = 0.73 and efficiency = 8.8% has been obtained using this design on "Silso" silicon.

Spectral response data were obtained using a Schoeffel GM100 monochromator and a reference cell calibrated at NASA-Lewis Research Center [2]. These data show the polycrystalline samples to have a lower infrared response than similar samples on single crystal silicon. The diffusion length was obtained using the technique outlined by Stokes and Chu [3] and showed a 15-50% lowered value when compared to 70 μm measured on single crystal silicon. Figure 1 shows a plot of J_{sc} as a function of

* Research supported by the Department of Energy.

** Rutgers University
Electrical Engineering Department
P.O. Box 909
Piscataway, New Jersey 08854

measured diffusion length. Data points for polycrystalline silicon cells are compared to a theoretical curve based on single crystal silicon.

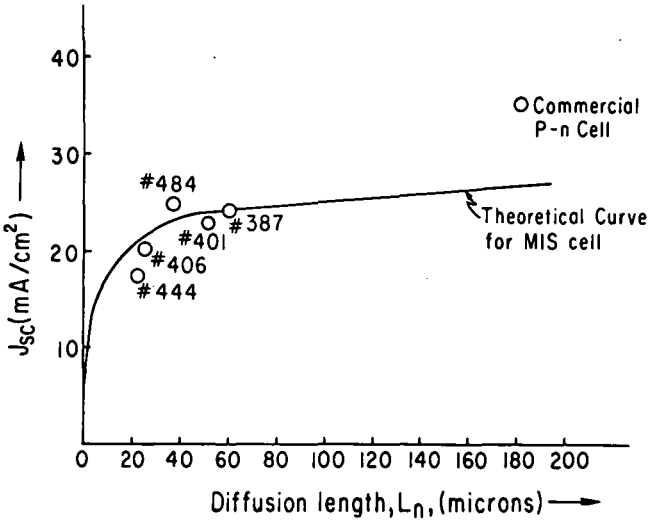

Figure 1: Short-Circuit current density as a function of diffusion length for polycrystalline Si. MIS solar cells.

Two laser scan studies were made to compare photocurrent response between Cr-MIS cells on single crystal and polycrystalline silicon substrates. A direct comparison is given in Figure 2 using single 6328 Å laser scans on the samples in question. A higher absolute response is given in the single crystal substrate case.

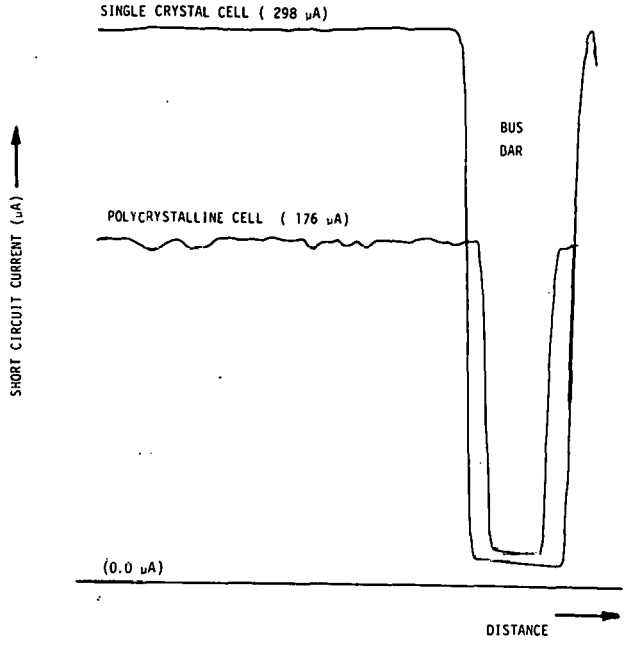

Figure 2: A single 6328 Å laser scan comparing MIS cells on single and polycrystalline Si.

Use of equation 1 [4] predicts a 4% decreased current at λ = 0.633 μm using L_p = 80 μm for a single crystal substrate and L_p = 40 μm for the

$$J_P = \frac{qF\alpha L_p}{\alpha L_p + 1} \; T \exp(-\alpha W) \qquad (1)$$

polycrystalline substrate. The greater experimental decrease was caused by grain boundary effects. A more thorough surface scan was performed at the National Bureau of Standards by Dr. D. E. Sawyer [5]. The photograph in Figure 3 shows the results of a 0.633 μm laser scan with 70 mA current bias on the 2 cm^2 sample. The dark regions at grain boundary locations are about 80 μm in width or 40 μm (one diffusion length) on either side of the grain boundary. This corresponds quite closely with data reported by Dared et.al. [6] in their grain boundary study.

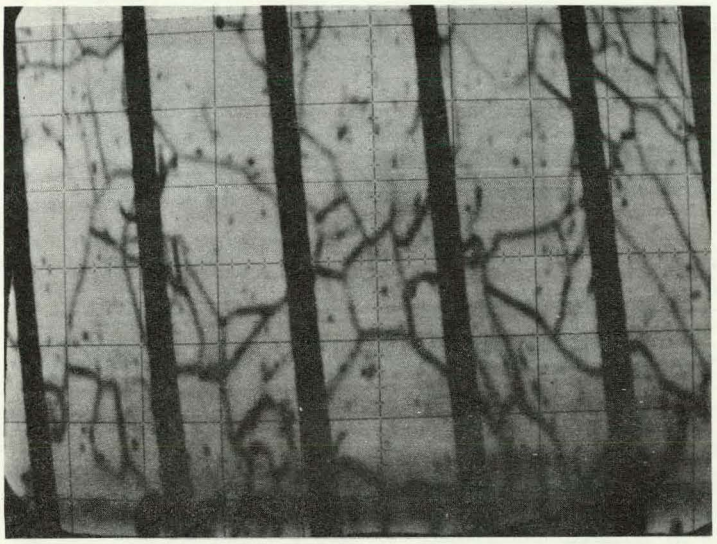

Figure 3: A multiple 6328 Å laser scan showing grain boundary recombination in polycrystalline Si.

Surface state studies on Cr-MIS solar cells have been previously reported [7]. The shape of the surface state distribution for MIS cells on single and polycrystalline substrates is similar but the latter substrate gives a factor of 10 increase in magnitude [1]. This predicts an open-circuit voltage (V_{oc}) of 0.51 V using a polycrystalline substrate compared to 0.64 V using a single crystal substrate according to the equation

$$V_{oc} = 0.65 - 2.1 \times 10^{14} D_s \qquad (2)$$

where D_s is interface state density. These values agree very closely with the experimentally verified decrease in V_{oc} from 0.60 V to 0.50 V when using poly rather than single-crystal substrates which is mainly attributed to the interface state effect.

Light I-V data served to reveal a 50% decrease in the n-value in the equation

$$J = J_o \left[\exp\left(\frac{qV}{nkT}\right) - 1\right] - J_{sc} \qquad (3)$$

as compared to the n-value from dark I-V data. This decreased n-value was accompanied by an increased barrier height (ϕ_b) from about 0.80 eV to 0.95 eV. Similar but lesser effects were reported by H. C. Card [8] for Au-nSi-MIS diodes on single crystal silicon. We interpret the data for Cr-MIS cells on p-type Wacker silicon to be due to trapping effects.

Traps are filled during illumination which reduces the loss of carriers due to unfilled trap states giving rise to a decreased n-value and increased ϕ_b. The large magnitude of change is indicative of the high trap density in this silicon both on the surface and at grain boundaries.

Small diodes on polished and un-polished Wacker Si have been tested using C-V tests, and I-V tests from 77° K to 300° K. The unpolished Si produces diodes which exhibit space charge limited behavior evidenced by a non-linear plot of $1/C^2$-V and ℓn (I) -V. A current-voltage behavior of

$$I = KV^n \tag{4}$$

was observed with $n \simeq 2$ for $V > 0.1$ V and $n \simeq 1$ for $V < 0.1$ V. This indicates severe space charge limited effects for $n \simeq 2$ and shunting effects for $n \simeq 1$ which are also verified by temperature data. Polishing the poly-Si prior to fabrication also results in diodes exhibiting space charge limited conduction. In this case, $n \simeq 7.5$ for $V > 0.1$ V. The value of n may be related to density of interface states which is significantly reduced by polishing the poly-Si.

In conclusion, several studies have been made using MIS solar cells on Wacker polycrystalline silicon. Effective diffusion length is limited by the silicon formation process and by grain boundaries. A laser surface scan shows the effects of grain boundary recombination to extend one diffusion length on each side of the physical boundary. An increased interface state density, caused by the silicon surface and by grain boundaries, is shown to decrease open circuit voltage. Space charge limited conduction has been observed.

References

1. W. A. Anderson, A. E. Delahoy, J. K. Kim, S. L. Hyland, and S. K. Dey, Appl. Phys. Lett., 33, pp. 588-590, 1 Oct. 1978.
2. S. K. Dey, W. A. Anderson, A. E. Delahoy, and C. Cartier, J. Appl. Phys., to be published.
3. E. D. Stokes, and T. L. Chu, Appl. Phys. Lett., 30, pp. 425-426, 15 Apr. 1977.
4. H. J. Hovel, Semiconductors and Semimetals: Vol 2: Solar Cells, Academic Press, New York, 1975.
5. D. E. Sawyer, Proc. 13th IEEE Photovoltaics Specialists Conference, Washington, D.C., pp. 1249-1250, 1978.
6. T. Dared, K. M. Koliwed, and F. G. Allen, Appl. Phys. Lett., 33, pp. 1009-1011, 15 Dec. 1978.
7. J. K. Kim, W. A. Anderson, and S. L. Hyland, Proc. IEEE Int. Elect. Dev. Mtg., Washington, D.C., pp. 90-92, 1978.
8. H. C. Card, Solid State Elec., 20, pp. 971-976, 1977.

NOTES

THIS PAGE

WAS INTENTIONALLY

LEFT BLANK

STUDY OF SPATIAL INHOMOGENIETIES IN PHOTOSENSITIVE MATERIALS USING DC AND MICROWAVE TECHNIQUES

by

P. Herczfeld, L. Hanlon* and J. Wargin*
Department of Electrical Engineering
Drexel University
Philadelphia, Pa. 19104

Introduction

Spatial inhomogenieties of photoconductivity are known to arise from nonuniform distribution of recombination centers and traps produced by molecular disturbances such as impurities, defects, and grain boundaries. These inhomogenieties may be characterized by DC and microwave biased photoconductive measurements. Such measurements have been performed on CdS crystals, polycrystalline films, and powders. Marked differences are observed between the DC and the microwave results.

Experimental Considerations

To observe the interaction of a microwave field with a photosensitive material, a photoconducting sample was placed on a microwave integrated circuit (MIC) transmission line, as shown in fig. 1., and from above. The section of the MIC coplanar waveguide containing the sample was made part of a 10-GHz microwave reflection bridge shown schematically in fig. 2. A change in the samples conductivity, due to illumination, or change in temperature, is detected by observing the change in the microwave reflection from the sample arm of the bridge. It is shown that the change of conductivity, $\Delta\sigma_s$, is given by the simple expression:

$$\Delta\sigma_s = \frac{2\Delta_\alpha}{Z_s}$$

where α is the attenuation constant in the sample arm of the bridge measured in nepers/m and Z_s is the impedance of the section of the microstrip line with the sample. The sample's environment was carefully controlled. The entire system could be evacuated and the temperature could be varied from cryogenic to room temperatures. Conventional ohmic contacts could be placed on the sample and standard DC measurements could be performed. All the DC and microwave measurements were carried out under indentical experimental conditions.

A variety of measurements were made including (i) photoconductive spectra, (ii) lux-ampere characteristics, (iii) optical quenching (iv) photoconductive rise and decay time and (v) noise spectra. The differences in the DC and microwave results are summarized below.

*Presently with Hewlett Packard Company.

Experimental Results

The results of various measurements performed on CdS crystals, thin films and powders are discussed below.

Photoconductive Spectra. For all the samples the microwave photoresponse versus wavelength curve was narrower than the DC biased curve and showed a shift in the peak response to shorter wavelengths. The magnitude of the microwave photoconductivity was typically two orders of magnitude higher than the DC conductivity of single crystals. For powders a difference of eight orders of magnitude was observed.

Photoconductive Rise and Decay Time. For all the samples we detected a faster rise and decay time with a microwave baising. The ratio of microwave biased decay time to DC biased decay time ranged from 1.4 to 3.5. Modulated light experiments gave similar results.

Infrared Quenching of Photoconductivity. Quenching of the photoconductivity due to infrared illumination was reduced by up to an order of magnitude in the microwave measurements compared to the DC measurements performed under identical conditions on the same CdS samples.

Lux-Ampere Characteristics. Lux-ampere characteristics in photoconductors are characterized by the relation

$$\sigma \alpha f^s$$

where f is the intensity of the light and the exponent s is a characteristic number. For the DC measurements three regions were identified. At low light intensities we had s = 1, at medium light intensities s = 1/2 dependences and finally at high illuminations s was less than 1/2 indicating saturation. For the microwave case we observed values for s between 1/2 and 1 for low and medium illumination, while at high intensities we found s = 1/2; i.e. no saturation.

Photoconductive Noise Spectra. The DC biased noise spectra was dominated by generation-recombination (g-r) and diffusion type frequency dependence. The microwave baised noise spectra, however showed no evidence of carrier diffusion.

Discussion

All the experimental observations could be explained on the basis that the photoconductive samples are spatially inhomogeneous. If crystal defects, impurities, and other localized disturbances exist they will cause localized trapping and deep recombination states. If these traps and recombination centers are non-uniformly distributed in the sample they will cause local variations in the carrier density and hence in the conductivity. The inhomogeneous sample will contain relative high and low conductivity regions. The microwave propagation interacts strongly with the high conductivity regions, but not with the low conductivity regions. The DC photocurrent on the other hand will be controlled by the high resistivity regions. The microwave measurements reflect

the material properties and carrier transport of the high conductivity regions while the DC experiments give the same information about the low conductivity regions. The combination of the DC and microwave study enables one to estimate the relative conductivities and relative size of these regions.

The microwave measurements are electrodeless (non destructive) and repeatable, so that they are well suited for process control applications. They are being evaluated at present to track the evolution of CdS from powder to completed device to improve fabrication yield.

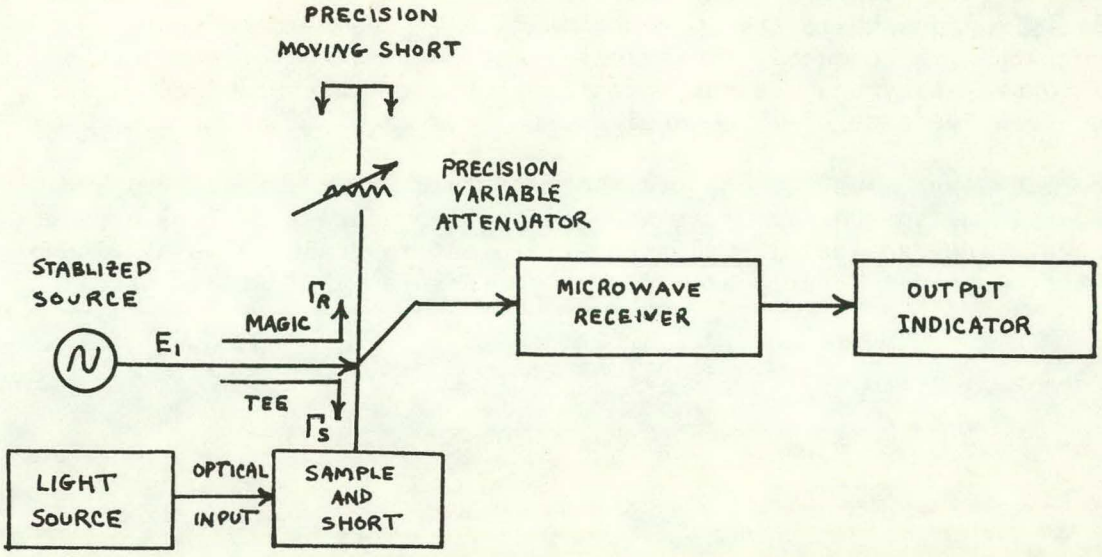

SCHEMATIC OF MICROWAVE BRIDGE

Fig. 1.

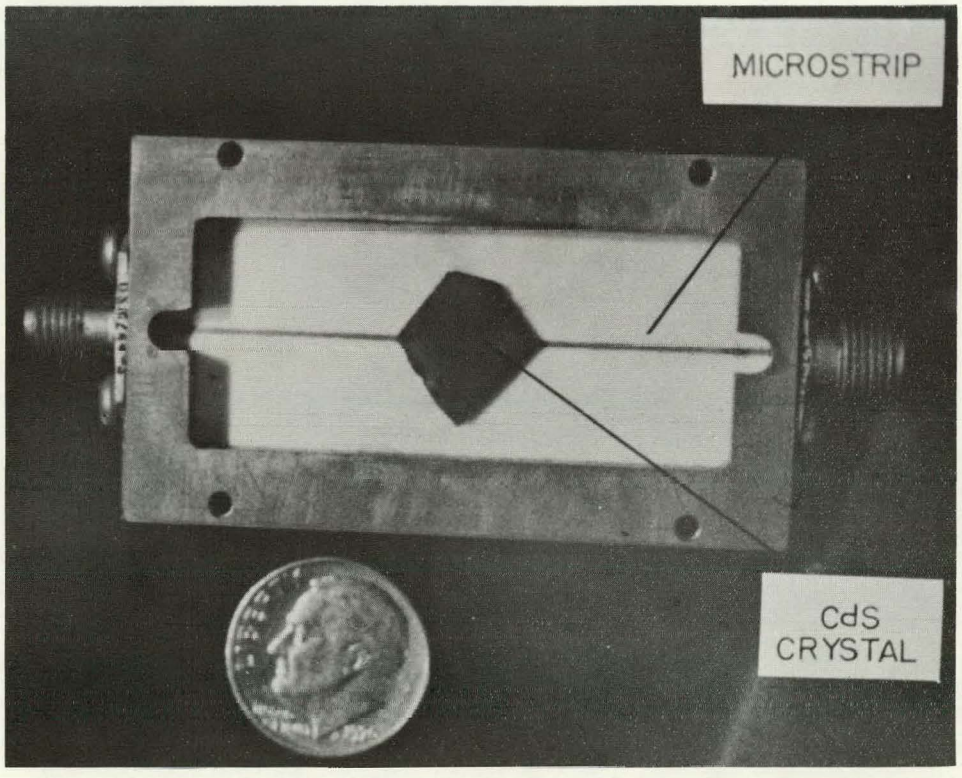

Microwave Integrated Circuit Sample Holder with CdS Samples.

Fig. 2.

CAPACITANCE AS A TOOL FOR INVESTIGATING THIN-FILM CdS/Cu_2S HETEROJUNCTIONS

W.J. Manthey and N.Convers Wyeth
Institute of Energy Conversion
University of Delaware
Newark, Delaware 19711

An important limitation of the efficiency of the CdS/Cu_2S cell results from recombination of electron-hole pairs at the junction interface, whereby some of the current is lost. We wish to measure and understand this interface recombination, determine its influence on the region near the interface, and relate the recombination to cell production and material characteristics.

The electronically active features of this region include interface states associated with lattice mismatch, and a population of donors and acceptors. The interaction of the various traps and interface states with each other and with free carriers will produce corresponding changes in the junction capacitance. This paper describes a technique that has been developed at the Institute of Energy Conversion to measure the capacitance of operational solar cells under varying conditions, and thereby elucidate key physical properties of the heterojunction regions.

Because of the high conductance of the illuminated cell under zero or forward bias, it is difficult to use a standard capacitance bridge. Our method, patterned after that of Shewchun and Waxman (1), uses a lock-in amplifier to measure the susceptive component of an AC signal, in such a way that the large conductive component does not interfere with the measurement. Figure 1 shows the circuit.

The DC bias of the cell can be set at any point on the I-V curve below about 200 mV forward bias using the function generator. An AC signal of 10 mV at 10 kHz is then superposed on the DC bias voltage. This AC signal is strong enough to produce a readable output but small enough ($V_{AC} < kT/e$) that the region swept thru can be considered uniform. The frequency is within the range where the oscillating charge in the junction region is able to respond, and the resulting cell current has a component 90° out of phase with the voltage and proportional to the cell capacitance C. The output of the lock-in amplifier is a DC voltage equal to the rms value of this out-of-phase component. The current amplifier allows one to measure the current in the cell without introducing any additional impedance.

CdS/Cu_2S cells are subjected to heat treatments during efficiency optimization during which copper ions diffuse into the CdS where they act as acceptors, reducing the positive charge in the space-charge region of the CdS. This increases the width w of this region and reduces both the junction capacitance and local electric field, which vary inversely with w.

The cell capacitance in the dark is typically in the range of 1 to 10 nF/cm^2. Under illumination the capacity increases and at an intensity equivalent to AM1 is usually in the range of 30 to 100 nF/cm^2. Under illumination holes were generated and trapped in the CdS causing the space-charge region to become more positive and therefore narrower. As a consequence the collection efficiency η_c also increases with illumination, often very substantially. Analysis of the variation of local electric field, obtained from C, with η_c indicates that interface recombination velocity is between 6×10^4 and 2×10^6 cm/sec^2.

A major advantage of the present technique is that the capacitance can be measured under actual operating conditions and capitalizes on the sensitivity of the capacitance to the intensity and spectral content of the illumination. More traditional photocurrent measurements are less able to differentiate between the various changes taking place. The use of this technique to monitor the influence of bias voltage and illumination on capacitance is described elsewhere (3).

Our technique is also well suited to the observation of transient variations of capacitance, provided that the time constants of interest are greater than both the response time of the lock-in amplifier, 1 msec, and the period of V_{AC}, here 0.1 msec. Because of the difference in energy gap between CdS and Cu_2S, trap loading and unloading is best accomplished by abrupt changes in illumination, rather than in junction bias (4). Analysis of these transients allows the evaluation of capture and emission constants, both optical and thermal, and the spatial distribution of traps. A typical transient response is shown in Figure 2. To simulate the actual operation of the cell we usually make use of multi-beam excitation. A steady, short-wavelength beam creates holes in the CdS which load the traps, and a second, long-wavelength beam is chopped to stimulate the transient responses.

A problem arises when large changes in capacitance are produced. The $C \propto 1/w$ relation is no longer valid if there are inhomogeneities in trap density so that the transient C(t) cannot be relied upon to vary exponentially. To overcome this difficulty, we have adapted the constant-capacitance method of Pals (5). Figure 1 shows the necessary circuit modification in dotted lines which automatically varies the bias voltage of the cell to maintain the capacitance at a constant value. The time decay of the negative feedback signal is characteristic of the traps at a constant depth in the junction.

References

(1) J. Shewchun and A. Waxman, Rev. Sci. Instr. 37, 1195 (1966).
(2) A. Rothwarf, J. Phillips and N. Convers Wyeth, Thirteenth IEEE Specialists Conference Rec. - 1978 (IEEE, New York, 1978) p. 399
(3) N. Convers Wyeth and A. Rothwarf, J. Vac. Sci. Tech., to be published.
(4) G.L. Miller, D.V. Lang and L.C. Kimerling, Ann. Rev. Mater. Sci. 7, 377 (1977).
(5) J.A. Pals. Sol. State. Elec. 17. 1139 (1974).

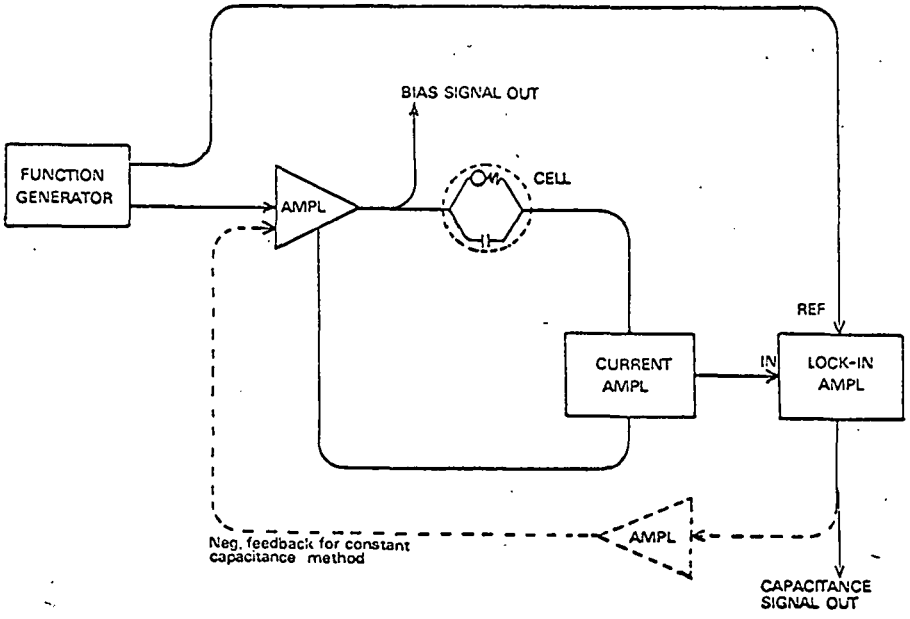

Fig. 1. Capacitance Measurement Circuit

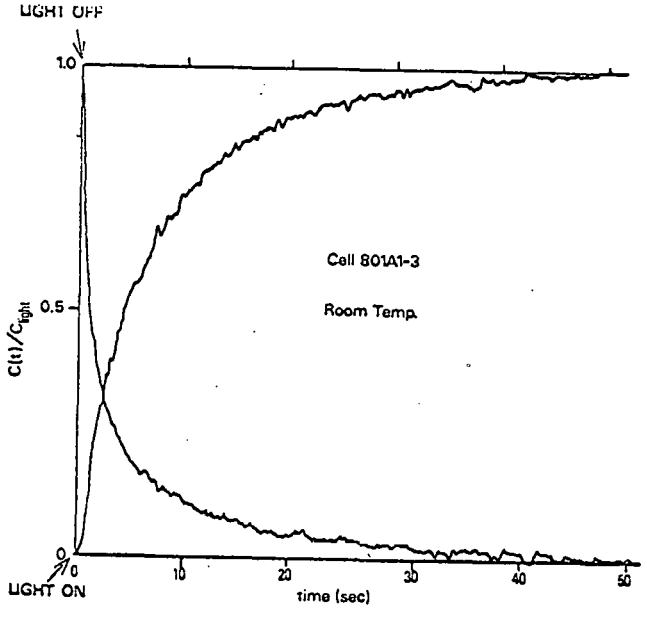

Fig. 2. Capacitance Transients

NOTES

Poster Session

CORRELATION OF GRAIN BOUNDARY ELECTRICAL PROPERTIES WITH GRAIN BOUNDARY IMPURITIES IN MULTIGRAINED SILICON USING SURFACE ANALYTICAL TECHNIQUES

L.L. Kazmerski and P.J. Ireland
Photovoltaics Branch
Solar Energy Research Institute
Golden, Colorado 80401

The applications of complementary surface analysis techniques - Auger electron spectroscopy (AES) and secondary ion mass spectroscopy (SIMS) - to the comparative compositional analysis of grain and grain boundary regions in multigrained silicon are presented. The method incorporates in-situ ultrahigh vacuum fracturing of the material with the surface sensitive techniques to delineate differences in elemental composition between the inter- and intra-grain regions. The method is used to provide the first direct physical evidence for the localization of impurities at the grain boundaries in silicon grown by the casting and directional solidification techniques.

The multigrained silicon samples used in this study were obtained from three different sources. Two of these (termed Si-A and Si-B) were produced by a "conventional" casting process in which the silicon was molten when poured into the shaping crucible held slightly below the melting point of the silicon. The third sample type (termed Si-C) was produced by the directional solidification process. This differs from casting in that solid silicon was initially loaded into the crucible and subsequently heated into the molten phase. In either case, the cooling and cooling rate were precisely controlled to provide optimum grain size and structure. Both carbon and mullite crucibles were used to form the multigrained silicon ingots which were then sliced into thin (<1 mm thick) sheets.

The surface analytical operations were performed in a Physical Electronics Industries model 590 scanning Auger microprobe (SAM) system with secondary ion mass spectroscopy capabilities. The minimum beam diameter of the SAM was measured to be 1600Å. A differentially-pumped ion gun was used for depth profiling and SIMS. Its beam diameter could be focused to 140 μm. The base pressure of the analysis chamber was 1.2×10^{-10} torr. An Extranuclear laboratories quadrupole mass analyzer was used for the SIMS, and elemental and molecular species 1-1000 AMU could be analyzed. The samples were inserted using an introduction/transfer system which preserved the UHV chamber conditions, minimizing contamination to this volume. A sample fracture stage permitted the in-situ,

ultrahigh vacuum exposure and comparison of both intragrain and grain boundary regions. By the UHV fracturing technique, potential contamination to these surfaces from sorbed species was minimized, thus ensuring that the resulting data were not artifacts of the experiment. The chamber environment was monitored during the experiment with a separate quadrupole mass analyzer with residual gas analysis capability.

This investigation involves the application of two surface analysis techniques, SAM and SIMS, to the solution of the impurity segregation problem. Although each contributes its inherent diagnostic quality (e.g. submicron spacial resolution, non-destructive analysis, monolayer surface sensitivity, quantifiable data and nearly uniform elemental sensitivity for SAM; increased sensitivity, usually 100 times better than Auger, isotope and molecular fragment identification for SIMS), the methods are complementary. Thus, they provide for more dependable and less ambiguous results if used, as in this study, for essentially simultaneous analysis during the diagnostic procedure.

Auger Studies

An Auger mapping of a grain boundary area is presented in Fig. 1. These data were taken on an internal region of cast sample Si-A, grown in a mullite crucible. The secondary electron image of the fractured grain boundary does show some irregularities as indicated at points 1 and 2. The Auger maps of this region do give evidence to impurity concentrations, Ni, Al and C, in these areas with oxygen prevalent throughout. It should be emphasized that the Auger maps here indicate build-up of the impurities, which can be remnants due to fracturing, and lower concentrations of each are detectable throughout the grain boundary regions. No impurities were found in the grain interior. The grain boundary localization of the Ni and Al (in the form of NiO and Al_2O_3, probably from the crucible) is verified by the depth-compositional profiles.

These Auger electron spectroscopy data are presented as representation examples of the localization evidence. Cast samples (Si-A and Si-B) and the directionally-solidified samples (Si-C) showed similar results. Only the elemental impurities, due to the difference in crucible and starting materials, differed between sample types. Essentially no impurities, outside of the C-inclusions for sample Si-C, were detected in the interior of the grains. Since the Auger technique is insensitive to concentrations at or below the $10^{18}/cm^3$-level, the determination of trace impurity content necessitated the use of another surface-sensitive method.

SIMS Studies

Generally, SIMS provides at least 100 times the sensitivity to trace elements than that attainable by Auger spectroscopy. It is, however, limited in spacial resolution by the broader diameters (usually greater than 100 μm) of the ion probes. In the configuration for those experiments, SIMS can be performed on the same region as the SAM investigations without moving or otherwise disturbing the sample itself.

The analysis once again could be performed on adjacent grain and grain boundary fractured regions. Fig. 2 presents a typical SIMS spectrum for a region found by fracturing through a grain - this from sample Si-A. A controlled oxygen leak (10^{-7}torr) is used to enhance secondary ion yields. The SIMS spectrum indicates primarily the presence of Si; the only impurity is the intentional dopant. The oxides result from the oxygen leak, and the Na and K result from the inevitable inclusion of the top and/or bottom surfaces of the thin samples (previously exposed to the atmosphere) in the SIMS analysis. In contrast, many impurities are observed in fractures at the grain boundary (see Fig. 3). These data are taken on the identical region as that presented in the Auger studies of Fig. 1. In addition to the C, Ni and Al, trace impurities including Ti, Cu, B and Mg are detected. None of these appear in the corresponding analysis performed on the grain region. SIMS profiles do confirm that the impurities are localized at the boundary and do not significantly penetrate the grain itself.

Electrical Characterization

The electrical properties of selected grain boundary regions are investigated using high-resolution SAM methods. Preliminary conductivity data correlating the grain boundary elemental composition with electrical behavior are presented. Some evidence is reported which indicates that the electrical activity of the grain boundaries differs in a given sample and depend upon the localization of impurities in that region.

Acknowledgement

The cooperation, help and consultation of T.F. Ciszek and T.E. Gilmer of the Photovoltaics Branch at SERI is gratefully acknowledged and sincerely appreciated.

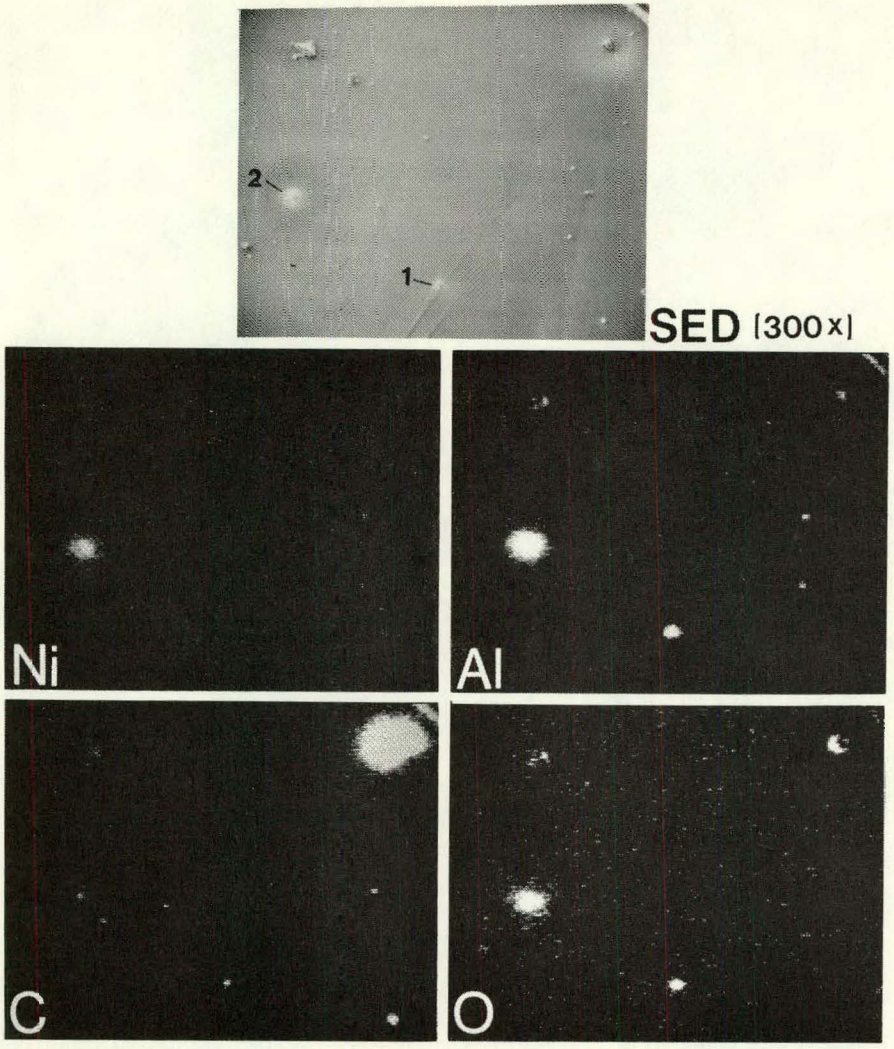

Fig. 1

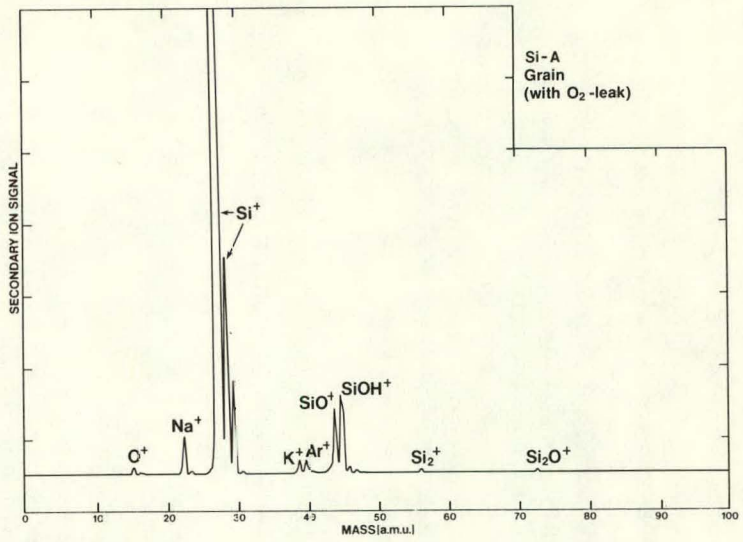

Fig. 2

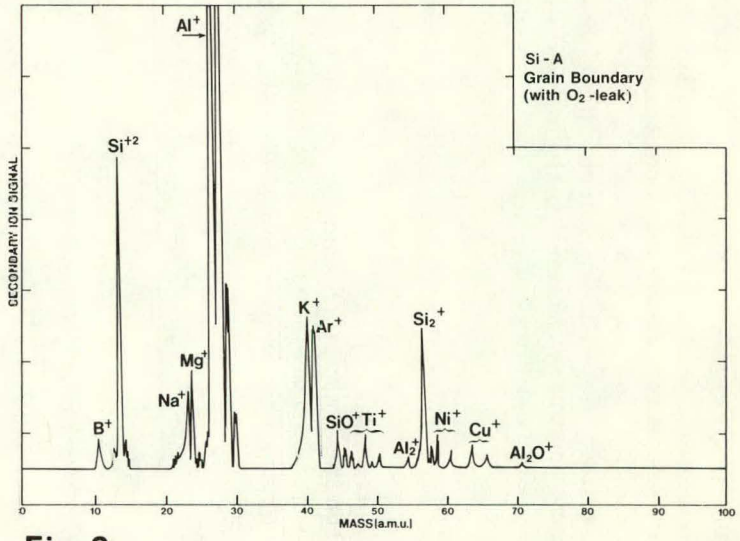

Fig. 3

NOTES

THIS PAGE

WAS INTENTIONALLY

LEFT BLANK

DIFFUSION LENGTH MEASUREMENTS IN Cu_2S

W. J. Biter and T. W. O'Keeffe
Westinghouse Research and Development Center
Pittsburgh, PA 15235

Detailed knowledge of the electronic properties of Cu_2S is essential to the understanding of the Cu_2S/CdS thin film cell. We wish to report measurements of diffusion length and other electronic properties of thin Cu_2S layers obtained by a scanned laser beam technique. CdS single crystals were used for the major portion of the work but some initial results will be reported with the Cu_2S formed on CdS thin film.

Light probes scanned across a beveled junction have been used by a number of authors (1,2) to measure the transport properties of various materials. Mechanically produced bevels suffer from the possible effect of surface damage introduced by the polishing upon the electronic properties of the material. The present work produced the required variation in Cu_2S thickness by depositing a CuCl layer onto the CdS by evaporation through a raised mask using a broad source. Subsequent processing (3) produced a Cu_2S layer of tapering thickness in the CdS substrate.

The thickness of the Cu_2S layer was determined by a direct measurement of the transmission using a silicon detector mounted behind the sample. The photocurrent from the heterojunction was monitored simultaneously with the measurement of the transmission using a scanned He-Ne laser. This apparatus is shown in Fig. 1. We choose to display this data directly as a plot of photocurrent versus transmission obtained from an oscilloscope trace. This method is insensitive to local variations in the Cu_2S thickness which would interfere with the usual method of measuring thickness based on position across the bevel. The technique was very simple to apply and allowed rapid comparison.

It was found more useful to make the theoretical predictions of photocurrent versus active layer thickness in terms of photocurrent versus transmission using the electronic properties as parameters. Experimental curves obtained were very close to theoretically predicted shapes. The most significant feature of the curve is the location and magnitude of the peak photocurrent response, which can give an immediate estimate of diffusion length and junction losses.

Figure 2 is a typical experimental curve taken directly from the oscilloscope (somewhat smoother) with the axes re-interpreted. The photocurrent (vertical axis) has been normalized to the laser beam

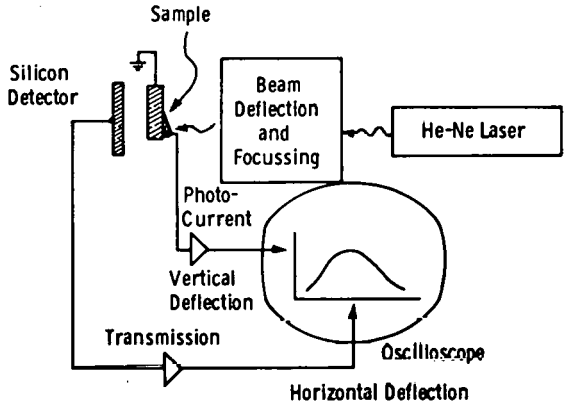

Fig. 1. Experimental Arrangement

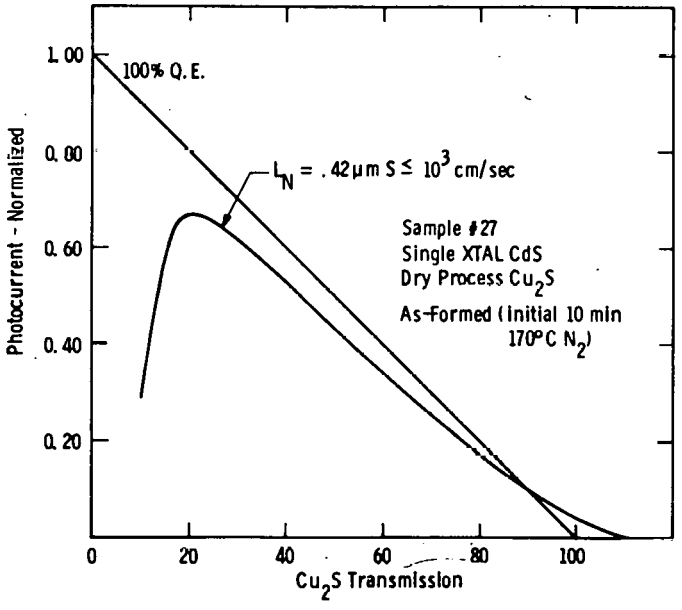

Fig. 2. Experimental Response of Tapered Cu_2S Layer

intensity as measured by the silicon detector using a previously determined value for the silicon quantum efficiency at 6328Å.

The Cu_2S transmission (horizontal axis) is more precisely the Cu_2S internal transmittance and represents the amount of light lost by absorption alone in the Cu_2S thickness, i.e., not including reflection losses. The appropriate correction for reflection and CdS losses have been made to the axis scale. The extension of the curve beyond 100% is due to optical interference effects which were not fully investigated.

The shape of the curve is very consistent with that expected theoretically. The value of transmission corresponding to the peak response can be used to extract diffusion lengths information. The height of the peak response gives information on other loss mechanisms, in particular the surface recombination. For the example shown, the diffusion length was .42 micrometers and the surface recombination velocity less than 10^3 cm/sec.

On other samples, diffusion lengths from .2 to .6 micrometers for photoelectrons in Cu_2S were obtained with no detectable change with heating while values for the surface recombination velocity appeared to be less than 10^4 cm/sec. A change in the losses associated with the junction seemed to be the dominant change with heat treatment.

References

1. M. Ettenberg, H. Kessel and S. J. Gilbert, J. Appl. Phys. 44, 327 (1973).

2. W. D. Gill and R. H. Bube, J. Appl. Phys. 41, 1694 (1973).

3. T. S. TeVelde, Solid State Electronics 16, 1305 (1973).

NOTES

MEASUREMENT OF RESISTIVITY OF THIN CdS FILMS ON BRASS SUBSTRATES

S. Hogan and S. Wagner
Solar Energy Research Institute, Golden, CO 80401

and

F. Barnes
Dept. of Elect. Engr., University of Colorado, Boulder, CO 80309

This paper reports a non-destructive resistivity measurement technique for thin semiconductor films deposited on metallic substrates. This technique addresses a serious measurement problem in current photovoltaic research. At present, samples are characterized after application of ohmic or Schottky barrier contacts by two point through-resistance or by capacitance-voltage measurements, respectively. Contact metallization is inconvenient for routine evaluation because it eliminates a sample from subsequent solar cell fabrication thereby preventing a one-to-one correlation of resistivity with photovoltaic behavior. The technique reported here involved determining the sample resistivity by a field perturbation analysis on a semi-confocal Fabry-Perot resonator. The sample is mounted within the cavity and quality factors both with and without the film present are related to resistivity.

Extensive use of microwave characterization of dielectric materials has been reported. Determination of semiconductor resistivity has also been accomplished using microwave methods. These techniques involved sample insertion into waveguides[1,2] and into cavities[3]. The methods employed, however, imposed strict restrictions on sample shape or thickness which prohibited their use on samples of arbitrary thickness backed by a conducting surface.

The resonator cavity and its important dimensions are shown in Figure 1. A nearly semi-confocal configuration was chosen so that the confocal requirement of d=b/2 was ignored. The value of d (~6 cm) was purposely kept smaller than b/2 (50 cm) to minimize diffraction losses out of the cavity. The 'M' sized waveguide was connected to the resonator with field coupling accomplished with a 0.107 cm diameter iris through the 0.025 cm thick wall.

The field distribution with the cavity under resonance has been shown[4] to most closely be described by combined Hermite-Gaussian functions. Although a solution in closed form is possible, it becomes necessary to perform numerical integrations for each new sample material or thickness in order to describe the fields at resonance as simple plane waves[5]. This is well suited in the near semi-confocal configuration for the

region near the flat plate where the sample is mounted.

The derivation of the film resistivity expression relies on several assumptions, the first of which is the assumption that the electric field effectively terminates at the film/substrate surface. This assumption is satisfied if two conditions are met; the skin depth in the metal is much less than the substrate thickness, and the semiconductor skin depth is much larger than the film thickness. Metals of typical conductivity satisfy the first requirement if they are greater than several μm thick. The skin depth in the semiconductor, δ, is given by

$$\delta = 1/\{\omega(\mu\varepsilon/2)^{\frac{1}{2}}[(1+1/\omega^2\varepsilon^2\rho^2)^{\frac{1}{2}}-1]^{\frac{1}{2}}\} \qquad (1)$$

where μ is the permeability of the semiconducotor. The experiment was set to operate at 92GHz which gave a range of δ from 30 μm for a ρ of 0.01 Ωcm to 29 cm for ρ=1000 Ωcm. Typical thin film processes involved in photovoltaic device fabrication give both film resistivity and thickness in the defined limits of operation. For the experiment as established at 92GHz, a substrate thicker than several μm is adequate, while acceptable skin depth restrictions allow measurements of samples whose ρ varies from 0.01 Ωcm to 1000 Ωcm.

Another condition to be satisfied is avoiding substantial phase shift within the semiconductor. This requires the wavelength within the film to be much larger than the film thickness, a requirement which is easily met for most applications of interest. The final important condition to be satisfied regards the physical dimensions of the sample. The sample diameter must be at least twice the field spot size (beam radius) at the flat plate. The spot size, W, is determined from

$$W = (2d\lambda/\pi)^{\frac{1}{2}}/[(4d/b)-(2d/b)^2]^{\frac{1}{4}} \qquad (2)$$

For the dimensions of the cavity used and the generator wavelength (λ) employed, a spot size of 1.5 cm was determined. The requirement of sample size to be greater than 3 cm to a side is generally met in current photovoltaic device structures.

The derivation of an expression for the resistivity can be accomplished using the above mentioned assumptions. The film ρ can be stated as

$$\rho = s/[\omega\varepsilon d(1/Q_s-1/Q_o)] \qquad (3)$$

where s is the sample thickness (film only), d the distance separating the reflectors, ω the angular frequency of resonance, ε the dielectric constant of the semiconductor, and Q_s and Q_o represent the cavity quality factor with the film sample mounted and the substrate only mounted, respectively.

Three polycrystalline CdS films deposited on 51 μm thick brass substrates were measured. The field generation was accomplished by use of a Klystron at around 92 GHz. The frequency was determined using a wavemeter, while the standing wave indicator method of determining cavity Q[6] was used. Measurements of Q_o were made by wax mounting a piece of brass,

the size of the sample, onto the flat reflector plate. The value of Q_s was then measured by mounting the sample of film on substrate to the plate, again by means of a low temperature wax. An alternate method using only the sample would be to make the measurements first with the film side face down, for Q_o, then reversing the sample to measure Q_s. [The method of measurement by hand is quite tedious, and it is recommended that microprocessor control be utilized to limit inaccuracies and minimize testing time.] For the three samples tested, a multitude of Q measurements were taken and averaged. Using those values and the others as listed in Table 1, the value of ρ was determined by use of equation 3. These values are also listed in Table 1 as ρ_{MW}, along with a value of ρ_{IV}. The ρ_{IV} values are resistivities determined from current-voltage measurements carried out independently on other portions of the sample using indium contacts pressed onto the CdS film.

Table 1

	Sample 740A	Sample 715	Sample 763 A
s (μm)	38.4	30.0	30.1
d (cm)	6.23	6.00	6.34
Q_s	423	2613	3678
Q_o	1437	6915	4179
f_o (Hz)	91.32×10^9	91.16×10^9	91.57×10^9
ρ_{MW} (Ωcm)	0.7	4.3	29.5
ρ_{IV} (Ωcm)	0.7	4.2	30.4

In conclusion, as seen from the excellent correlation in measured values, we have demonstrated a technique for resistivity determination of thin semiconductor films on metal substrates. Because of the open cavity the sample is accessible. This permits the possibility of expansion of the technique to measuring photoconductivity by illumination as well as determining temperature effects. The measurement of carrier lifetime is also possible.

We would like to express our appreciation to Dr. R. Hall of the Institute of Energy Conversion for providing the CdS samples and the ρ_{IV} data. We also thank Drs. R. Hayes and E. Kuester for helpful discussions.

REFERENCES

1. J. Lindmayer and M. Kutsko, Solid State Electronics 6, 377 (1963).
2. R.L. Ramey and T.S. Lewis, J. Appl. Phys. 39, 1747 (1968).
3. T. Kohane and M.H. Sirvetz, Rev. Scientific Instruments 30, 1059 (1959).
4. G.D. Boyd and J.P. Gordon, Bell System Tech. J. 40, 489 (1961).
5. W. Culshaw and M.V. Anderson, National Bureau of Standards Report 6786, July 1961.
6. E.L. Ginzton, Microwave Measurements (McGraw-Hill, New York, 1957).
7. M. Orgeret et al., Conf. Record of the 11th IEEE Photovoltaics Specialists Conference, May 6-8, 1975, Scottsdale, AZ: IEEE, New York, 1975; pp 62-66.

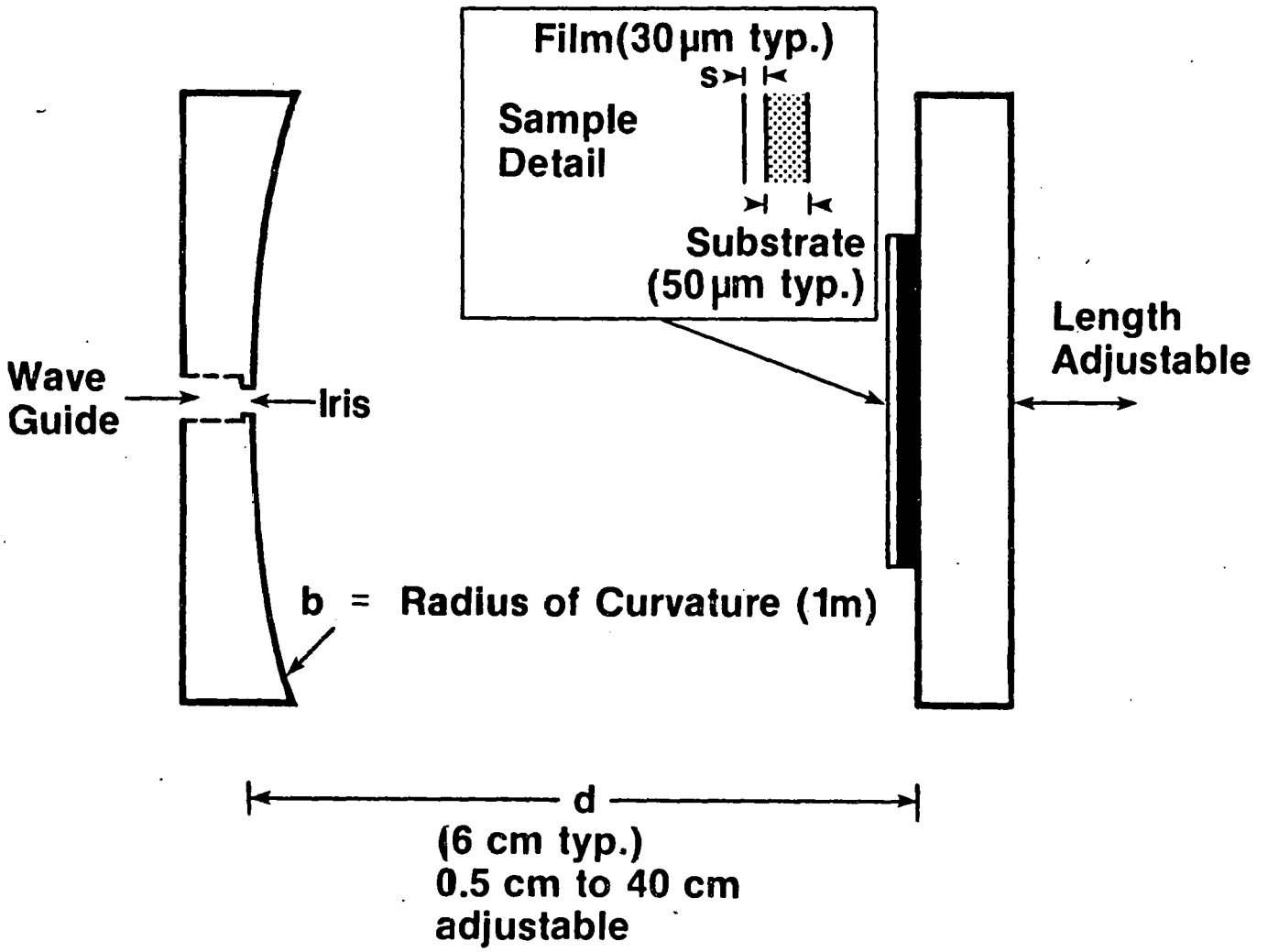
Film(30 µm typ.)
s
Sample
Detail
Substrate
(50 µm typ.)
Length
Adjustable
Wave
Guide
Iris
b = Radius of Curvature (1m)
d
(6 cm typ.)
0.5 cm to 40 cm
adjustable

FIGURE 1

NOTES

THIS PAGE

WAS INTENTIONALLY

LEFT BLANK

ELLIPSOMETRY OF THIN SILICON DIOXIDE FILMS ON ROUGH POLYCRYSTALLINE SILICON SURFACES

T. David Burleigh*, Sigurd Wagner, and Theodore F. Ciszek
Solar Energy Research Institute, Golden, Colorado 80401

Thickness and refractive index of oxides were determined with an automatic ellipsometer equipped with a He-Ne laser source (λ = 632.8 nm). Measurements were carried out on wafers prepared from two types of cast polygrain and one CVD polycrystalline rod. The surface roughness ranged from fine polish (with 0.05 μm alumina) to as-cut. Roughness values were derived from surface profiler traces.

On polished single crystal reference samples, the oxide thickness ranged from ~3.5 nm (room temperature oxidation) to ~130 nm (oxidation at 950 C). For roughness substantially below the measuring wavelength, the oxide thickness is equal to that of the reference sample. Roughness in the vicinity and above the measuring wavelength results in thickness values higher than on reference samples for thin oxides, and comparable to the reference samples for thicker oxides. The data are reproducible. They can be used to determine the - at least apparent - oxide thickness on a rough surface once a calibration curve has been established.

The apparent refractive index of the oxide exhibits a maximum for roughness values comparable to the measuring wavelength.

*Summer Student.
Present Address: Department of Metallurgy and Materials Science, Massachusetts Institute of Technology, Cambridge, MA 02139

NOTES

Experimental Determination of the Photon Economy in Polycrystalline Thin Film Photovoltaic Materials and Devices

J. A. Bragagnolo

Institute of Energy Conversion

E. A. Fagen

Department of Electrical Engineering
University of Delaware
Newark, Delaware 19711

ABSTRACT

A full quantitative analysis of the photon economy of a photovoltaic device requires that every incident photon be accounted for. This information in turn serves as input to the analysis of charge transport and by combining these two analyses it is possible to relate the current at the external terminals of the device to the number of incident photons. If photovoltaic devices consisted of plane-parallel layers of homogeneous isotropic media, the photon economy problem would yield to known analytical methods. In practice, however, polycrystalline thin film devices depart from this prescription in every particular. Among the consequences are diffuse scattering at all interfaces due to roughness, either adventitious or deliberately introduced, and diffuse volume scattering due to grain boundaries and orientation effects. On one hand these effects greatly complicate the measurement of intrinsic optical properties, while on the other, they afford the device engineer certain degrees of freedom which can be turned to advantage.

In this paper we describe the techniques of optical measurement and analysis employed by the Photovoltaic Device Analysis group at the Institute of Energy Conversion of the University of Delaware. The key element in this body of techniques is the use of a Gier-Dunkle model SP-220 absolute directional reflectance attachment ("integrating sphere") in a manner which compels the user to account for all residual absorptance. The power and utility of this technique are illustrated by its application to two hitherto unsolved problems:

1. Determination of the Intrinsic Absorption Edge of Polycrystalline Thin Films of Zn_3P_2.

Vacuum evaporated thin films of this material exhibit slightly textured or non-specular surfaces whose apparent roughness increases with film

thickness. Transmittance measurements in the specular mode with ca. f/10 detector collection geometry (Beckman 'Acta' MIV) yield pronounced ($\alpha > 10^3$ cm^{-1}) and substantially wavelength-independent absorption tails at energies below the nominal bandgap. Insertion of supplementary beam condensing lenses, however, which effectively enlarge the aperture ratio of the detector to ca. f/1, sharply reduces these tails, indicating that the absorption is largely spurious and due to light scattered out of the detected beam. We therefore perform all thin film transmittance and reflectance measurements in the integrating sphere, using a procedure[1] shown in Fig. 1.

The essential feature of this procedure is that the longitudinal axis of the sphere is rotated slightly with respect to the optic axis of the monochromator by means of a nodal slide, permitting the sample beam to clear the sample mounting post. The sample in turn is slightly offset from this post in such a way that it can be flipped up into the beam or down out of the way, while remaining near the center of symmetry. In step (a) both beams are permitted to strike the sphere wall and a reference spectrum is run. In step (b) the sample, backed by an absorber, is flipped up into the beam and the total reflectance spectrum R (λ) is measured. In step (c) the absorber is removed, and the sum of reflectance and transmittance spectra, R (λ) + T (λ), is measured. The total transmittance spectrum T (λ) is then obtained by subtraction.

Comparison of the reference spectrum obtained in step (a) with that obtained in step (c) far in the passband of the sample affords a direct and sensitive test for residual absorbance. Similarly, comparison of the reflectance spectrum obtained in step (b) far in the stop band of the sample with that obtained on polished bulk samples ensures the accuracy of reflectance measurements and the correctness of surface preparation techniques. By assigning relatively low ($\leq$ 1%) tolerances to permissible discrepancies, and discarding all data-taking runs which fail to meet these criteria, data with a high degree of internal consistency are obtained. As a result, the intrinsic absorption edge of evaporated thin films of Zn_3P_2 was revealed to be exponential and to conform to Urbach's rule,[2] contrary to earlier reports on analogous materials.[3]

2. Analysis of Photon Collection Efficiency of Polycrystalline CdS/Cu_2S Cells.

Thin-film polycrystalline CdS/Cu_2S cells of over 9.0% efficiency and AM1 short-circuit currents in excess of 27 mA/cm^2 have been recently reported by the Institute of Energy Conversion.[4] Reflection measurements as a function of incidence angle with the cell at the geometrical center of the sphere, showed that the specular component of reflected light is negligible. Further analysis using reflectance and transmittance measurements, indicates that as many as 80% of the incident photons are absorbed in the Cu_2S layer, which generates 95% of the minority carriers (Fig. 2).

The morphology of the strongly textured Cu_2S layer and CdS/substrate interface is the dominant factor in determining the high optical efficiency of thin-film CdS/Cu_2S cells. The latter arises from both light

capture at textured front cell surface and trapping caused by diffuse reflection at the CdS/Cu_2S and CdS/substrate interfaces. This leads to total internal reflection of outgoing photons at the outer cell boundary and reduces re-emission losses of thin-film Cu_2S/CdS cells to a fraction of their value for a specular multi-layer device.

REFERENCES

1. We are indebted to Keith Nelson of Gier-Dunkle Instruments for showing us this technique.
2. E. A. Fagen, J. Appl. Phys. (submitted for publication).
3. W. Zdanowicz and J. M. Pawlikowski, Acta Phys. Polon. A38, 11 (1970).
4. A. M. Barnett, J. A. Bragagnolo, R. B. Hall, J. E. Phillips and J. D. Meakin, Proceedings 13th IEEE Photovoltaic Specialists Conf. pp 419-420 (1978).

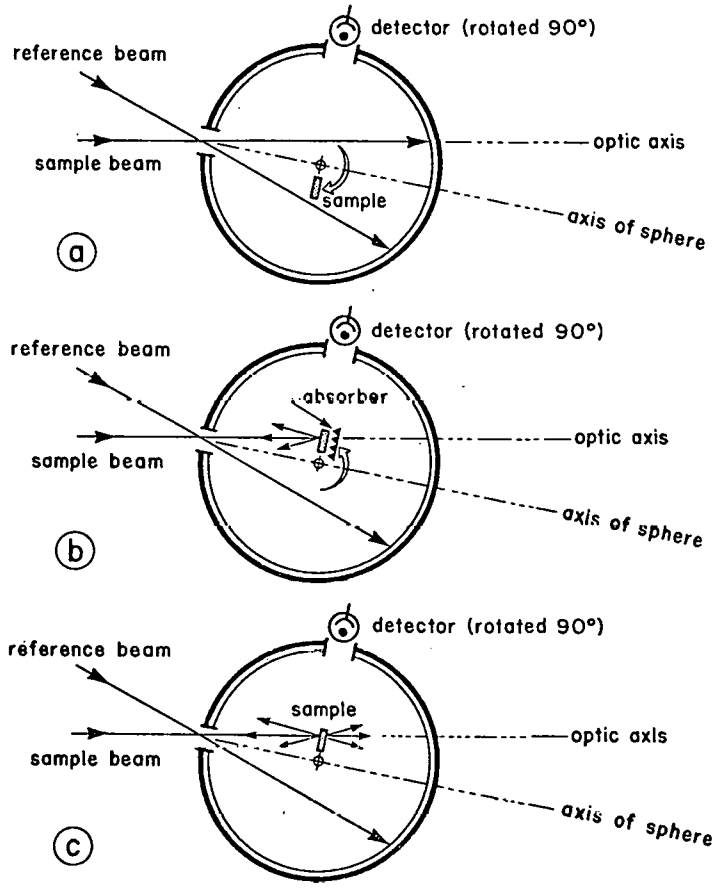

Figure 1. Utilization of an integrating sphere to give total reflectance and transmission data. See text.

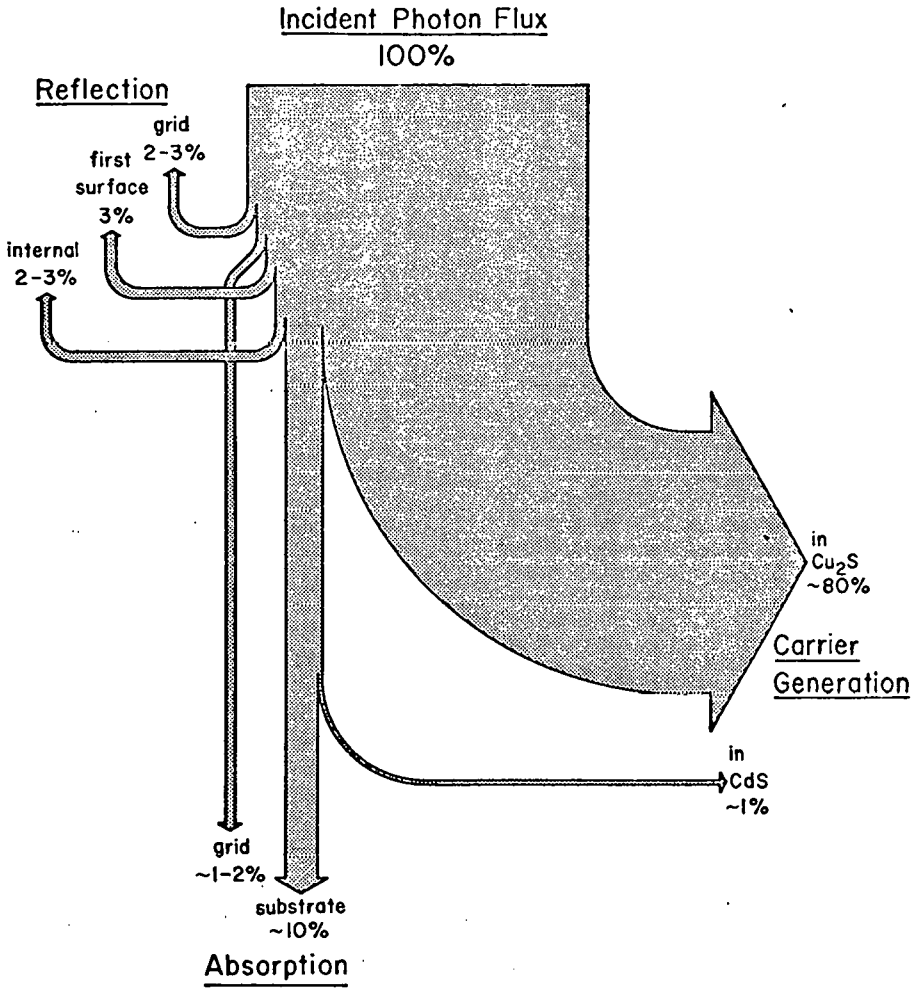

Figure 2. The photon economy for a high efficiency textured CdS/Cu_2S Solar Cell.

NOTES

THIS PAGE

WAS INTENTIONALLY

LEFT BLANK

EXPERIMENTAL TECHNIQUES USED TO EVALUATE GRAIN BOUNDARY DEFECTS IN THIN SEMICRYSTALLINE SILICON SHEET MATERIAL

Zimri C. Putney
Semix, Incorporated
15809 Gaither Road
Gaithersburg, Maryland

William F. Regnault
Semix, Incorporated
15809 Gaither Road
Gaithersburg, Maryland

ABSTRACT

Various test techniques have been applied to evaluating the effect of grain boundary defects on the electrical performance of solar cells made from thin semicrystalline silicon sheet material. Two types of defect structures have been investigated. The first is an "open" grain structure, which leads to an ohmic solar cell shunt by allowing either diffusion or metal evaporation to proceed from the front to the back of the cell. A second type of structure also is highly shunted; however, in this case the cause is apparently a high density of recombination centers arising from defects at the grain boundaries. Grain boundaries in semicrystalline silicon generally have little or no effect on the electrical performance of the cell.

A variety of experimental techniques were used to study the physical and electrical characteristics of semicrystalline samples. First, the physical structure of the surface was investigated using both SEM and optical methods. In order to emphasize the crystal structure of the surface, samples were prepared using a preferential chemical etch. Optical studies were also carried out on samples that were angle lapped and stained using a copper solution to clearly delineate the diffused regions. High quality single crystal and semicrystalline wafers were used as controls in all processing steps.

Second, the electrical response of the completed solar cells was investigated. After the illuminated cell response was measured, leakage tests were conducted as a function of temperature under both forward and reverse bias, revealing major differences in the analytical form and activation energy of the defect leakage mechanisms.

The spectral response of the cells was measured as a function of the wavelength of the incident illumination. In order to calculate the photogenerated current as a function of the number of photons hitting the device surface it was necessary to measure the reflectance of the cell surface. Again the results of the polycrystalline samples were compared with the results obtained from the single crystal controls.

The net result of these tests was a differentiation between the types of structural defects and resulting electrical performance. It is believed that this type of comprehensive investigation will lead to a better understanding of defect structure of devices made from semicrystalline and polycrystalline thin film sheet material.

NOTES

ETCHING OF CdS FILMS AND ITS EFFECT ON THE MORPHOLOGY OF THE Cu_2S LAYER OF CdS THIN FILM SOLAR CELLS

F. A. Shirland
Westinghouse Research and Development Center
Pittsburgh, PA 15235

High output CdS thin film solar cells have generally been made using a strong HCℓ etch of the CdS film prior to formation of the Cu_2S layer. The etch has been used because appreciably higher cell outputs, by a factor of 2 or more, are obtained. However, there has been little understanding of the function of the HCℓ pre-etch. Very little data have been reported on the effect of different etching parameters even though different laboratories have used different etching conditions.

A study of the morphology of the Cu_2S layer of CdS thin film solar cells (1) showed that one of the results of the HCℓ pre-etch is the formation of etch pits in the CdS film, and that the Cu_2S layer which is subsequently formed penetrates into CdS grain boundaries from the side walls of the etch pits as well as from the upper surface of the film. These penetrations appear to be beneficial to cell output. The purpose of the present study was to investigate the effect of etching parameters on variously processed CdS films to better understand how the pre-etch affects the topography of the upper CdS film surface and thence the morphology of the Cu_2S layer. Preliminary results are presented on the effect of different etchant concentrations, temperatures and times on the formation of etch pits and on the texturing of variously processed CdS films.

Vacuum evaporated CdS films are polycrystalline. Films that have been most successful for thin film solar cells have crystallite diameters of about 1 to several micrometers. The crystallites are preferentially oriented with the +c axes growing approximately up from the substrate but with their a axes randomly oriented to each other. HCℓ attacks these films more rapidly at grain boundaries and at regions of high strain. There are two principal effects: texturing of the upper film surface, and randomly scattered etch pits. The pyramiding of the grains appears to result from the anisotropic nature of the etch. It is beneficial for solar cells since films so textured are effective light traps - that is, the surface is antireflecting.

The formation of etch pits is somewhat more complex. Etch pits probably occur at regions where there is severe strain built into the film, or where there is a concentration of dislocations. The etch pits formed on representative films are large (from about 1 to several

micrometers across), and deep (from about 10 to about 20 micrometers). As noted, these etch pits appear to start between grains rather than within grains, and a whole grain or even several grains may be consumed in the formation of a pit.

The number and distribution of etch pits for a given etching treatment varies widely for differently prepared CdS films. Systematic data have not been obtained on this aspect, but in general it has appeared that CdS films grown at more rapid deposition rates develop a higher density of these etch pits. Also, the topography of the substrate of the film appears to have a major effect on the density of the etch pits. It has been noted that the higher output cells made at the Westinghouse R&D Center, and earlier cells made at the Clevite Laboratory, are usually characterized by a high density of distributed etch pits. Lower output cells are usually characterized by fewer etch pits or by etch pits that are bunched in scattered clusters.

Texturing and etch pitting occur simultaneously. However, there are indications that weaker etching solutions may favor texturing over pitting while very strong etching solutions seem to cause pitting to occur more rapidly than texturing.

A number of experiments have been carried out using weaker concentration etchants and lower temperature in order to slow the etching enough to observe more clearly how the reaction proceeds. As etching time increases the edges of the crystallites are attacked more and more until a blunt pyramid with an apex angle of about 90° is formed at the top of each crystallite. With further etching, the edges continue to be attacked more rapidly than the apexes resulting in a sharper delineation of individual crystallites and an increase in upper surface area. The apex angle becomes more acute. Also, as the etching time is increased, the depth of penetration of the etch pits (at the surface), and the number of etch pits per unit area also increases, but not in proportion. Increasing the temperature of the etch speeds up the reaction, as would be expected. The increase in temperature does not appear to change the nature of the pyramiding nor of the etch pits.

It has long been recognized that the substrate of the CdS film, and the preparation of the substrate surface prior to film deposition have a major effect on the output efficiency that can be obtained from cells made from the films. Featureless substrates, those with a very fine surface texture, and those with variable surface features generally yield low output cells. Those substrates with a somewhat coarser, but uniform, surface texture generally yield higher output cells. This seems to be at least partially correlatable with the degree of pitting which occurs during the pre-barrier etch. It seems that the most successful substrates impart a degree of disorder to the grown CdS films which is conducive to deep etch pitting, and probably also to deep penetration of the Cu_2S into grain boundaries.

SEM photographs of variously etched CdS films are presented which led to the observations and preliminary conclusions discussed above. However, it is emphasized that a limited number of such observations have been possible to date, on CdS films deposited under a relatively narrow range

of conditions. More extensive work is needed to corroborate the preliminary conclusions and to optimize CdS film etching.

Reference

1. To be published, J. Appl. Phys.

NOTES

EFFECT OF SUBSTRATE ORIENTATION ON THE PROPERTIES OF THE PbS-Si HETEROJUNCTION

H. Elabd, A. J. Steckl, and W. Vidinski
Rensselaer Polytechnic Institute
Troy, New York 12181

ABSTRACT

The PbS thin film deposited at room temperature from chemical solution on a monocrystalline Si substrate [1,2] should approximate most closely an abrupt junction between the two materials. Since no appreciable interdiffusion is thought to occur at room temperature, the interface between a PbS grain and the Si substrate should be atomically sharp. PbS-Si heterostructures were studied by electron microscopy, X-ray diffraction and analysis and Auger electron spectroscopy. Thin PbS films (t = 1000 - 6000 Å) were deposited on Si substrates with (100) and (111) orientation. The as-grown PbS has been found to consist of a uniform polycrystalline film and chain-like clusters. The PbS grain size as estimated from the SEM experiments falls in a range of 1500 to 4000 Å, as shown in Table 1. For (111) Si and glass substrates, the grain size is in the 1800 - 2000 Å range. For (100) Si, the grain size is significantly larger, ∿3500 Å. The crystallite orientation was also found to be very strongly substrate dependent, as shown in Fig. 1. For the PbS-Si (111) case, the crystallite preferred orientations are along the [220] and [311] directions as evident from the dominant intensity of the d_{220} and d_{311} lines. On the other hand, for the PbS-Si (100) heterostructure, the dominant line is d_{200} signifying a strong [100] orientation. PbS films grown on amorphous glass substrates exhibit a similar but much weaker [100] orientation. Films grown on unpolished Si (100) substrates exhibit no dominant line but rather resemble the PbS powder diffraction pattern. The diffraction data for PbS films grown on different Si and glass substrates is presented in Table 2. The experimental evidence therefore suggests that, in spite of the large lattice mismatch (∿8.9%) and different crystal structures in the PbS-Si heterostructure, there is a close crystallographic relationship between the Pb and S atoms and the Si surface.

Auger electron spectroscopy was utilized to detect the presence of foreign atoms at the PbS-Si interface. The spatial distribution of interface constituents was determined by repeating the AES scans at several locations at the film-substrate interface. No impurity peaks with the exception of a minor oxygen peak (∿1 at. %) were detected at the interface between PbS and either Si (100) or (111), indicating the absence of any significant insulative barriers. A typical composition depth profile of the PbS (100) Si heterostructure is shown on Fig. 2. The interface oxygen concentration in the PbS-Si (100) structure is roughly twice that present in the PbS-Si (111) structure. It is possible that the presence of foreign atoms, such as oxygen, at the heterojunction interface is the result of interaction with dangling bonds rather than uniform oxidation.

A physical three-dimensional model was constructed in order to study the relative orientation of PbS and Si crystallographic planes at the heterostructure interface. The type and density of dangling bonds at the interface was calculated for various substrate and film orientations. Correlations and comparisons between the experimental X-ray diffraction data and the theoretical calculations based on the model are presented.

REFERENCES

(1) H. Elabd, and A. J. Steckl, J. Vac. Sci. Tech., 15, 264 (1978).

(2) J. L. Davis, and M. K. Norr, J. Appl. Phys., 37, 1670 (1966).

Substrate	Mean Crystallite Dimension X-ray Diffraction (Å)	SEM Estimate of Grain Size (Å) A ≃ B
Si (100)	3430	3400 - 3800
Si (111)	1850	1500 - 2000
Glass *	2020	1400 - 2700

Table 1. Tabulation of Various Estimates of the Average Grain Size in 4000 Å PbS Films
* Grain size of PbS-Glass reported here compares closely to that reported by G. W. Mahlman, Phys. Rev., 103, 6, (1956).

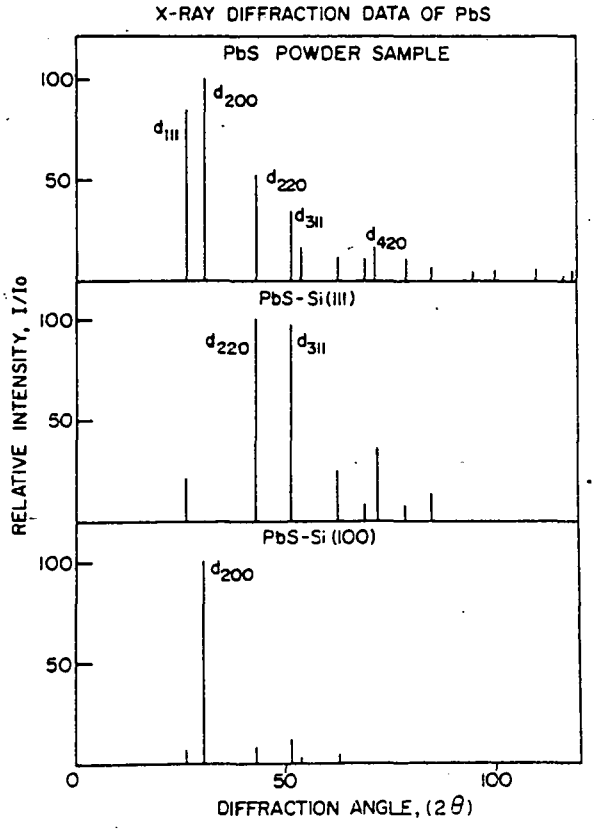

Fig. 1. X-Ray Diffraction Data of PbS Film [on Si (111) and (100)].

d(Å)	HKL	2θ°	I/I0, Galena* Powder Sample	I/I0, PbS-Si(100) Unpolished	I/I0, PbS-Si(100) Polished	I/I0 PbS-Si(111)	I/I0 PbS - Glass
3.429	111	26.09	84	81.13	6.25	21.05	56.25
2.969	200	30.11	100	100	100	UNDETERMINED	100
2.099	220	42.62	57	59.12	7.5	100	32.14
1.790	311	51.04	35	33.96	11.5	97.89	18.75
1.714	222	53.48	16	18.24	1.25	-	4.46
1.484	400	62.63	10	8.81	3.5	26.32	4.46
1.362	331	68.98	10	UNDETERMINED		7.89	1.79
1.327	420	71.07	17	18.87	-	36.84	8.04
1.212	422	79.04	10	10.69	-	7.89	2.68
1.1424	511	84.92	6	6.60	-	13.16	-
1.0489	440	94.66	3	1.26	-	-	-
1.0034	531	100.46	5	3.77	-	-	-
0.9393	600	110.38	6	5.03	-	-	-
0.9386	620	110.51	4	4.09	-	-	-
0.9050	533	116.90	2	-	-	-	-
0.8952	622	118.97	4	-	-	-	-

Table 2. Tabulated Diffraction Data of PbS Film Grown on Different Substrates
* Diffraction Data of the A.S.T.M. Data File.

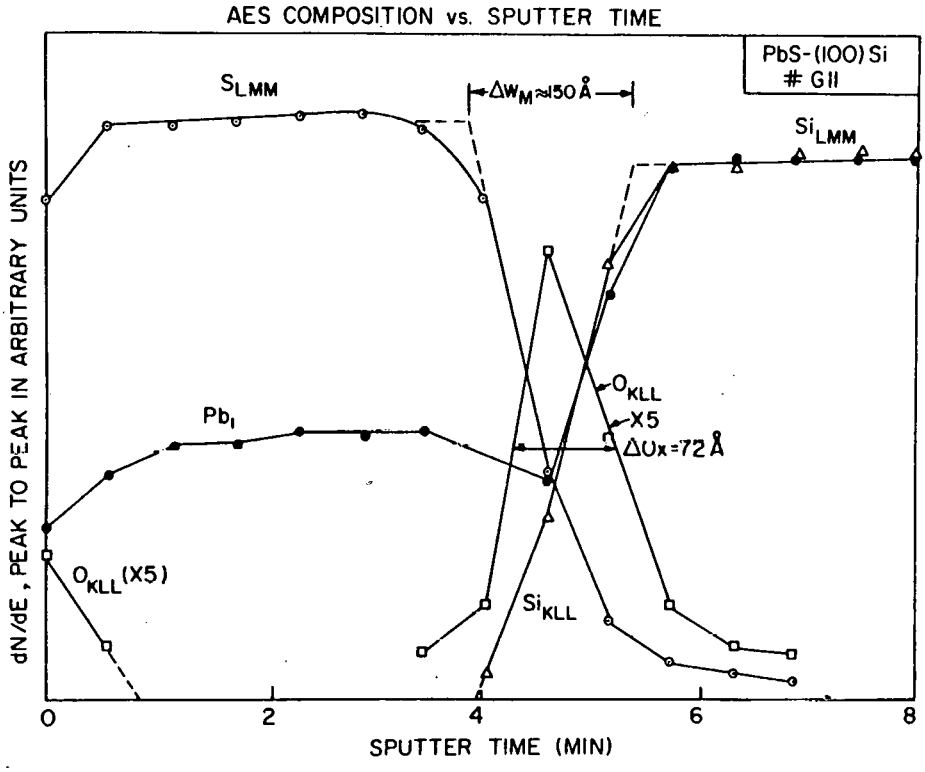

Fig. 2. Auger Electron Spectroscopy Composition vs Sputter Time (the interface width ΔW_M and Oxygen Peak Width ΔOx are estimated using the etch rate of SiO_2).

NOTES

THIS PAGE

WAS INTENTIONALLY

LEFT BLANK

MEASUREMENT TECHNIQUES IN THIN FILM POLYCRYSTALLINE MATERIALS AND DEVICES (SOLAR CELLS)

H. K. Charles, Jr. and R. J. King

PRC Energy Analysis Company
7600 Old Springhouse Road
McLean, Virginia 22102

A. P. Ariotedjo

Solar Energy Research Institute
1536 Cole Boulevard
Golden, Colorado 80401

A discussion of the theory relevance and applicability of basic bulk material and single crystal semiconductor measurement techniques to thin film polycrystalline materials and devices will be made. The measurement techniques to be emphasized include resistivity (i.e., in-line four point, Van der Pauw and spreading resistance methods) and the Hall effect. Parametric expressions for resistivity and the Hall effect will be presented which include correction factors for film thickness, grain size, grain boundary conductivity and the influence of the substrate. The use of other electronic measurement techniques in obtaining materials parameters necessary for the resistivity and the Hall effect expressions will also be reviewed. These measurements include: surface photovoltage, diode reverse recovery time, photo conductivity, capacitance-voltage methods, and thermo-electric conductivity. Materials characterization and analysis techniques such as scanning electron microscopy (SEM), secondary-ion mass spectrometry (SIMS), Auger electron spectroscopy (AES), and X-ray crystallography will be presented in their dual role of providing necessary sample parameter values for the derived analytical expression and also serving as an independent means of verification for some of the results determined by the basic electronic measurement techniques. The material characterization methods provide information on grain size, morphology, and many other parameters including: impurity content, film thickness, doping profiles, and device junction depth.

The technical literature will be surveyed to determine the most widely applied thin film resistivity and Hall effect analytical and experimental measurement methods. Widely used measurement techniques for other relevant parameters (e.g., minority carrier lifetime, diffusion length, etc.) will also be identified, and an estimate of their efficacy in yielding results (i.e., parameter values) for thin films consistent with overall device performance will be made. To facilitate the dissemination and widespread utility of this information, key device parameters and their respective measurement methods will be identified and discussed using matrix methods. Measurement techniques producing the most effective performance indicators will then be analyzed for needed improvements, greater measurement reproducibility, etc.

Special emphasis will be placed on the influence of grain size and grain size measurements on key device parameters and overall device performance. Curves for the resistivity and Hall effect coefficient as a function of grain parameters will be developed. The problems associated with the extension of single crystal semiconductor measurement theory to polycrystalline thin films will be reviewed. Consideration will be given to new (or little used) techniques which offer promise in thin films for estimating the relevant or potentially useful parameters. The aspects and importance of test device fabrication methods (e.g., junction delineation, sample sectioning, selective etching, capacitive and ohmic contact application) to the measurement results will be discussed. Particular attention will be paid to ohmic contacts on polycrystalline thin films.

NOTES

THIS PAGE

WAS INTENTIONALLY

LEFT BLANK

*U.S. GOVERNMENT PRINTING OFFICE: 1979--0-677-083/24